JSTR
ASEAN Journal of Scientific and Technological Reports
Vol. 25 No. 3
July - September 2022
ISSN 2773-8752 (online)

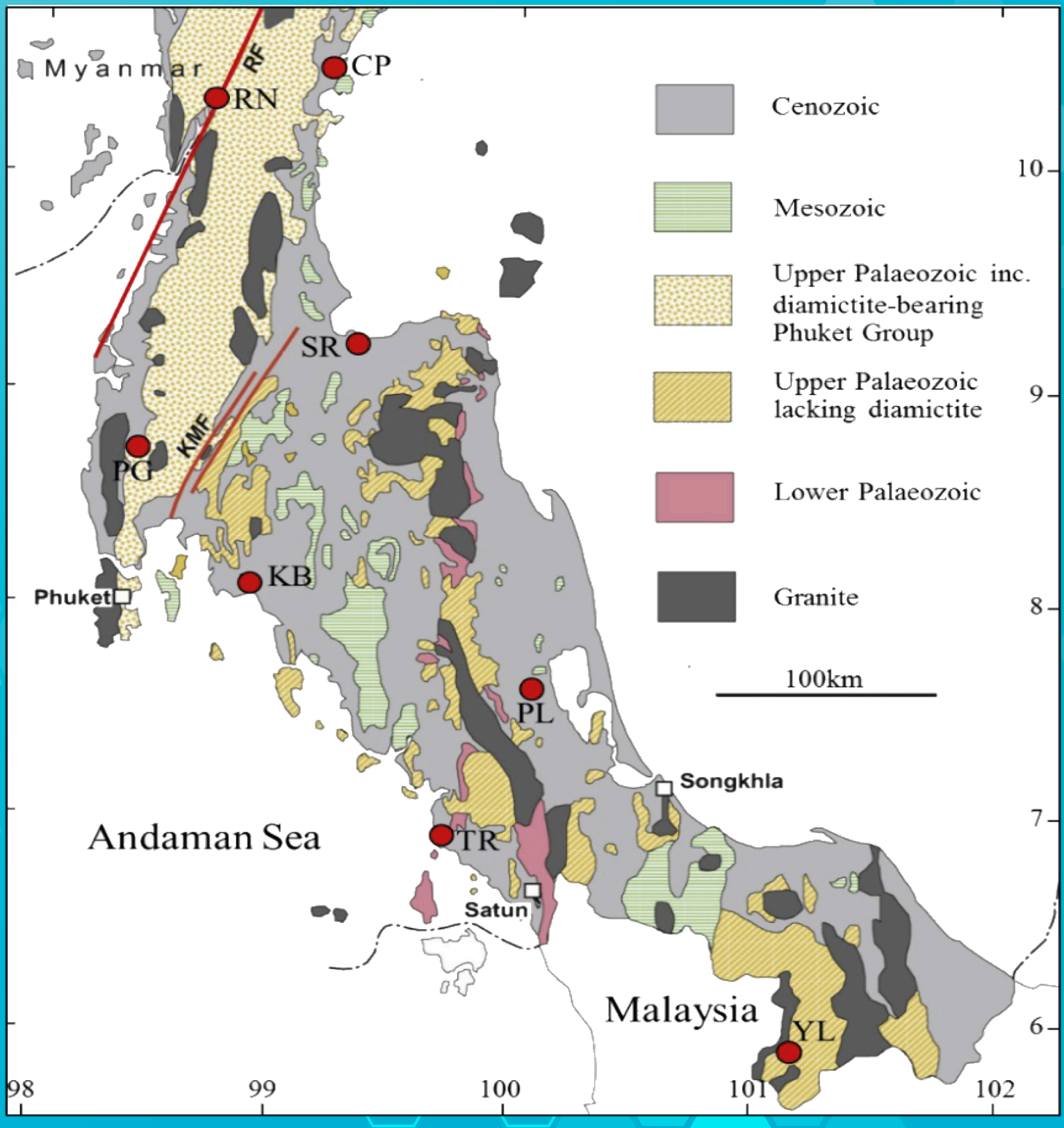

ASEAN Journal of Scientific and Technological Reports (AJSTR)

Staff: Journal Management Division

1. Miss Kanyanat Liadrak, Thaksin University, Thailand
2. Miss Ornkamon Kraiwong, Thaksin University, Thailand

Contact Us Research and Development Institute Thaksin University 222 M. 2 Ban-Prao sub-district, Pa-Pra-Yom district, Phatthalung province, Thailand

Tel. 0 7460 9600 # 7242 , E-mail: aseanjstr@tsu.ac.th

Editorial

The ASEAN Journal of Scientific and Technological Reports (AJSTR) Vol. 25 No. 3 (July-September 2022) ISSN 2773-8752 is the third issue under AJSTR. This issue published eight worth-reading research articles. These exciting research articles were reviewed and answered by experts from various universities and institutions. We sincerely hope that some of the research papers will help guide and motivate our active researchers to produce and create more valuable research shortly. The AJSTR has served our energetic readers and customers on an international level.

For this reason, all selected and accepted research articles will be written and organized in English. Furthermore, the new international editorial board of AJSTR has also been set up and started to administrate and manage all the journal's business simultaneously. From now on, the AJSTR and a new editorial team are ready to organize, manage, publish, and deliver all good quality articles written in well-organized English to the world of academic society. I would like to introduce AJSTR's editorial board members as below.

Assoc. Prof. Dr. Sompong O-Thong
Journal Editor-in-Chief

List of Contents


มหาวิทยาลัยทักษิณ THAKSIN UNIVERSITY


JSTR
ASEAN Journal of Scientific
and Technological Reports


มหาวิทยาลัยทักษิณ THAKSIN UNIVERSITY

JSTR
ASEAN Journal of Scientific and Technological Reports

Research article

Geothermometry in High-Temperature Reservoirs of the Geothermal Springs in Southern Thailand: Insights from Cations and Silica Geothermometers

Wipada Ngansom[1*], Dumrongsak Rodphothong[1] and Helmut Duerrast[2]

[1] Department of Physics, Faculty of Science, Ramkhamhaeng University, Thailand; wipada.n@rumail.ru.ac.th; dumrongsak.r@rumail.ru.ac.th
[2] Geophysics Research Center, Faculty of Science, Prince of Songkla University, Thailand; helmut.j@psu.ac.th
* Correspondence: wipada.n@rumail.ru.ac.th

Abstract: Geothermal springs have provided a unique opportunity to study the geothermal system of geological processes. A reservoir temperature estimation based on the chemical geothermometers is vitally essential for assessing the exploration and development of geothermal resources. The paper represents the various techniques of geothermometers with comparisons between the silica (quartz and chalcedony) and the cation geothermometers (Na–K–Ca and K–Mg) for the high exit temperature (temp. ≥55°C) of geothermal springs in southern Thailand. The Na–K–Ca geothermometer presented more elevated reservoir temperatures than the K–Mg, silica and chalcedony geothermometers, about 20–30◦C. The preliminary assumed difference between the geothermometers may indicate that the shallow subsurface conditions are mixed with groundwater.

Keywords: Geothermometer; reservoir temperature; geochemistry; geothermal spring; southern Thailand

Citation:
Ngansom, W.; Rodphothong, D.; Duerrast, H. Geothermometry in High-Temperature Reservoirs of the Geothermal Springs in Southern Thailand: Insights from Cations and Silica Geothermometers. *ASEAN J. Sci. Tech. Report.* **2022**, *25*(3), 1-8. https://doi.org/10.55164/ajstr.v25i3.246596.

Article history:
Received: May 4, 2022
Revised: June 25, 2022
Accepted: July 6, 2022
Available online: July 19, 2022

1. Introduction

Variations in chemical constituents of geothermal spring waters indicate the changes experienced by sampled fluid in its past flow [1, 2, 3]. Most essential parameters like reservoir temperatures, flow patterns, sources of recharge, and type of reservoir rocks can be estimated through chemical analysis of fluids reaching the surface of natural hot springs or wells [4, 5]. A geochemical concentration has estimated reservoir temperatures and the ratio of certain elements; these are called "geothermometers" comprising silica (quartz and chalcedony) and cation (e.g., Na-K-Ca and K-Mg) geothermometers [6, 7]. Significantly, the geothermometers rely on the temperature-dependent equilibrium with time constants, used to estimate specific temperatures at depth [8, 9]—resulting in geothermal reservoir temperatures reflected by solute concentrations of solute ratios. Significantly, the silica geothermometer is reservoir temperature controlled by SiO_2 solubility [8, 9].

An efficiency factor of the silica geothermometer of geothermal reservoirs consists of (1) mixing and boiling processes as the most significant interference, (2) a defective crystalline structure of chalcedony, and (3) a pH value of geothermal waters (not exceed 9) [7, 8, 9]. Cation geothermometers (e.g., Na-K, Na-K-Ca, and K-Mg) with slow re-equilibration are theoretically more effective in accurately assessing a deep-reservoir temperature. Still, they are often affected by shallow processes. In this study, we focus on non-volcanic geothermal areas (e.g., Malaysia and Thailand) where low to medium temperature reservoirs are ranged from 100 to 180°C (10, 11). For this condition, some geothermal springs in Southern Thailand are of distinctive importance in estimating subsurface temperature as a key parameter for evaluating the economic potential for a geothermal electricity plant. Overview the geothermal springs in Southern Thailand are characterized by medium to high exit temperatures of approximately 40 to 80°C with a wide range of dissolved chemical compositions [4, 5]. Most of the hot spring waters are hot-types with bicarbonate-rich waters. Observations of surface and groundwater and geothermal fluids discharged from geothermal springs and drilling show that the chemical compositions vary within wider limits [3, 5]. For all geothermal springs in southern Thailand, the accurate heat sources are unknown. It can be either an igneous body where radioactive decay produces heat or a higher heat flow onshore basin development [2, 4].

2. Methodology

2.1 Field Overview

At least 30 geothermal spring sites are located in eight geothermal provinces in the southern region of Thailand, which consist of Chumphon (CP), Ranong (RN), Surat Thani (SR), Phang Nga (PG), Krabi (KB), Trang (TR), Phatthalung (PL), and Yala (YL) provinces, as shown in Figure 1. Exit temperatures are between 40 and 80°C. A summary of information for the study sites can be briefly described.

2.1.1. Ranong geothermal province (RN1-RN6)

As one of the larger geothermal systems in the southern region, the RN geothermal field is located in Ranong Province. It is famed for natural hot springs, thus drawing the attention of local and foreign visitors (Figure 1). Altogether, seven natural hot spring sites are located in the RN geothermal field, with exit temperatures between 40 and 75 °C; RN1 and RN6 areas have the highest temperature in this system. The RN1 site is praised as the famous landmark of Ranong City, also providing spa and hot massage therapy nearby. While the RN6 site was discovered in the deep forest in Kapoe District, located approximately 60 km south of Ranong city, the site is protected by the Ranong Forest Preservation and Protection Division. All hot spring sites located close to the Ranong Fault Zone are on major strike-slip faults [2, 5].

2.1.2. Surat Thani geothermal province (SR1-SR9)

The SR geothermal field is located in the western part of the southern region, with nine natural hot springs recorded. The exit temperatures range from 40 to 70 °C, while the SR3, SR7, and SR9 sites show the highest exit temperature in this system (Figure 1). SR3 is in Tha- Chang District, located on public land close to the main railway line (Bangkok - Hat Yai) and relatively close to Thailand's Gulf. SR7 is already developed for tourism; its larger pond is visible from the main road. In contrast, SR9 is located in a national park area. The general geology surrounding the SR geothermal field is characterized by isolated steep-sided hills of Permian limestones, tower karsts and granitic mountains on the western margins [1, 3].

2.1.3. Phang Nga geothermal province (PG1-PG3)

The PG geothermal field on the western side of the southern region, approximately 100 km north of Phuket city, is shown in Figure 1. At least three natural hot spring sites can be found in this geothermal system, with exit temperatures recorded from 45 to 78 °C; only one place, PG1, has an exit temperature of up to 78 °C. The PG1 site can be found close to and on the banks of the Pai Phu River. Rocks in and around the PG1 site are predominantly granites distributed in the southeastern and sedimentary/metamorphic rock units, which cover other regions [2, 5].

2.1.4. Phatthalung geothermal province (PL1-PL4)

The PL geothermal field is located in Phatthalung Province, as shown in Figure 1. This system has four hot spring sites with exit temperatures between 41 and 57 °C. A general geological setting is exposed, containing Cambrian to Quaternary rocks. Cambrian rocks comprise white to light grey-coloured fine-grained sandstone and quartzite, and Ordovician rocks are mainly grey-coloured, finely crystalline to coarse-grained limestones [1, 3].

2.1.5. Yala geothermal province (YL1)

The Yala geothermal field is located in southernmost Thailand near the border with Malaysia, as shown in Figure 1. Detailed investigations have been affected by continuous armed conflicts in this area since 2004; therefore, geological and geophysical survey data are limited. However, the YL site is a famous tourist attraction, mainly for Malaysian guests, and has an exit temperature above 80 °C [1, 3].

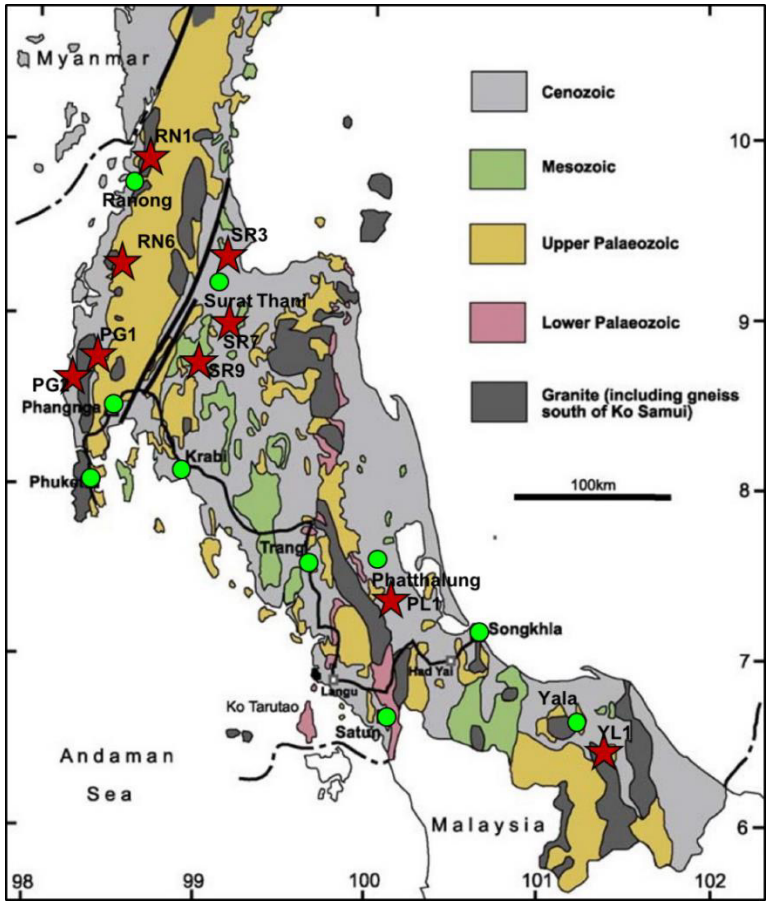

Figure 1. Simplified geological map and location of geothermal hot spring systems part of Southern Thailand (based on Department of Mineral Resources, 1999)

2.2. Samples and Analytical Methods

Based on the property of the geothermal groundwater is usually mixed with freshwater/saltwater and has undergone various chemical reactions during its flow through different geological formations. Therefore, investigating the appropriate reservoir temperatures of geothermal groundwater in southern Thailand was expressed with specific geochemical signatures to the other components of the various operations in water sampling and analysis. Nine water samples with high exit temperatures greater than or equal to 55°C were collected in five geothermal provinces, comprising Ranong (RN1 and RN6), Surat Thani (SR3, SR7 and SR9), Phang Nga (PG1 and PG2), Phatthalung (PL1), and Yala (YL1) sites. All the water samplings were carried out in April 2021. The multi-parameter water quality analyser measured exit temperature and pH values at the sampling sites. One litre of each sample collected for the major and trace element analysis was filtered on-site

and stored in polyethene bottles cleaned by rinsing several times with the waters sampled solution. Whereas a nitrogen oxoacid (HNO3) was utilized to acidify (pH < 2) a portion of the water samples for cations analysis. In contrast, significant anions were kept unacidified for chemical analysis. The geochemical analysis was performed at the Laboratory of Water Analysis Co., Ltd. (ISO/IEC 17025:2017), Phra Nakhon Si Ayutthaya, Thailand. The methods of chemical analysis and detection limits of these parameters are exhibited in Table 1. The ionic balance error of cations and anions of all water samples is ranged from 0.15 to 6.23%.

Table 1. Methods used and Detection limits of geochemical analysis

Parameters	Method used	Detection limits (mg/L)
pH	In-house method: TM 001	-
Total dissolved solids, TDS	In-house method: TM 017	25
Chloride, Cl^-	In-house method: TM 008	6
Calcium, Ca^{2+}	EDTA Tritrimetric	0.01
Magnesium, Mg^{2+}	EDTA Tritrimetric	0.01
Potassium, K^+	Direct Air-Acetylene Flame	0.01
Sodium, Na^+	Direct Air-Acetylene Flame	0.005
Sulfate, SO_4^{2-}	Turbidimetric	1
Bicarbonate, HCO_3^-	Titration	1
Silica, SiO_2	In-house method: TM 030	1.1

2.3. Chemical Geothermometers

The site-specific selection of the geothermal springs in Southern Thailand among the high exit temperatures greater than or equal to 55°C consisted of nine hot springs located in five geothermal provinces that included Ranong (RN1 and RN6), Surat Thani (SR3, SR7 and SR9), Phang Nga (PG1 and PG2), Phatthalung (PL1) and Yala (YL1). Various silica and cation geothermometers were used to estimate reservoir temperatures (tR, in °C) of the geothermal springs in southern Thailand. Silica geothermometers, which are the most common types to estimate subsurface temperatures of geothermal reservoirs, are based on the solubility of quartz and chalcedony (SiO_2 content, unit; mg/L) [7, 9], whereas cation geothermometers (Na-K-Ca and K-Mg geothermometers) are based on the ion exchange reaction of Na^+, K^+, Ca^{2+} and Mg^{2+} concentrations (unit; mg/L) with a temperature-dependent equilibrium constant [6, 7, 8, 9], as shown in Eq. (1) to (4):

Quartz $$t_R(°C) = \left[\frac{1309}{5.19-\log(SiO_2)}\right] - 273.15 \quad (1)$$

Chalcedony $$t_R(°C) = \left[\frac{1032}{4.69-\log(SiO_2)}\right] - 273.15 \quad (2)$$

Na-K-Ca $$t_R(°C) = \left[\frac{1647}{\log\left(\frac{Na}{K}\right)+\beta\left[log\left(\frac{\sqrt{Ca}}{Na}\right)+2.06\right]+2.47}\right] - 273.15 \quad (3)$$

when $\beta = 4/3$ for t<100 °C; $\beta = 1/3$ for t>100 °C

K-Mg $$t_R(°C) = \left[\frac{4410}{14-\log(K^2/Mg)}\right] - 273.15 \quad (4)$$

3. Results and Discussion

3.1. Groundwater properties

Geochemical characteristics analyzed from the local groundwater samples of geothermal springs in Southern Thailand are listed in Table 2. The relative errors of ion balance (cation and anion) were below 5% in each sample. High TDS (total dissolved solids) value of 12,610 mg/L was found at the SR3 geothermal spring. All the geothermal groundwater samples were near-neutral to weakly alkaline; pH value was 6.8 at the SR9 geothermal spring and greater than 7.0 at the other hot springs, and was up to 8.0 at the RN1, RN6 and YL1 geothermal springs. A concentration of Na^+ is ranged from 12.1 to 64.5 mg/L in most geothermal spring sites, except the SR3 (Na^+=3,655 mg/L) represented a saltwater intrusion into the geothermal aquifer (Table 2). Cl^- the content was the dominant anion in the SR3 (6,630 mg/L), while HCO_3^- the content was the dominant one in the PG2 and PL1 geothermal spring waters. Moreover, Mg^{2+} concentrations were very low to the medium of approximately 0.02 to 42.5 mg/L in most geothermal waters except the SR3 and SR7 hot springs.

Table 2. Exit temperatures (Exit temp., °C), pH values, and concentrations of major geochemical constituents in geothermal spring waters (mg/L) from southern Thailand

Hot spring	Exit temp. (°C)	TDS (mg/L)	pH	Content (mg/L)							
				SiO_2	Na^+	K^+	Ca^{2+}	Mg^{2+}	Cl^-	HCO_3^-	SO_4^{2-}
RN1	65	330	8.3	79.3	48.4	2.8	44.1	0.02	4.8	182	19.3
RN6	75	580	8.1	111.0	51.3	3.5	28.1	0.90	13.3	177	10.0
SR3	60	12,610	7.9	58.5	3,655.0	115.0	840.0	148.00	6,630.0	117	746.0
SR7	70	1,980	7.9	60.7	64.5	13.6	381.0	75.20	21.0	117	1,180.0
SR9	62	1,300	6.8	62.0	12.1	4.6	265.0	42.50	8.9	131	830.0
PG1	78	280	7.8	77.7	84.0	3.3	6.9	0.18	5.8	145	11.9
PG2	55	390	7.7	25.5	39.1	3.7	45.5	10.80	8.1	250	4.3
PL1	57	255	7.8	97.6	76.6	6.4	16.7	0.45	5.8	200	3.1
YL1	80	335	7.9	98.2	75.8	7.2	17.2	0.52	6.1	195	2.9

3.2. Geothermometers

The reservoir temperatures estimated from the cation geothermometers (Eq., 3-4) are usually higher than those obtained from silica geothermometers (Eq., 1-2) [8, 9,10], as shown in Table 3 and Figure 2. The Na–K-Ca geothermometer (Eq., 3) gives anomalously high temperatures ranging from 128 to 182°C, whereas the K–Mg geothermometer (Eq., 4) yields the maximum temperature of around 114°C;. In contrast, the silica geothermometer (Eq., 1) and chalcedony geothermometer (Eq., 2) estimated temperatures vary between 80 and 135 °C. Therefore, the K–Mg geothermometer results are considered more consistent with reservoir temperature estimates from the silica (particularly chalcedony) geothermometer [11, 12, 13]. Reservoir temperatures estimated by the quartz geothermometer are about 20–30 °C higher than those by the chalcedony geothermometer [12, 13, 14] shown in Figure 2.

Table 3. Calculating results of the silica and cation geothermometers (°C) for the geothermal springs in Southern Thailand

Hot spring	Reservoir temperature (°C) computed by different chemical geothermometers			
	quartz (Eq.1)	chalcedony (Eq.2)	Na-K-Ca (Eq.3)	K-Mg (Eq.4)
RN1	124.6	96.7	127.9	113.5
RN6	113.9	84.9	154.3	46.1
SR3	109.3	79.9	142.9	92.9
SR7	111.1	81.9	176.9	50.9
SR9	112.1	83.0	182.0	35.2
PG1	123.6	95.5	132.4	87.8
PG2	112.5	83.4	128.9	96.5
PL1	127.9	100.2	142.0	111.8
YL1	135.8	109.0	158.9	93.0

Whereas the comparisons for quartz, chalcedony, Na-K-Ca, and K-Mg geothermometers used to calculate reservoir temperatures corresponding to all hot spring sample sites are shown in Figure 2.

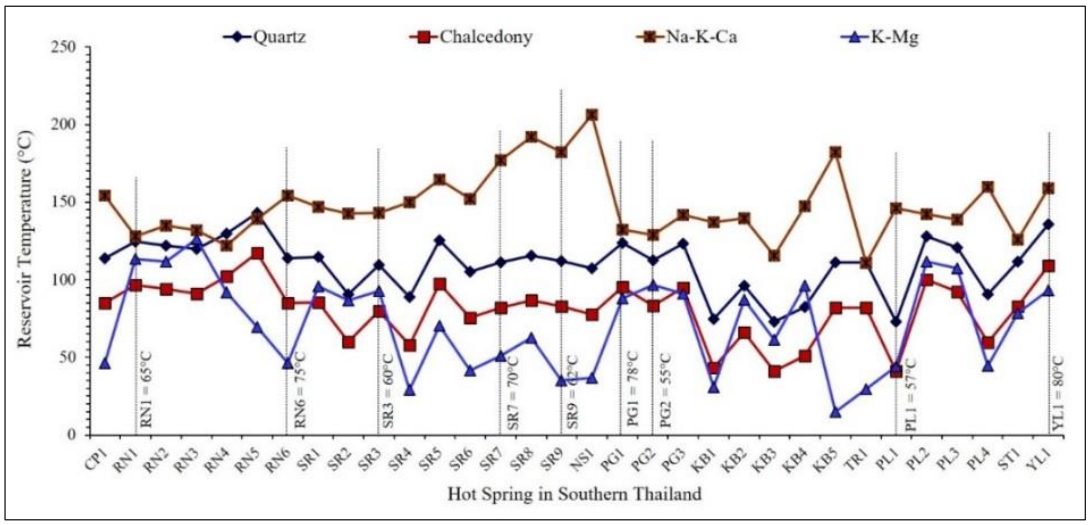

Figure 2. Reservoir temperatures calculated using different geothermometers.

On the other hand, the relationships between silica contents, exit temperatures, and reservoir temperatures calculated with the quartz-silica geothermometer using the hot spring water composition are plotted in Figure 3a. These parameters are strongly correlated except for some geothermal spring samples from low exit temperature hot springs. For the Na–K geothermometer, the relationship between log (K/Na) composition, the exit temperature, and reservoir temperature is shown in Figure 3b. Na/K ratios of geothermal spring water samples are more sensitive to temperature changes than the silica contents, as shown in Figure 3. Also, except for some geothermal spring samples from low exit temperature hot springs, these parameters are negatively correlated but not strong. Therefore, the subsurface temperatures estimated by the silica-quartz geothermometer could represent a suitable reservoir temperature for the geothermal springs (exit temperature, ≥55°C) ranging from 110 to 135°C.

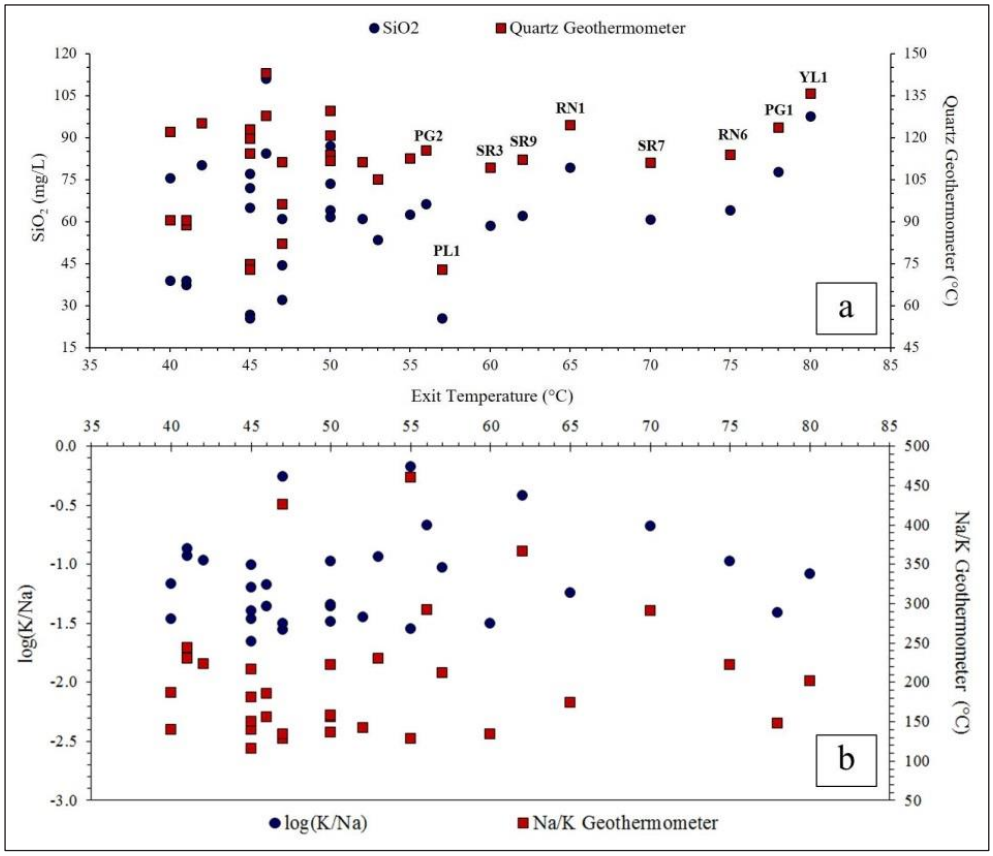

Figure 3. (a) Quartz and (b) Na–K geothermometer temperatures, as well as SiO_2 and log (K/Na) contents in relation to exit temperatures for hot springs from Southern Thailand.

4. Conclusions

The application of chemical geothermometers in geothermal springs of southern Thailand is an essential technique for understanding the chemical composition and for the estimation of geothermal reservoir temperatures. However, conducting detailed studies at the geothermal spring sites is also necessary to better understand the geological setting where these natural hot springs are found. As silica is chemically more inert, the silica geothermometer temperatures can be assumed to provide more reliable reservoir temperatures. The quartz geothermometer has better values than the chalcedony one, as the chalcedony relates to the quartz content. Variations in the cation geothermometers, Na-K-Ca and K-Mg, derived from the mixing of the hot water can explain temperatures with shallow groundwater; at some locations near the shoreline, also with seawater. Silica geothermometers, and especially the quartz ones, provide more realistic reservoir temperatures, but the absolute values are relatively low in comparison.

5. Acknowledgements

The authors are very grateful to Geophysics Research Center, Faculty of Science, Prince of Songkla University, for the survey equipments.

References

1. Ngansom, W.; Dürrast, H. Geochemical Characterization of Hot Spring Waters from Southern Thailand as The Base for Geothermal Energy Utilization. *Environment Asia.* 2021, *14*, 37–49.
2. Ngansom, W.; Pirarai, K.; Dürrast, H. Geological setting and hydrogeothermal characteristics of the Kapong non-volcanic hot spring area in Southern Thailand. *Geothermics.* 2020, *85*, 101746.

3. Ngansom, W.; Dürrast, H. Assessment and Ranking of Hot Springs Sites Representing Geothermal Resources in Southern Thailand using Positive Attitude Factors. *Chiang Mai Journal of Science.* 2019, *46*, 592–608.
4. Ngansom, W.; Dürrast, H. Saline hot spring in Krabi, Thailand: A unique geothermal system. *Society of Exploration Geophysicists.* 2016, 1949–4645.
5. Ngansom, W.; Dürrast, H. Integrated geoscientific investigations of the Phang Nga geothermal system, southern Thailand. *Society of Exploration Geophysicists.* 2017, 5427– 5431.
6. Fournier, R.O.; Rowe, J.J. Estimation of underground temperatures from the silica content of water from hot springs and wet- steam wells. *American Journal of Science.* 1966, *264*, 685–697.
7. Fournier, R.O.; Truesdell, A.H. An empirical Na-K-Ca geothermometer for natural waters. *Geochimica* et *Cosmochimica Acta*. 1913, *31*, 515–525.
8. Fournier, R.O. Chemical geothermometers and mixing models for geothermal systems. *Geothermics* 1977, *5*, 41–50.
9. Fournier, R.O. A method of calculating quartz solubilities in aqueous sodium chloride solutions. *Geochimica* et *Cosmochimica Acta.* 1983, *47*, 579–586.
10. Baioumy, H.; Nawawi, M.; Wagner, K.; Arifin, M.H.J. Geochemistry and geothermometry of non-volcanic hot springs in West Malaysia. *Journal of Volcanology and Geothermal Research*. 2015, *290*, 12–22.
11. Dávalos-Elizondo, E.; Atekwana, E.A.; Atekwana, E.A.; Tsokonombwe, G.; Laó-Dávila, D.A. Medium to low enthalpy geothermal reservoirs estimated from geothermometry and mixing models of hot springs along the Malawi Rift Zone. *Geothermics.* 2021, *89*, 101963.
12. Li, J.; Zhang, L.; Ruan, C.; Tian, G.; Sagoe, G.; Wang, X. Estimates of reservoir temperatures for non-magmatic convective geothermal systems: Insights from the Ranwu and Rekeng geothermal fields, western Sichuan Province, China. *Journal of Hydrology.* 2022, *609*, 127668.
13. Mao, X.; Dong, Y.; He, Y.; Zhu, D.; Shi, Z.; Ye, J. The effect of granite fracture network on silica-enriched groundwater formation and geothermometers in low-temperature hydrothermal system. *Journal of Hydrology*. 2022, *609*, 127720.
14. Huang, Y. H.; Liu, H. L.; Song, S. R.; Chen, H. F. An ideal geothermometer in slate formation: A case from the Chingshui geothermal field, Taiwan. *Geothermics*. 2018, *74*, 319-326.

JSTR
ASEAN Journal of Scientific and Technological Reports

Research article

Effects of Dietary Protein Levels on the Stage Development and Production Performance of Nile Tilapia

Nisarat Tippayadara[1], Kanokkan Worawut[2*] and Baramee Phungpis[2]

[1] Faculty of Interdisciplinary Studies, Khon Kaen University Nong Khai Campus, Nong Khai, 43000, Thailand; nisati@kku.ac.th
[2] Faculty of Natural Resources, Rajamangala University of Technology Isan Sakon Nakhon Campus, Sakonnakhon, 47160, Thailand; barameephungpis@yahoo.com
[2] Faculty of Natural Resources, Rajamangala University of Technology Isan Sakon Nakhon Campus, Sakonnakhon, 47160, Thailand; kanokkan_pom@hotmail.co.th
* Correspondence: kanokkan_pom@hotmail.co.th

Abstract: Lack of understanding in selecting age-appropriate protein levels in the tilapia diet would result in low growth and productivity. Therefore, the effect of dietary protein levels on tilapia development and the productive potential of fry raised in concrete ponds according to the CRD experimental protocol was investigated using three treatments with four replications. Fifteen breeder fish/ponds with a male-to-female ratio of 1:2 were fed with 15.5, 25, and 30% protein for 20 weeks. The water quality was monitored and the fish's mouth was tapped every 2 weeks. The results showed that feeding of 25% protein affected egg development at all stages (Zygote, Cleavage, Gastrula, Segmentation, Pharyngula, Hatching, Early larva, and Late larva) as well as production cost better than other feeds ($p<0.05$). Breeders fed 30% protein had a higher average weight, specific growth rate, condition factor, and feed efficiency but the lowest feed intake, feed rate, and feed conversion rate ($p<0.05$). A 25% protein diet provides adequate nutrition for hatching and fries production while keeping the pond water safe for their lives.

Keywords: Nile tilapia; Dietary protein; Fish growth; Fish egg; Water quality

Citation:
Worawut, K.; Phungpis, B.; Tippayadara, N. Effects of Dietary Protein Levels on the Stage Development and Production Performance of Nile Tilapia. *ASEAN J. Sci. Tech. Report.* **2022**, *25*(3), 9-17. https://doi.org/10.55164/ajstr.v25i3.246355.

Article history:
Received: March 28, 2022
Revised: June 26, 2022
Accepted: August 30, 2022
Available online: September 28, 2022

1. Introduction

Nile tilapia (*Oreochromis niloticus*) is one of the fish farmed on every continent in the world, including 135 countries [1]. This fish farming tends to increase and is the world's second-largest fish farming, inferior to the carp group. Thailand is the world's fifth-largest producer of tilapia [2] and tilapia is the first rank fish farming industry in Thailand. Tilapia produces up to 217.9 tons, accounting for 52.7% of all freshwater aquaculture [3]. Tilapia fry can be made in earthen ponds, net pens, and concrete ponds. The production of tilapia fry in concrete ponds is widely popular in Thailand. The pond size will be in the range of 2-10 meters in length, 2-4 meters in width, and 0.8-1 meters in depth, with breeders in the ratio of 1:3 (3-4 fishes per square meter) [4]. Producing fry in concrete ponds results in more accessible fry collection than in earthen ponds and net pens. Still, its production cost is higher, which is a significant weakness in the production system, especially the cost of food, which accounts for more than 50% of the total cost. Besides, it is necessary to manage the water system in

the fishpond for suitable quantity and quality or to improve quality for tilapia farming, such as pH 6.5-8.0 and dissolved oxygen concentration (DO) of not less than 4 mg/L [5].

Fish feeds protein mainly significantly impacts the growth, survival rate, cost-benefit analysis, yield, and quality of farmed fish. A feed with appropriate protein levels for the development of fish of various ages and species is critical, whereas a meal with lower protein levels than the fish requires results in low growth rates and yields. [6]. The protein requirement from nutrients for tilapia is approximately 1 g/kg of fish per day, and breeders require protein in the range of 25-50% [6], fat in the range of 5-9% [8], and digestible energy in the range of 8.2-9.4 kcal/g protein [9]. Most aquaculture farms in Thailand use commercially available ready-made pellets with varying protein levels, including some using low-quality raw materials to reduce production costs. When the farmers use them to raise fish, they will impact the fish's development rate, low survival rate, and loss—as such, selecting the proper feed for tilapia production in concrete ponds is critical.

This study aims to determine the production potential of fry in small concrete ponds fed with various protein levels. The types of feeds with different protein levels have been selected from the local commercially available to assist the farmer in selecting the best feeds for fish farming.

2. Materials and Methods

2.1 Fish sample preparation

The male and female breeders of 180 and 120 tilapia (*O. niloticus*) were taken from the Nong Khai Inland Fisheries Research and Development Center in Nong Khai Province, Thailand. They were raised in six concrete ponds of two square meters in size, separated by sex, and filled with about 1 cubic meter of freshwater so that the fish could adapt to the experimental conditions. The fish were fed twice a day (9 a.m. and 3 p.m.) at a satiation level with a 25% protein diet (Charoen Pokphand Foods Public Co., LTD, Samut Sakhon, Thailand) for one week at the Faculty of Interdisciplinary Studies, Khon Kaen University Nong Khai Campus.

2.2 Experimental design

The study used a Completely Randomized Design (CRD) with four replications. Three commercially available floating pellet diets fed the fish: a 15.5% protein diet (herbivorous fish feeds, T1), a 25% protein diet (large catfish feed, T2 control) [4], and a 30% protein diet (small catfish feed, T3), with pellet sizes of approximately 5, 5, and 3 mm, respectively. The male and female breeders from each protein level were randomly weighed and placed in concrete ponds 1.8 x 1.8 square meters in size filled with water at a depth of 0.55 meters at a sex ratio of 1:2 (male:female) or 15 fish/pond with a mean weight of 107.51 ± 2.25 g and 92.79 ± 2.12 g of male and female fish, respectively. They were fed saturated diets (1-2% of their body weight) twice daily (9 a.m. and 3 p.m.) for 20 weeks. Also, the water was changed to 100% of its total volume every two weeks. Throughout the experiment, there were no substitutions of breeders, and their mouths were tapped every two weeks using Sousa's method. [10]

2.3 Data collection

Water quality was measured weekly, including water temperature (T) and dissolved oxygen concentration (DO), by using YSI (model 52, Yellow Spring Instrument Co., Yellow Springs, OH, USA). The pH of the water was measured with a pH meter (Digital Mini-pH Meter, 0-14PH, IQ Scientific, Chemo-science (Thailand) Co., Ltd, Thailand), and total ammonia in nitrogen form (NH_3-N) was determined by using the Phenate-hypochlorite method [11]. Biomarkers were analyzed every two weeks, including total bacteria and coliforms of *Escherichia coli* and *Streptococcus* sp., using colony count techniques. [12]

Fish growth was measured by weighing the fish on a 2 decimal scale, and the total length was measured at the end of the experiment with a vernier (no feeding for one day before weighing). Fish weight gain, remaining fish, and the weight of feed eaten by the fish were all recorded to calculate weight gain, specific growth rate, condition factor (K) = (100 x bodyweight) ÷ (total length)^3, feed conversion rate, and feed efficiency. Eggs were collected every two weeks and separated by egg stage, according to [13] before being calculated: spawning rate = 100 x (number of tapped mouth female breeder ÷ total female breeder released),

fecundity = number of eggs ÷ female breeder weight (g), egg output = (number of eggs ÷ area (sq.m.)) ÷ day, female productivity = (number of eggs ÷ total weight of initial female breeder (kg)) ÷ day and egg production according to Surajit method [14]. The costs and benefits of the products were determined according to Shaha's method [15].

2.4 Data analysis

Observed data were analyzed for variance (ANOVA) according to the CRD experimental scheme. The mean difference ± standard error (SE) was compared using Duncan's Multiple Range Test at 95% confidence levels by the SPSS package.

3. Results and Discussion

3.1. Results

The results of mouth-tapping egg development in female breeders revealed that egg development of fish fed 15.5% protein had the highest cleavage and segmentation stages at 6.77 percent, followed by zygote stage (2.26%) and pharyngula, hatching, and only 1.50% of late larva stage. Still, no egg development was found in the gastrula and early larva stages. Egg development in fish fed 25% protein was discovered at various stages, in descending order: Late larva (10.53%) > segmentation (9.02%) > hatching (8.27%) > cleavage stage (7.51%) > zygote stage (5.26%) > early larva stage (4.51%) > pharyngula stage (3.01%), but no eggs were developed during the gastrula stage. Egg development was observed in descending order in fish fed 30% protein: As shown in Figure 1 and Table 1, cleavage (8.27%) > segmentation (6.77%) > zygote, pharyngula, and late larva (3.76%) > early larva (3.01%) > hatching (1.50%) > gastrula (0.75%).

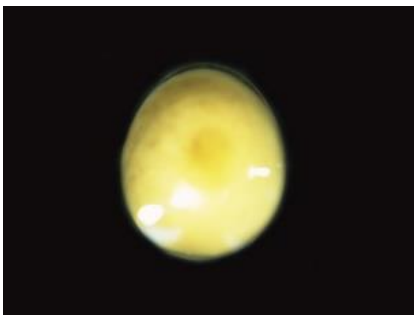

a. Zygote period

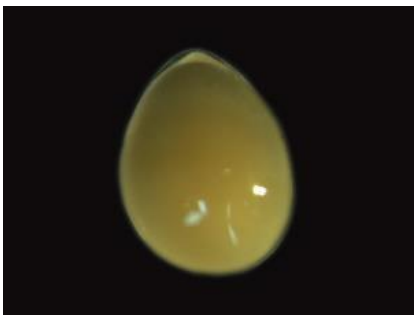

b. Cleavage period

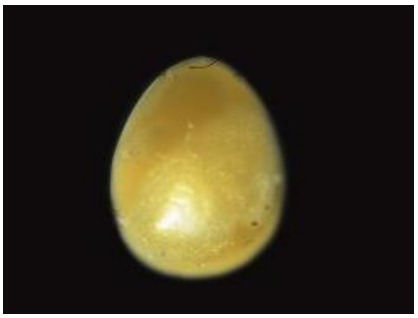

c. Gastrula period

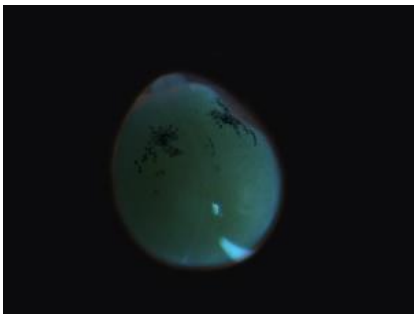

d. Segmentation period

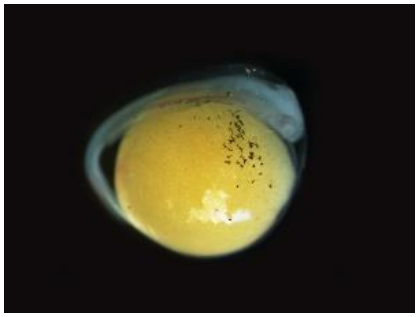

e. Pharyngula period

f. Hatching period

g. Early larva period

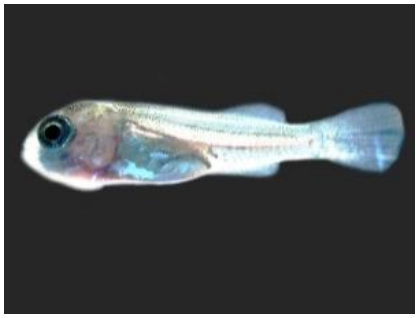

h. Late larva period

Figure 1. The developmental egg stages observed on Nile tilapia

Table 1. Percentages in developmental stages of Nile tilapia eggs as influenced by various percentages of feed protein diets (n=120)

Periods	Diet (% protein)		
	15.5	**25.0**	**30.0**
Zygote	2.26	5.26	3.76
Cleavage	6.77	7.51	8.27
Gastrula	None	None	0.75
Segmentation	6.77	9.02	6.77
Pharyngula	1.50	3.01	3.76
Hatching	1.50	8.27	1.50
Early larva	N/A	4.51	3.01
Late larva	1.50	10.53	3.76

The spawn rate per cycle of the female breeder ranged from 1.29 to 1.67% when the fish were fed 30, 25, and 15.5% protein, respectively, which was not statistically different (Table 2). The female breeder fed 30 percent protein had the highest fecundity at 5.20 eggs/g, which was significantly different. The total egg production, egg output, and female productivity of tilapia were 820.59 eggs, 1.81 eggs/m²/day, and 4.14 eggs/kg total initial female/day, respectively when fed 30% protein. The results were not significantly different from those fed 25% protein ($p < 0.05$).

Table 2. Mean values of spawning rate, fecundity, egg production, egg output, and female productivity of Nile tilapia, measured at two weeks intervals (n=120)

Diet (% protein)	Spawning rate (%)	Fecundity (eggs/g female spawned)	Egg production (eggs)	Egg output (eggs/m²/day)	Female productivity (eggs/kg total initial female/day)
15.5	1.67 ± 0.30	2.03 ± 0.23^{c}	411.92 ± 111.60^{b}	0.91 ± 0.25^{b}	2.06 ± 0.50^{b}
25.0	1.60 ± 0.13	3.89 ± 0.25^{b}	815.17 ± 90.68^{a}	1.80 ± 0.20^{a}	4.07 ± 0.46^{a}
30.0	1.29 ± 0.11	5.20 ± 0.33^{a}	820.59 ± 92.92^{a}	1.81 ± 0.20^{a}	4.14 ± 0.49^{a}
F-test	ns	**	*	*	*
C.V. (%)	5.87	3.84	6.43	6.13	7.69

Letter (s) in each column indicated statistically significant presented as standard errors of means (ns=p > 0.05; *=p < 0.05; **=p < 0.01). C.V. = coefficient of variation.

Tilapia breeders fed different diets for 20 weeks revealed that the water temperature ranged from 27.22 to 27.66 °C, which was not statistically different (Table 3). The dissolved oxygen concentration, pH, and total bacterial count ranged from 5.20 to 5.29 mg/L, 8.01 to 8.04, and 201.33 to 214.80 CFU/mL, respectively, which were not statistically different. However, the highest amount of ammonia was 0.104 mg/L, and the lowest was 0.044 mg/L when the fish were fed 30 and 15.5% protein, respectively, which differed significantly. *Escherichia coli* and *Streptococcus* sp. were not found in water throughout the culture.

Table 3. Mean water temperature values, dissolved oxygen, pH, and the total amount of ammonia. These were measured at week intervals, while total bacteria and coliforms of *Escherichia coli and Streptococcus* sp. were measured at two weeks interval

	Diet (% protein)			F-test	C.V. (%)
	15.5	**25.0**	**30.0**		
Water temperature (°C)	27.66 ± 0.18	27.35 ± 0.14	27.22 ± 0.10	ns	4.11
Dissolved oxygen (mg/L)	5.29 ± 0.05	5.23 ± 0.07	5.20 ± 0.02	ns	9.45
pH	8.01 ± 0.02	8.04 ± 0.01	8.04 ± 0.01	ns	1.50
Total ammonia (mg/L)	0.044 ± 0.002^{c}	0.088 ± 0.002^{b}	0.104 ± 0.003^{a}	**	5.62
Total bacteria (CFU/mL)	201.33 ± 44.82	207.73 ± 33.12	214.80 ± 29.68	ns	5.93
Coliforms (cfu/mL)					
Escherichia coli	None	None	None	-	-
Streptococcus sp.	None	None	None	-	-

Letter(s) in each row indicated statistically significant effect due to treatments presented as standard errors of means (ns=p > 0.05; **=p < 0.01). C.V. = coefficient of variation.

The initial mean weight of fish was in the range of 95.26-100.92 g, which was not statistically different. At the end of the experiment, tilapia breeders had a 100% survival rate across all treatments, with the highest mean values of final weight, weight gain, specific growth rate, and condition factor (*K*) of 256.93 g, 161.68 g, 0.71%/day, and 2.20, respectively, when fish were fed 30% protein. When the data were statistically analyzed, it was discovered that the mean final weight, mean weight gain, specific growth rate, and condition factor (*K*) were all significantly different (Table 4).

Table 4. Mean values of final weight, weight gain, specific growth rate, and condition factor *(K)* of Nile tilapia as influenced by various percentages of protein diets (n=120)

Diet (% protein)	Mean initial weight (g)	Mean final weight (g)	Weight gain (g)	Specific growth rate (%/day)	Condition factor (K)
15.5	100.92 ± 6.42	213.86 ± 8.43^{b}	112.94 ± 4.07^{c}	0.54 ± 0.03^{c}	1.89 ± 0.01^{b}
25.0	96.90 ± 3.95	233.98 ± 2.98^{b}	137.08 ± 1.92^{b}	0.63 ± 0.02^{b}	1.97 ± 0.01^{b}
30.0	95.26 ± 5.35	256.93 ± 6.70^{a}	161.68 ± 2.51^{a}	0.71 ± 0.02^{a}	2.20 ± 0.09^{a}
F-test	ns	**	**	**	**
C.V. *(%)*	2.94	5.49	4.34	7.46	5.02

Letter *(s)* in each column indicated statistically significant presented as standard errors of means *(*ns=$p > 0.05$; **=$p < 0.01$*)*. C.V. = coefficient of variation.

Mean values of total feed intake and feed intake rates were the lowest at 4,482.66 g and 2.13 g/fish/day, respectively, when fed 30% protein. According to the statistical analysis, the mean values of total feed and feed intake rates differed significantly (Table 5). The lowest feed conversion ratio was 1.85, while the highest feed efficiency was 54.11% when fed 30 % protein, which was statistically significantly different.

Table 5. Mean values of total feed intake, rates of feed intake, feed conversion ratio, and feed efficiency of Nile tilapia fed with various levels of protein diets (n=120)

Diet (% protein)	Total feed intake (g)	Rates of feed intake (g/fish/day)	Feed conversion ratio	Feed efficiency
15.5	4,739.99 ± 46.49^{a}	2.26 ± 0.02^{a}	2.81 ± 0.09^{a}	35.73 ± 1.14^{c}
25.0	4,814.28 ± 62.40^{a}	2.29 ± 0.03^{a}	2.34 ± 0.05^{b}	42.74 ± 1.01^{b}
30.0	4,482.66 ± 81.07^{b}	2.13 ± 0.04^{b}	1.85 ± 0.02^{c}	54.11 ± 0.50^{a}
F-test	*	*	**	**
C.V. *(%)*	2.77	2.78	5.14	4.18

Letter *(s)* in each column indicated statistically significant presented as standard errors of means *(*=$p < 0.05$; **=$p < 0.01$*)*. C.V. = coefficient of variation.

The production costs per fish from 4 replication treatments were 185.44, 221.94, and 227.12 baht when fed 15.5, 25, and 30% protein, respectively, which were significantly different (Table 6). When the fish were fed 25 and 15.5% protein, the highest benefit was 43.83 baht, and the lowest use was 12.51 baht, which was significantly different. The benefit-to-cost ratios were 0.07, 0.20, and 0.13 when the fish were fed 15.5, 25, and 30% protein, respectively, and the opportunity cost at 1.35 percent interest was the highest at 1.48 and the lowest at 1.17 when the fish were fed 30 and 15.5 percent protein.

Table 6. Cost, benefit, benefit: cost ratio and the opportunity cost of Nile tilapia as affected by various levels of protein diets (n=120)

Diet (% protein)	Cost (Bath)	Benefit (Bath)[1/]	Benefit: Cost	Opportunity cost [2/]
15.5	185.44[c]	12.51[c]	0.07	1.17
25.0	221.94[b]	43.83[a]	0.20	1.41
30.0	227.12[a]	30.60[b]	0.13	1.48
F-test	**	**	-	-
C.V. (%)	10.40	7.40	-	-

Letter(s) in each column indicated the least significant differences in probability (**=$p < 0.01$). C.V. = coefficient of variation.

[1/] Sale price of seed Nile tilapia = 0.05 Bath

[2/] The deposit rate reading was 1.35% (Bank for Agriculture and Agricultural Cooperatives, 2019)

3.2. Discussion

Egg production, egg output, and female productivity were lower than those reported by [14] when bred tilapia with an average weight of 150 g in a 1:1 or 6 fish/pond ratio for 8 weeks. They noted that the average egg production, output, and female productivity were 29,621.1 eggs, 22.73 eggs/m^2/day, and 51.67 eggs/kg of female breeders/day, respectively. Furthermore, [16] reported that tilapia raised in concrete ponds had egg production and female productivity in the range of 19-77 eggs/m^2/day and 72-312 eggs/kg of female breeders/day, respectively. This is likely due to female breeders did not spawn at the same time. This fish can spawn throughout the year, and the spawning cycle lasts about 28-30 days [17]. The egg development was mainly obtained from the female breeder's mouth, with 22.56% and 22.55% of the egg developmental stages in the segmentation and cleavage stages, respectively. This is consistent with previously reported [14] that most eggs found in a female breeder's mouth are in the eyed egg stage and head-tail egg stage. Both are segmentation stages, according to [13].

Tilapia fed with a higher protein diet had a statistically significant increment in the mean fish weight gain and specific growth rate. This result is consistent with a study by [8] on tilapia (*O. niloticus*) by feeding a 25-45 percent protein diet; this could be due to the fish's ability to utilize proteins for adequate growth. On the other hand, the feed conversion rate tends to decrease as the protein level in the diet increases, which is consistent with a study published by [8] in which the feed conversion rate decreased from 2.5 to 1.6 when tilapia were fed an increased protein diet of 25% to 45%, respectively.

The water in the pond had a pH of 8.01-8.04 and a dissolved oxygen concentration of 5.20-5.29 mg/L, both suitable for tilapia culture. The ammonia concentration in the water in the closed system is primarily caused by fish excretion and overfeeding in the pond. The study discovered that when the fish were fed protein diets ranging from 15.5 to 30%, ammonia concentrations tended to increase (T1 to T3). The protein content of the feed caused this increment in ammonia concentration; when the feed had high protein, the fish excreted high ammonia levels. The results are consistent with studies of [18] in rainbow trout (*Oncorhynchus mykiss*) and [19] in grass carp (*Ctenopharyngodon idella*). The ammonia concentrations found in this study are in the range of 0.044-0.104 mg/L, which is a suitable level, that tilapia can survive harmlessly [20]. However, when fed 25 and 30% protein (T2 and T3), the ammonia concentrations were 0.088 and 0.104 mg/L, respectively, which may result in tilapia fertilization, hatching, and embryo toxicities. [21] discovered that increasing the ammonia concentration in water (0.05-0.6 mg/L) would decrease the number of fertilized eggs and hatching rates while increasing the number of deformed eggs.

4. Conclusions

The effects of dietary protein levels on tilapia development and the productive performance of tilapia fry in concrete ponds for 20 weeks were investigated in this study. Dietary protein levels influenced egg development in female breeders' mouths, with 25 percent protein providing enough nutrition for breeders to

hatch eggs and produce hatchlings. Furthermore, it has the lowest production cost, feeding 30 and 15.5% protein in second and third place, respectively.

5. Acknowledgements

This research was completed due to a research grant from the Faculty of Interdisciplinary Studies, Khon Kaen University Nong Khai Campus.

Author Contributions: Nisarat Tippayadara and Baramee Phungpis participated in data analysis and drafted manuscript. Kanokkan Worawut conceived the study, designed the study, coordinated the study, carried out data analysis, interpreted the results and aided in drafting the manuscript. All authors gave final approval for publication.

Funding:

Conflicts of Interest: The authors declare that there is no conflict of interest regarding the publication of this article.

References

[1] FAO. *The State of World Fisheries and Aquaculture*, Rome, Italy, 2014, 223.

[2] Tveteras, R.; Nystoyl, R. *Fish Production Estimates & Trends 2011-2012*, Global Outlook for Aquaculture Leadership (GOAL). Santiago. 2011, 57.

[3] Department of Fisheries. *Fisheries Statistics of Thailand 2017, No. 9/2019, Fisheries Development Policy and Strategy Division*, Department of Fisheries, Ministry of Agriculture and Cooperatives, Bangkok, 2019, 92.

[4] Bhujel, R.C.; Yakupitiyage A.; Turner W.A.; Little D.C. Selection of a commercial feed for Nile tilapia (*Oreochromis niloticus*) broodfish breeding in a hapa-in-pond system. *Aquaculture*. 2001, *194*(3), 303-314.

[5] Svobodová, Z.; Lloyd, R.; Máchová, J.; Vykusová, B. *Water quality and fish health*. EIFAC Technical Paper. No. 54. Rome, FAO. 1993, 59.

[6] Chitmanat, C.; Makaw, S. Effects of protein levels and feed pellet types on the growth and production of red tilapia cage culture in Huai Pae reservoir, Tombon Naprang, Amphoe Pong, Phayao province. *Proceedings of 48th Kasetsart University Annual Conference: Fisheries:* 2010, 271-278. (in Thai)

[7] Bhujel, R.C. On-farm feed management practices for Nile tilapia (*Oreochromis niloticus*) in Thailand. In; M.R. Hasan and M.B. New, eds. On-farm feeding and feed management in aquaculture. FAO Fisheries and Aquaculture Technical Paper No. 583. Rome, 2013, 159-189.

[8] Al Hafedh, Y. S. Effects of dietary protein on growth and body composition of Nile tilapia, *Oreochromis niloticus* L. *Aquaculture Research*. 1999, *30*(5), 385-393.

[9] Popma, T.; M. Masser. *Tilapia: Life History and Biology*. SRAC Publication No. 283. Southern Regional Aquaculture Center, Stoneville, MS. 1999.

[10] Sousa, S.M.D.N., Freccia, A.; Santos, L.D.D.; Meurer, F.; Tessaro, L.; Bombardelli, R.A. Growth of Nile tilapia post-larvae from broodstock fed diet with different levels of digestible protein and digestible energy. *Revista Brasileira de Zootecnia*. 2013, *42*(8), 535-540.

[11] APHA. *Standard Methods for the Examination of Water and Wastewater*. American Public Health Association. Washington, DC. 1989; 1, 268.

[12] APHA. *Compendium of methods for the microbiological examination of foods*, 4th ed. American Public Health Association. Washington, D.C. 2001, 676.

[13] Fujimura, K.; Okada N. Development of the embryo, larva and early juvenile of Nile tilapia *Oreochromis niloticus* (Pisces: Cichlidae). *Developmental staging system. Development, growth and differentiation*. 2007, *49*(4), 301-324.

[14] Surajit, T.; Yoonpundh, R.; Srisapoome, P.; Satienjitr, S.; Thaitungchin, C. Comparition study on breeding systems of nile tilapia (*Oreochromis niloticus*) fry production in earthponds, tanks and hapas suspended in an earthen pond. *Proceedings of 47th Kasetsart University Annual Conference: Fisheries*. *17-20 March 2009. Bangkok*. 2009, 434-443.

[15] Shaha, D.C.; Kundu S.R.; Hasan M.N. Production of organic grass carp (*Ctenopharyngodon idella*) and GIFT tilapia (*Oreochromis niloticus*) using napier grass, Pennisetum purpureum. *Journal of Fisheries*. 2015, *3*(1), 233-238.

[16] Tsadik, G. G.; Bart A. N. Effects of feeding, stocking density and water-flow rate on fecundity, spawning frequency and egg quality of Nile tilapia, *Oreochromis niloticus (L.). Aquaculture*. 2007, *272*(1), 380-388.

[17] Srisakultiew, P. *Studies on the reproductive biology of Oreochromis niloticus* (*L.*). Ph.D. thesis, Stirling: University of Stirling. Scotland. 1993, 310.

[18] Cheng, Z.J.; Hardy R.W.; Usry J.L. Plant protein ingredients with lysine supplementation reduce dietary protein level in rainbow trout (*Oncorhynchus mykiss*) diets, and reduce ammonia nitrogen and soluble phosphorus excretion. *Aquaculture*. 2003, *218*(1), 553-565.

[19] Gan,L.; Liu Y.J.; Tian L.X.; Yang H.J.; Yue Y.R.; Chen Y.J.; Liang J.J.; Liang G.Y. Effect of dietary protein reduction with lysine and methionnine supplementation on growth performance, body composition and total ammonia nitrogen excretion of juvenile grass carp, *Ctenopharyngodon idella*. *Aquaculture Nutrition*. 2012, *18*(6), 589-598.

[20] Evans, J.J.; Pasnik D.J.; Brill G.C.; Klesius P.H. Un-ionized ammonia exposure in Nile tilapia: toxicity, stress response, and susceptibility to *Streptococcus agalactiae*. *North American Journal of Aquaculture*. 2006, *68*(1), 23-33.

[21] El-Greisy, Z.A.E.B.; Elgamal A.E.E.; Ahmed N.A.M. Effect of prolonged ammonia toxicity on fertilized eggs, hatchability and size of newly hatched larvae of Nile tilapia, *Oreochromis niloticus*. *The Egyptian Journal of Aquatic Research*. 2016, *42*(2), 215-222.

JSTR
ASEAN Journal of Scientific and Technological Reports

Research article

Formulation of Borneol Camphor Solution from Essential Oil of *Amomum biflorum* Jack: a literature review

Teeradej Thewtanom[1], Katekeaw Sarunyakasitarin[2], Suni Prajitr[3] and Karunrat Tewthanom[4*]

[1] Faculty of Management Sciences, Nakhon Pathom Rajabhat University, Nakhon Pathom, 73000, Thailand; kikquman@gmail.com
[2] Faculty of Pharmacy, Silpakorn University, Nakhon Pathom, 73000, Thailand; SARUNYAKASITRIN_K@su.ac.th
[3] Faculty of Business Administration, Thonburi University, Bangkok, 10170, Thailand; Suni.burin@gmail.com
[4] Faculty of Pharmacy, Silpakorn University, Nakhon Pathom, 73000, Thailand; tewthanom_k@su.ac.th
* Correspondence: tewthanom_k@su.ac.th

Abstract: Wan Sao Long is a plant in the Zingiberaceae family, scientific name: *Amomum biflorum* Jack has heart-nourishing properties, an anti-flatulent, aromatic essential oil. Therefore, it is applied as a component of water pimple products in various forms such as spray, air conditioning gels or solution. In principle, the preparation of water pimples relies on the Eutectic phenomenon: the main elements of the recipe consist of volatile oil, borneol, camphor, menthol, and fatty acid. Preparing is to mix the substances that will produce eutectic, borneol, camphor, and Menthol, and then mix in the part of the oil, such as fatty acids. Stir well-using heat, leaving to cool, so add the volatile oil and Wan Soa Long extracted oil. Among the considerations for the recipe is the proportion of substances that will be mixed to achieve the Eutectic phenomenon, the amount of Wan Sao Long extracted oil, and the proper heat to make the soluble parts and fatty acids compatible.

Keywords: Wan Sao Long; Borneol camphor solution; Eutectic; *Amomum biflorum*

Citation:
Thewtanom, T.; , Sarunyakasitarin K.; Prajitr, S.; Tewthanom, K. The Principle of Formulation of Borneol Camphor Solution from Essential Oil of *Amomum biflorum* Jack. *ASEAN J. Sci. Tech. Report.* **2022**, *25*(3), 18-24. https://doi.org/10.55164/ajstr.v25i3.247035.

Article history:
Received: July 7, 2022
Revised: September 21, 2022
Accepted: September 24, 2022
Available online: September 28, 2022

1. Introduction

The Borneol camphor solution is currently one of the most favorite products during the COVID-19 epidemic era. Since the inhale preparations are useful for the respiratory system. Many products of Borneol camphor solution have been launched, such as inhale solutions, sprays, and aroma stickers. The market investigation of these products seems to have a great possibility channel for receiving the benefit and increasing income. This article reviewed the possibility and principle of formulation of Borneol camphor solution from Wan Sao Long or Amomum biflorum Jack, a useful herb in Thailand. This review article was divided into four parts. The first part mentions the characteristic of this herb to make the reader familiar with it. The second part was about the principle of formulation of Borneol camphor solution from Wan Sao Long and the eutectic principle, which is important knowledge to apply for preparation. The third part explains **th**e step of preparation. After the understanding of

preparation, the last part before a conclusion reveals the key points that should be considered during the preparation step to make a qualified and stabilized product, ending up with the conclusion of all main 3 parts concept. This reviewed article provided the information for decision-making in establishing the Borneol camphor solution business.

2. Materials and Methods

The information on *Amomum biflorum* Jack and the principle of formulation of borneol camphor solution reviewed from the literature in the following steps

2.1 Keywords: this article use these keywords; *Amomum biflorum*, Borneol camphor, Eutectic, Wan Sao Long

2.2 The secondary sources: this article use google scholar and PubMed as secondary source for searching and gathering paper materials. The inclusion criteria of the paper were the English language. The relavance of the preparation of borneol camphor soution.

2.3 Retrieved the papers evaluated and summarized in the results and discussion part.

The process of the literature review is illustrated in Figure 1

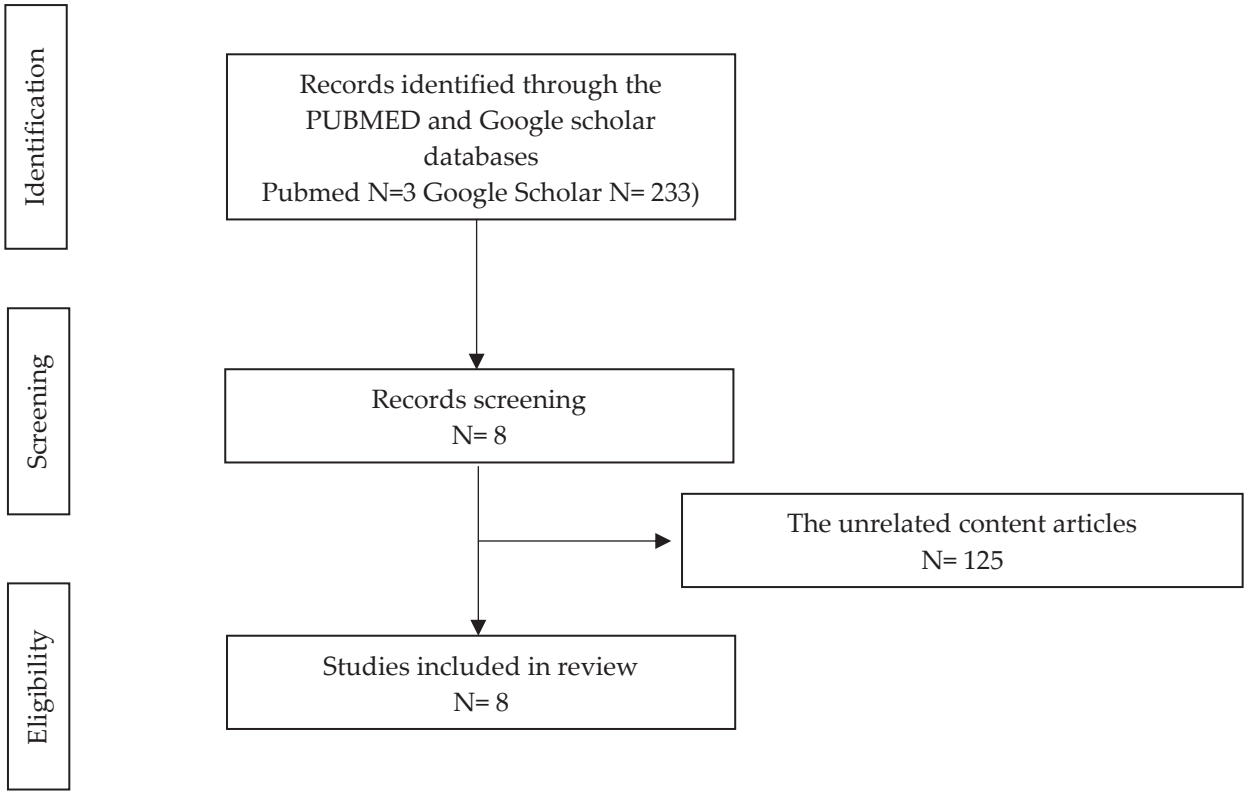

Figure 1. The literature review process

3. Results and Discussion

From the literature, we also reviewed and discussed papers on the following topic

3.1. What is Wan Sao Long?

3.1.1 Characteristics

Wan Sao Long is herbal in the *Zingiberaceae* family; the scientific name for this plant is ***Amomum biflorum Jack***. It's a fallen plant. There are rhizomes underground, above the soil 30-80 cm high, with parallel-edged leaves. Red leaves, soft hairy leaf plates covering small inflorescences. The plant is born at the rhizome,

away from the base of the artificial stem. Rhizomes, petals and white petals form a small number of flowers. The petals have a yellow stripe in the middle and white pollen. A beak extending to the top is three-pointed, round, yellowish-green.. Red thorns cover. [1-2] The picture of this plant illustrates in Figure 2

There was a study about the morphology of plants in the Amomum family, the researcher collected indigenous species of Amomum from various areas in Thailand. The scanning electron microscope (SEM) picture was used to study morphology. The study found that the reproductive part morphology applied to the identity of *Amomum biflorum* Jack from the other species. Amomum's pollen grains are spherical to subspherical, inaperturate, and the exine sculpture is either echinate or psilate. Pollen characteristics agree with the previous reports but do not correspond with the classification earlier based on morphological traits. Therefore, the pollen morphology is less useful for the subgeneric classification of Amomum [3].

3.1.2 Usages

This plant has fragrant rhizomes. It is a component of compresses and medicines for steaming herbs to nourish the heart. In addition, applying essential oils is believed to make lovers masturbate, [1-2] including relaxation [4].

3.1.3 Component

The main component of Wan Sao Long are the following [1]

(E)- but-1-enyl-4-methoxybenzene 85%

Limonene 2.2%

β- pinene 2.1%

Camphor 1.8%

Figure 2. *Amomum biflorum* Jack (Wan Sao Long)

The method of extraction of essential oil [5]

According to the literature review [5], the method of extraction of Wan Sao Long is described as the following;

The essential oils were extracted by water distillation; the distillation conditions were water steaming for 6 hours. The steaming temperature was 100 °C, and the cooling downed to 10 °C to collect the essential oils.

From this analysis review that this product contained the following volatile oil

Benzene, 1-(1-butenyl)-4-methoxy-, trans- = 92.63%

Eucalyptol = 2.13%

Bicyclo[3.1.1]heptane, 6,6-dimethyl-2-methylene-, (1S) = 1.82%

D-Limonene = 1.75%

Camphor = 1.66%

The literature review found that there has been the development of various products from Wan Sao Long essential oil in cosmaceutical, spa, [6] including inhaler products [7] which found that the customers were satisfied with the smell of 5% essential oil from Wan Sao Long. In addition, the essential oil from that plant can apply to air freshener gel [8-9].

Based on this information, Wan Sao Long is herbal and a practical challenge to develop to increase value and be a source of income for future growers.

3.2 The principle of formulation of Borneol camphor solution from Wan Sao Long

3.2.1 Core principle

Borneol camphor solution recipes use a pharmaceutical technology principle called Eutectic, in which the direction of Eutectic compound formation, by definition, belongs to two combinations that usually do not react with each other as new compounds. But if mixed in runaway proportions, there is a process of inhibiting the crystalline formation of another substance, giving the system a lower melting point than the original substance. [10, 11] Such a process can be summarized as a diagram to make it easier to understand as follows: (Figure 3)

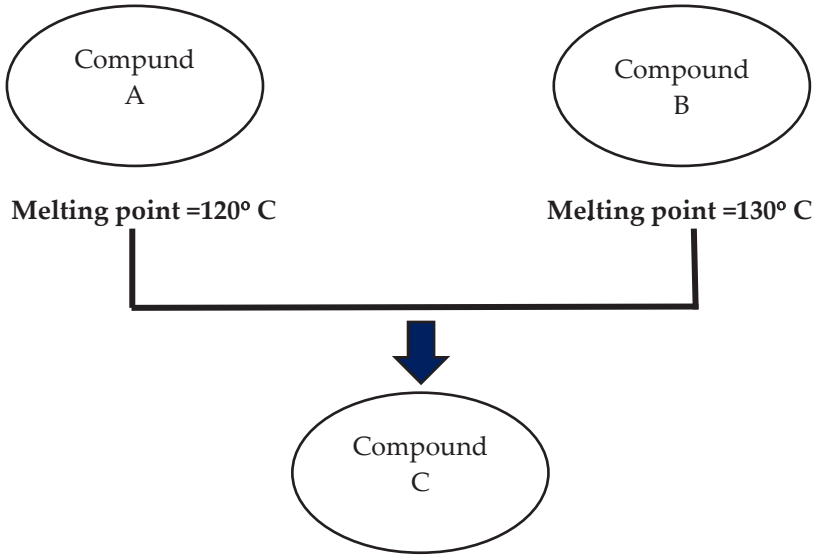

Figure 3. The Eutectic process

As a result of this principle, combined with the properties of substances that can cause eutectic reactions, liquid products are obtained from solid substances. The eutactic system, for example, is used in the pharmaceutical industry to improve drug solubility, permeability, and absorption. Based on this theory, a deep eutectic solvent was used to create a preparation from a eutactic system [10]. Examples of widely used substances with such properties include borneol, camphor, and mint, which have led to the development of a product known as "water pimpsen," which is commonly used to relieve dizziness and nasal congestion due to the presence of volatile aromatic substances in the terpenes group that, when inhaled, feel fresh and reduce nasal congestion, which in the latter, especially during the COVID-19 pandemic, is a product that has grown in popularity.

Borneol camphor solution product models that can be developed include various types. Solutions, sprays, and even stickers can be attached to clothing and face masks to reduce odors. This is because studying the principles for developing such a product is fascinating.

3.2.2 The core component of Borneol camphor solution

The core component of Borneol camphor solution is

1. Essential oils: It is the part that will cause the aroma. This recipe comes from Wan Sao Long
2. Borneol: The component in the eutectic phenomenon
3. Camphor: The component in the eutectic phenomenon
4. Menthol: The component in the eutectic phenomenon
5. Fatty acid

Borneol, camphor, and menthol, When mixed, Eutectic processes form a liquid compound at room temperature. Due to the lower melting point than the substrate. Therefore, we can use this principle to prepare it as a Borneol camphor solution product.

3.2.3 The step of preparation

The preparation process is illustrated in Figure 4.

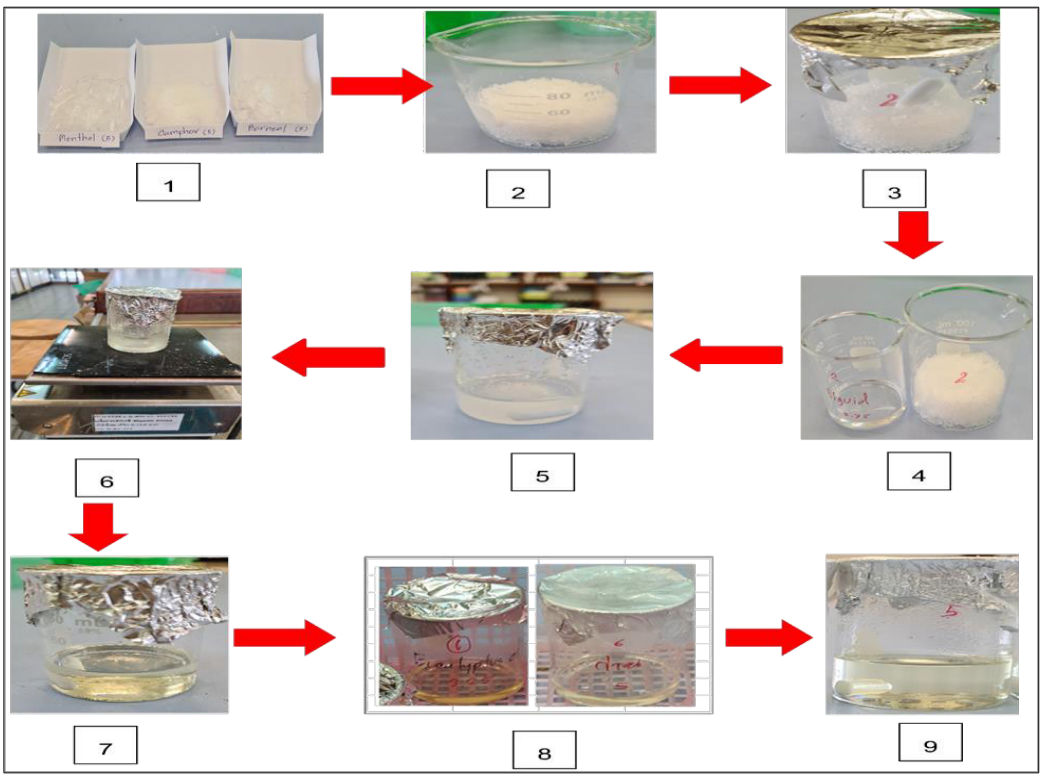

Figure 4. The process of Borneol camphor solution preparation

Step one: Mix the three compounds, camphor, borneol, and menthol, and the mixing proportions must be adjusted to make it appropriate to create a eutectic process and obtain a liquid state in the final, where the ratios used are as varied as 1:1:1, 2:1:1, 3:2:1 [6].

Step two: If there is a part of a fat-soluble substance (fatty acid) such as Liquid Paraffin, add it and stir well, it may be possible to use heat to dissolve fatty acids or oil-soluble substances early.

Step three: Leave the solution to cool and add essential oils, including essential oil from Wan Sao Long.

Step four: Stir well. They were packed in tight containers.

3.2.4 The key consideration

The are some points for consideration as the following

1. When mixing the three substances, Camphor, Borneol, and Menthol, it is important to consider about phase diagram of each substance; the example of the phase diagram is shown in Figure 5 [10].

The experiment's phase diagram must be derived to determine an optimum condition capable of producing stable eutectic systems.

As previously stated, the intended purpose is the proportion of the three substances that will remain liquid in the final state. An appropriate ratio will result in a stable and favorable end product.

2. The amount of wandering oil, as well as the appropriate essential oil, because too much may be incompatible. It appears as a floating oil droplet, affecting the product's livability and stability.

3. Heating during the fatty acid addition process If the amount of heat used is insufficient, fatty acids will clump. Liquids are incompatible. This renders the product useless.

4. Another critical point to consider before launching a product is testing finished product properties such as rheology, viscosity, surface tension, contact angle measurement, and infrared spectroscopy.

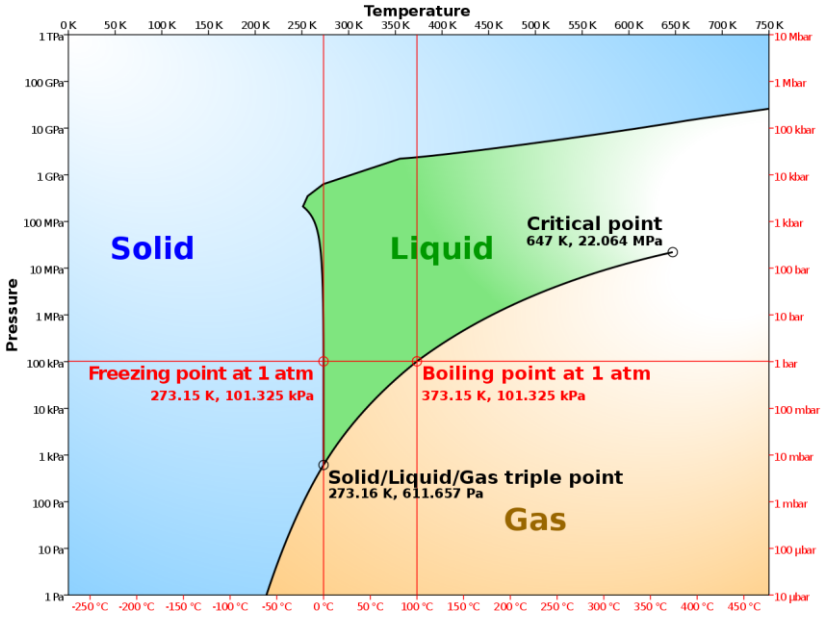

Figure 5. The phase diagram

Therefore, the quality assurance of the finished product should be considered. However, there is no standard specification of the quantity of essential oil in *Amomum biflorum* Jack established because of the variation (depending on the area and the agricultural method). Therefore the certificate of analysis is also reported as the physical and some chemical characteristics such as appearance, color, and specific gravity. The quantity of the active ingredient is not specified. No changes in appearance and smell may detect the stability of the product. If some laboratory can be developed to quantify the essential oil, it may be implemented to check the changes in the essential oil composition to confirm the stability. The analysis and identification of volatile oil can be used by gas chromatography (GC) or Differential Scanning Calorimetry (DSC). [7-9] However, the instruments were expensive. Moreover, before launching the product or producing a large scale, the satisfaction of the product should be confirmed.

4. Conclusions

To prepare borneol camphor solution products from Wan Sao Long. Despite the few steps and minimal equipment, knowing the principles of Eutectic and considerations will make the preparation of the product even more accurate and make the product more pleasant to use.

5. Acknowledgements

The author would like to send a great acknowledgment to all members of the overall project, especially CPS pharma, that gave a helpful idea and support of information. Pichayapa Yendee, Bunnada Kaewdee, the

undergraduate; Settthapong Senarat; Ph.D. student from the Faculty of Pharmacy Silpakorn University, participated in the project.

Author Contributions: Conceptualization, Teeradej Thewtanom. and Karunrat Tewthanom.; methodology, Karunrat Tewthanom, Teeradej Tewthanom, and Katekeaw Sarunyakasitarin.; resources; Karunrat Tewthanom, Teeradej Tewthanom, Katekeaw Sarunyakasitarin and Suni Prajitr.; data curation, Karunrat Tewthanom.; writing—original draft preparation, Karunrat Tetwhanom; writing—review and editing, Karunrat Tewthanom, Teeradej Tewthanom, Suni Prajitr .; project administration, Karunrat Tewthanom.; funding acquisition, Karunrat Tewthanom. All authors have read and agreed to the published version of the manuscript.

Funding: This research was funded by the Pre-talent project, Silpakorn University.

Conflicts of Interest: The authors declare no conflict of interest.

References

[1] Singtothong, C.; Gagnon, M.J.; Legault, J. Chemical composition and biological activity of the essential oil of Amomum biflorum. *Nat Prod Commun*. 2013, *8*(2), 265-7.

[2] Polsena, P., *Khoa Hin Son Botanic Gardens(Complete version)*. 2007, Bangkok, Thailand: Jetanaromphan Printing.

[3] Kaewsri, W; Paisooksantivatana, Y. Morphology and Palynology of Amomum Roxb.in Thailand. *Gardens' Bulletin Singapore. 59*, 2007(1&2), 105-112.

[4] Subhadhirasakul, S.; K, Moosigapong, K. Relaxation Effect on Volunteers of Essential Oil from Amomum biflorum Jack. *Thaksin University Journal*. 2014. 17, 7-25.

[5] Namphon P.; Santhawat, T.; Surachet, S.; Mongkol, M.; Ratchadawan, A. Essential oil distillation from Amomum biforum jack with 500 liter essential oil distillation machine. *35th MENETT National conference (MENETT 2021)*. 2021.

[6] Uthairung, A.; Rattarom, R.; Mekjaruskul, C. Cosmeceutical Applications of Essential Oils of Amomum biflorum Jack from Whole Plant and Rhizome. *Thai Journal of Science and Technology*. 2020. 9, 680-692.

[7] Srisuwan, T.; Keereekoch, T.; Watchasit, N.; Chomprang S; Subhaddhirasakul, S., Satisfaction Test of Borneo Camphor Liquid Inhaler from Essential Oil of Amomum biflorum Jack. *Thaksin University Journal*. 2019, *22*(2), 33-41.

[8] Keereekoch, T.; Srisuwanet, T.; Kaewpitak, P.; Dangnam, S.; Subhaddhirasakul, S . Formulation of Amomum biflorum Jack Air Freshener Gel. *Thaksin University Journal*. 2019, *22*(2), 15-21.

[9] Belarmino Dantas, M.G.; Bromfim Reis, S.A.G.; Dias Damasceno, C.M.; Araújo Rolim, L.; Rolim-Neto, P.J.; Oliveira Carvalho, F.; Quintans-Junior, L.J.; Silva Almeida, J.R.G.D. Development and Evaluation of Stability of a Gel Formulation Containing the Monoterpene Borneol. *The Scientific World Journal*. 2016, 1-4.

[10] Tuntarawongsa, S; Phaechamud, T. Menthol, Borneol, Camphor and WS-3 Eutectic Mixture. *Advanced Materials Research*. 2012, 506, 355-358.

[11] Wikipedia. *Phase diagram*. Available online: https://en.wikipedia.org/wiki/Phase_diagram. (accessed on 2 Sept 2022).

JSTR
ASEAN Journal of Scientific and Technological Reports

Research article

Improving Cluster-Based Index Structure for Approximate Nearest Neighbor Graph Search by Deep Learning-Based Hill-Climbing

Munlika Rattaphun[1], Amorntip Prayoonwong[2*], Chih-Yi Chiu[3], and Kritaphat Songsri-in[4]

[1] Faculty of Science and Technology, Nakhon Si Thammarat Rajabhat University, 80280, Thailand; munlika_rat@nstru.ac.th
[2] Faculty of Science and Technology, Suratthani Rajabhat University, 84100, Thailand; aprayoonwong@gmail.com
[3] Department of Computer Science and Information Engineering, National Chiayi University, Taiwan; cychiu@mail.ncyu.edu.tw
[4] Faculty of Science and Technology, Nakhon Si Thammarat Rajabhat University, 80280, Thailand; kritaphat_son@nstru.ac.th
* Correspondence: E-mail: aprayoonwong@gmail.com

Abstract: This study presents a novel approach to archive an excellent tradeoff between search accuracy and computation cost in approximate nearest neighbor search. Usually, the *k*-nearest neighbor (*k*NN) graph and hill-climbing algorithm are adopted to accelerate the search process. However, using random seeds in the original hill-climbing is inefficient as they initiate an unsuitable search with inappropriate sources. Instead, we propose a neural network model to generate high-quality seeds that can boost query assignment efficiency. We evaluated the experiment on the benchmarks of SIFT1M and GIST1M datasets and showed the proposed seed prediction model effectively improves the search performance.

Keywords: Inverted indexing; Nearest Neighbor Search; Nearest Neighbor Graph; Hill-climbing; Neural network;

Citation:
Rattaphun, M.; Prayoonwong, A.; Chiu, C.Y., Songsri-in, K. Title. *ASEAN J. Sci. Tech. Report.* **2022**, *25*(3), 25-33. https://doi.org/10.55164/ajstr.v25i3.247183.

Article history:
Received: August 3, 2022
Revised: September 20, 2022
Accepted: September 21, 2022
Available online: September 28, 2022

1. Introduction

The nearest neighbor (NN) search technique is widely applied in numerous fields, including computer vision, pattern recognition, signal processing, information retrieval, recommender systems, and so on [1-2]. Typically, the feature of each object of interest (such as an image) is represented in a high-dimensional space. A distance function is used to calculate distances between all data points and a given query. The NN is the data point with the smallest distance to the given query. When the number of data points and the number of data dimensions increase, an exhaustive search becomes impractical due to the expensive computation cost. To accomplish this task, numerous approximate nearest neighbor (ANN) [3-9] search methods are proposed to address the tradeoff between speed and accuracy.

The graph-based method is one of the most popular approaches to addressing the ANN search problem. The basic idea is that a neighbor of a neighbor is also likely to be a neighbor [5]. Most graph-based methods are based on constructing the *k*-nearest neighbor graph (*k*NN graph), built in the offline phase. A straightforward way to create the *k*NN graph is an exhaustive comparison

between each pair of vectors. Then, the top-*k* nearest neighbors for each reference vector are selected to be the connected node in the *k*NN graph. When the query is given, the search process is started by traversing the chart to find the NN candidates.

Two main challenges are considered to improve the graph-based index structure performance: (1) how to effectively generate the *k*NN graph and (2) how to traverse the *k*NN graph to find the NN candidates efficiently. The first challenge focuses on reducing the computation cost of constructing the *k*NN graph. It can be addressed using an approximate *k*NN graph [5] [10-11]. In this paper, we focus on the second challenge. One popular method is the hill-climbing algorithm [12-13] which utilizes the *k*NN graph for ANN search. It generates multiple random seeds to traverse the *k*NN graph and takes several iterations to refine the traverse result. However, random seeds are easily trapped in local optima and frequently visit unlikely NN candidates. To address the problem and speed up the process, Zhao et al. [12] proposed using inverted indexing in the residual vector space and applying cascaded pruning to avoid redundant candidates. Still, it may take a long time to converge. We thus propose an index method that employs the *k*NN graph to accelerate the search process. The contributions of the proposed method are emphasized as follows:

- We propose to modify the hill-climbing algorithm with a novel seed generation method. Instead of using random seeds in the original hill-climbing algorithm, we generate high-quality seeds based on a neural network.
- The proposed model learns the relation between query features and clusters in the *k*NN graph, which can estimate the cluster probabilities for a given query and provides a better way to select the initial seed without constructing an extra index table.
- We evaluated the experiment on the benchmarks of SIFT1M and GIST1M datasets and showed the proposed methods effectively improve the search performance.

The remainder of this paper is organized as follows. Section 2 presents a brief review of the NN search related to the *k*NN graph and hill-climbing algorithm. Section 3 offers the detail of the proposed method. We demonstrate some experimental results in section 4 and give the conclusion in Section 5.

2. Related Works

To improve index structure for better performance of ANN search, we are interested in the collaboration of the following three techniques: *k*-nearest neighbor graph (*k*NN graph), hill-climbing algorithm, and inverted file-based (or inverted index) method. The detail of each process are summarized as follows:

The *k*NN graph is a graph-based index structure widely used for ANN search. A graph structure is added to the index structure to make the search more efficient. To avoid exhaustive search and decrease the computation cost in ANN search tasks, the *k*NN graph construction process can be performed in the offline phase. The *k*NN graph is a directed graph defined for a set of *N* points in a metric space. The chart has a vertex for each data point, in which two vertices are connected by an edge whenever. The distance between those two vertices is among the k^{th} smallest distances. An exhaustive comparison between each pair of vectors is performed until the top *k* nearest neighbors are selected for each reference vector to generate a *k*NN graph. The computation complexity is about $O(DN)^2$, where *D* is the number of data dimensions and *N* is the number of data points [14]. Over the years, many researchers have applied and developed graph structures to increase the performance of ANN search in many forms. Zhang et al., 2013 [10] and Wang et al., 2012 [15] both constructed the *k*NN graph by randomly partitioning their samples into a small number of subsets with different technical details. [15] used the hierarchical random projections technique while [10] exploited the locality-sensitive hash functions. Combining the neighborhood graph with a bridge graph yields superior performance over large-scale datasets [16]. Two more popular graph-based index structure techniques are deployed to speed up searches: HNSW [8] and NSG [17]. HNSW is a hierarchical multi-level proximity graph that enables hopping with multi-scales on different graph layers. NSG intends to reduce the density of the graph edges while the search performance remains accurate.

The hill-climbing algorithm [12-13] is a mathematical optimization algorithm that often utilizes the *k*NN graphs for ANN search to find the best solution together with various possible solutions. The hill-climbing algorithm is a local search algorithm with the following working principles. First, it tries to find the best solution to the given problem by starting with a random seed (node or solution). It then evaluates the neighbor nodes. If the best of those neighbor nodes is better than the current node, it replaces the current

solution with this better solution. It subsequently continues to move in the direction of elevation or increasing values to find the peak of the local mountain or the best solution. The algorithm terminates when it reaches a peak value where no neighbor has a higher value. By starting to traverse the *k*NN graphs from a random seed and applying the abovementioned working principles, there is no guarantee that the best solution will always be found. It is easy for the algorithm to trap in a local maximum. Many researchers have proposed several approaches to address that problem in terms of speed and optimized values. For example, [12] used the combination of the inverted indexing in residual vector space and cascaded pruning to speed up the search by avoiding redundant candidates. [14] avoided using the random seed by incorporating new hash-based methods for seed generation: LSH [18] and ITQ [19]. These principles have been applied to generate higher quality seeds, which lead to increased accuracy and a lower computation cost.

The inverted file-based (or inverted index) method is another popular framework in multimedia retrieval. In text retrieval, an inverted index is used as a vocabulary of words, where each word has a list of the associated documents that contain this word. For image retrieval, the inverted index is used to store the codewords from the quantization process, and each codeword has a list of all vectors belonging to these codewords. The non-exhaustive search performs by checking only items in the codeword list. The inverted file-based method can be operated on the billion-scale dataset to avoid the exhaustive search and achieve good recall and speed in many works [20-22]. For instance, the inverted multi-index (IMI) [21] built a multi-dimensional index table, which is the Cartesian product of codebooks. IMI showed better accuracy without increasing the query time. The jointly inverted indexing [22] is a method that generates multiple quantizers and jointly optimizes all the codewords instead of computing the multiple quantizers independently. IVFADC [3] showed that the combination of inverted indexing with Product Quantization (PQ) [3-4] and Asymmetric Distance Computation (ADC) could handle billion-scale datasets efficiently.

In the past years, the learned index structure employed by machine learning techniques has been used in place of the existing index structure in many studies. For example, [23] proposed a combination of supervised classification and graph partitioning to build better-balanced graph partitioning. [9] presented the learned index structure by using the nearest neighbor probabilities model that employed neural networks to characterize the neighborhood relationships, which can rank and find candidate clusters of the given query effectively. A previous work [14] used the hashing approaches to generate a compact binary code to index the associated clusters in the inverted index table. When the query is given, the same hashing function is used to create binary code for each query. The query hash codes and hash code index in the inverted index are then mapped to retrieve the initial seeds for the hill-climbing algorithm. In this paper, the proposed method also brings up a higher quality seed generation method by utilizing the learned index structure. We present a novel method based on a neural network that predicts cluster probabilities. Then, top-*R* clusters are then selected as the initial seeds for hill-climbing.

3. Methods

The proposed method consists of two parts. Figure. 1 shows an overview of the proposed method. First, we construct a *k*NN graph using a clustering approach integrated with inverted indexing. Second, we offer a novel seed selection method based on the neural network approach. The model learns the relationship from the training data to produce the cluster probabilities. Then, the clusters are ranked based on their possibilities, and the top-*R* clusters are selected as the initial seeds in the hill-climbing algorithm to find a set of NN candidates. The details for each part are elaborated in the following subsections.

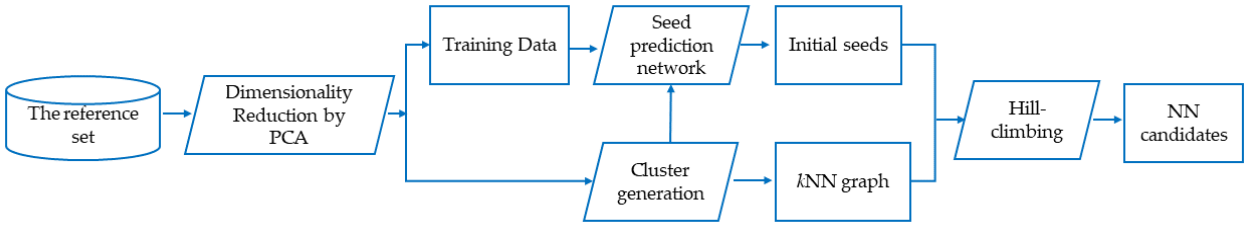

Figure 1. Overview of the proposed method

3.1. Cluster and kNN graph construction

To further reduce the memory space and time complexity of building a *k*NN graph, we adopt Principal Component Analysis (PCA) to perform dimensionality reduction.

Given a reference set of data points $\{x_i \in \mathbb{R}^D | i = 1,2, \dots, N\}$, where N is the number of data points and D is the number of data dimensions. First, we applied PCA to reduce the dimensionality of x_i. To d dimensions, where $d < D$. The PCA process is done by a linear transformation of x_i from the original space $\mathbb{R}^D$ into a lower space $\mathbb{R}^d$. We first standardize the data by subtracting each x_i with the mean and dividing it by the standard deviation of the reference set. Next, a covariance matrix, which is a $D \times D$ symmetric matrix, is computed. Each element in the covariance matrix reflects the covariance of the corresponding variables. After that, we can identify the principal components by computing the eigenvectors and eigenvalues of the covariance matrix. We selected the highest d principal components to construct a projection matrix. Then, each data point x_i is transformed into a new space with the projection matrix.

After we performed dimensionality reduction, the *k*-means clustering is adopted to divide the compressed data space into M clusters, $\{c_j | j = 1,2, \dots, M\}$ where c_j represents the centroid of the *j*th cluster. Finally, we construct the *k*NN graph by calculating the distance between cluster centroids to find k nearest clusters. So, each cluster is associated with a list of k nearest centroids. After that, the inverted index is used to store k indexes.

3.2. Hill-climbing seed generation using neural network

The main idea of our approach is to build a model that can estimate cluster probabilities for a given query. Then, n clusters with the highest probabilities are selected as a set of the initial seed in the hill-climbing algorithm. Function Z implicitly models the neighborhood relationships expressed as $Z(x_i) = \{p_1, p_2, \dots, p_m\}$, which maps a data point x_i to the NN probabilities $= \{p_1, p_2, \dots, p_M\}$, where p_M represents the NN probability of the *m*th cluster. The following training process constructs it. Let $Q = \{q^{(1)}, q^{(2)}, \dots, q^{(T)}\}$ be the training dataset of T queries. The *t*th query $q^{(t)} \in \{\mathbb{R}^d\}$ is associated with the weighted ground truth of *k*NNs, denoted as $G^{(t)} = \{g^{(t,1)}, g^{(t,2)}, \dots, g^{(t,K)}\}$ and $W^{(t)} = \{w^{(t,1)}, w^{(t,2)}, \dots, w^{(t,K)}\}$ where $g^{(t,k)}$ is the *k*th NN of $q^{(t)}$and the corresponding weight is $w^{(t,k)}$. In $Z(x_i)$, the input x_i is the query feature representation $q^{(t)}$. The output, also known as the target, is a vector of NN probabilities of M clusters, denoted as, $Y^{(t)} = \{y_1^{(t)}, y_2^{(t)}, \dots, y_M^{(t)}\}$, where $y_M^{(t)}$ is defined by:

$$y_m^t = \frac{\sum_k \{w^{(t,k)} | g^{(t,k)} \in c_m\}}{|G^t|} \tag{1}$$

where $|\cdot|$ denote the set cardinality.

We characterized Z by a fully-connected neural network to learn the neighborhood relationships from the training data $\{x^t, y^t | t = 1,2, \dots, T\}$. The input layer receives $x^{(t)}$ and the output layer predicts NN probabilities for M clusters, denoted as $p^{(t)} = \{p_1^{(t)}, p_2^{(t)}, \dots, p_M^{(t)}\}$. Based on the cross-entropy loss between the predictions $p^{(t)}$ and the target $y^{(t)}$, we computed the error derivative concerning the output of each unit, which is propagated backward to each layer to tune the weights of the neural network. The proposed seed prediction model is shown in Figure 2.

Given a query q, by using the learned mapping function Z, the model can predict the NN probability among clusters. We then rank these clusters based on their likelihood in descending order to return the top-R cluster used as the initial seed in the hill-climbing algorithm.

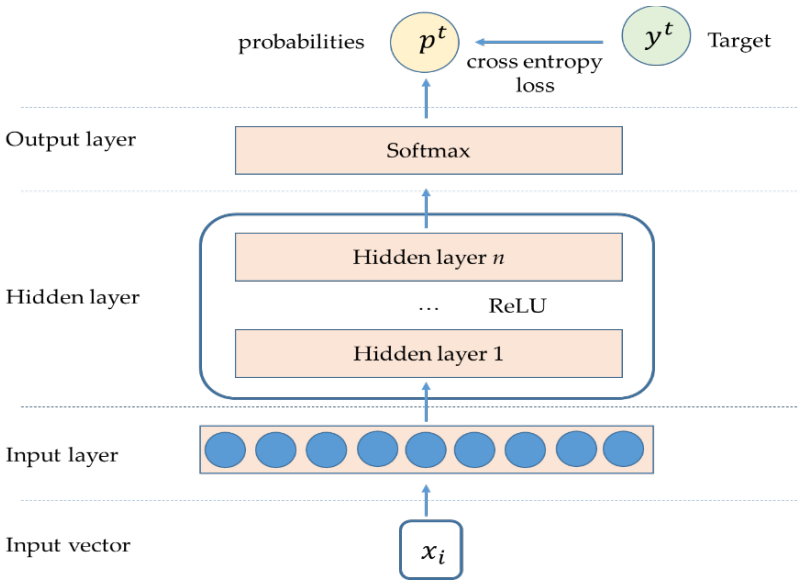

Figure 2. The seed prediction network

4. Experimental results

We performed experiments to evaluate the proposed method on the SIFT1M and GIST1M datasets of BIGANN. Each contains one million SIFT, GIST, and 10,000 and 1,000 query vectors, respectively. Each query is provided with the first 100 nearest neighbors of ground truth with the smallest Euclidean distances. The properties of the two datasets are summarized in Table 1. We applied PCA to reduce the dimensionality of SIFT1M from 128 to 32 dimensions and that of GIST1M from 960 to 120 dimensions. Afterward, we used *k*-means clustering to generate *M* clusters where $M \in \{256, 1024, 4096\}$.

Table 1. Summary of SIFT1M and GIST1M datasets

Datasets	SIFT1M	GISR1M
#data dimensions	128	960
#Reference set	1,000,000	1,000,000
#Training set	20,000	20,000
#Queries set (Test set)	10,000	1,000
#Ground truth set (per query)	100	100

The neural network model is characterized by a three-layer fully connected neural network, including an input layer, two hidden layers, and an output layer. The input layer receives the query feature as input, where the number of units equals the dimension of the input vector. The two hidden layers use ReLU as an activation function, each having an *M* unit. The output layer also has *M* units that predict the probability for *M* clusters using the softmax activation function. The detail of the configuration is elaborated in Table 2.

Table 2. The configurations of the neural network model with various sizes of the cluster.

	The number of units						Activation function
	SIFT1M			GIST1M			
#clusters	256	1024	4096	256	1024	4096	-
Input	32	32	32	128	128	128	-
Hidden	256	1024	4096	256	1024	4096	ReLU
Hidden	256	1024	4096	256	1024	4096	ReLU
Output	256	1024	4096	256	1024	4096	Softmax

A training set is generated by randomly selecting 20,000 data points from the reference set to train the neural network model. We provide 100 NNs of ground truth calculated from Euclidean distance for each training data point. We set the batch size to 128 and ran 100 epochs for training. The test set consists of 10,000 and 1,000 queries, respectively, provided by the SIFT1M and GIST1M, as shown in Table 1.

We implemented several configurations for the hill-climbing algorithm as follows:

- **Exhaustive search**. This method uses the Euclidean distances to calculate the distance between a given query and cluster centroids and select clusters in a particular way so that the hill-climbing algorithm is not applied here.
- **Random seed hill-climbing** [12-13]. Initial seeds for hill climbing are generated randomly.
- **8-bit, 10-bit, and 12–bit LSH seed hill-climbing** [14]. LSH [18] is used to transform data points into 8, 10, and 12-bit hash codes.
- **8-bit, 10-bit, and 12-bit ITQ seed hill-climbing** [14]. ITQ [19] is used to transform data points into 8, 10, and 12-bit hash codes.
- **DNN** seed hill-climbing. This approach uses the proposed neural network model to rank the cluster according to their probabilities.

Other parameters were set as follows: the number of the neighboring clusters kept in the *k*NN graph of a cluster $k \in \{20,30\}$, and the number of seeds for hill-climbing search $s = \{10, 20, 30\}$. Experiments were run on a PC using Windows 10, with an Intel Core i7 3.4 GHz CPU and 32 GB of Ram. The program was implemented in Python.

We use the recall rate to measure the correctness of the NN search. Let $Q = \{q^1, q^2, \dots, q^T\}$ be a set of T queries and $G = \{g^1, g^2, \dots, g^T\}$ be the ground truth, where g^t is the first NN of ground truth for q^t. A recall is defined as:

$$recall = \frac{1}{T}\sum_{t=1}^{T} f(R^t), \qquad f(R^t) = \begin{cases} 1 & if\ g^t \in (R^t) \\ 0 & otherwise. \end{cases} \tag{2}$$

where R^t is the retrieved set corresponding to the q^t. In addition, we counted the number of Euclidean distances calculated between query and cluster centroids to reflect the computation cost for each configuration.

Figures. 3 and 4 show the results under different *M* in SIFT1M and GIST1M, respectively, where *k* and *s* are fixed to 20. The X-axis denotes the number of Euclidean distance computations during the search process, and the Y-axis denotes the recall rate. The exhaustive method yields the best recall, which is served as the accuracy upper bound. However, the computation cost is the highest due to the exhaustive comparisons between the given query and all clusters. The other methods, such as random, LSH, ITQ, and DNN, run five iterations in the hill-climbing algorithm. It shows the recall rates get close to the upper bound with a few iterations and spend much fewer computations. More iterations are required to converge in a more significant number of clusters. The proposed deep learning-based methods outperform the random and hashing methods. It can get the highest recall rate at the first iteration. Using our seed prediction model can provide a better initial seed in a hill-climbing algorithm since the model can learn the relationship between the query feature and cluster to predict the probability for each cluster. Moreover, compared to the previous version of hash-based seeds [14], the proposed DNN method yields better results but requires no additional memory space to store the inverted index lookup table.

Figures. 5 and 6 show the results against different $k \in \{20, 30\}$ and number of seeds $s \in \{10, 20, 30\}$, where *M* is fixed at 4096. We observe that increasing *k* makes the convergence of recall faster than increasing *s*. However, it needs more space to store a larger *k*NN graph.

We also analyzed the memory usage of the proposed DNN model compared with the hash-based seed. The memory space consumed by the hash-based seed method is the inverted lookup table loaded into memory for real-time searching. The number of clusters determines the size of the inverted lookup table. Assume that *M* is the number of clusters, and it takes 2 bytes to store cluster-ID, $2M$ bytes are required for hash-based seed index. The neural network used for seed prediction occupies $8(\tau\lambda\text{^}2 + M\lambda)$, where the model has τ hidden layers, each of which contains λ units, and each nan 8-bytes floating-point number represents each network coefficient.

The time complexity mainly involves two parts: index time and candidate calculation. The time spent on the index depended on the machine and the environment. Some programs merely cannot run very well in the same environment. Therefore, it would be better to analyze the complexity by calculating the number of candidates, making the result more comparative. The results in terms of the number of candidates are shown in figures 3-6.

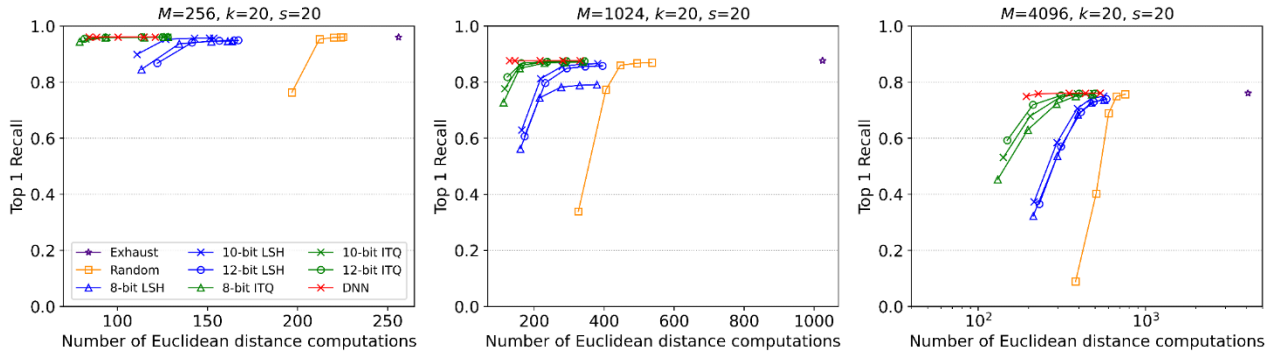

Figure 3. Recall in SIFT1M with different sizes of cluster, where *k* and *s* are fixed at 20

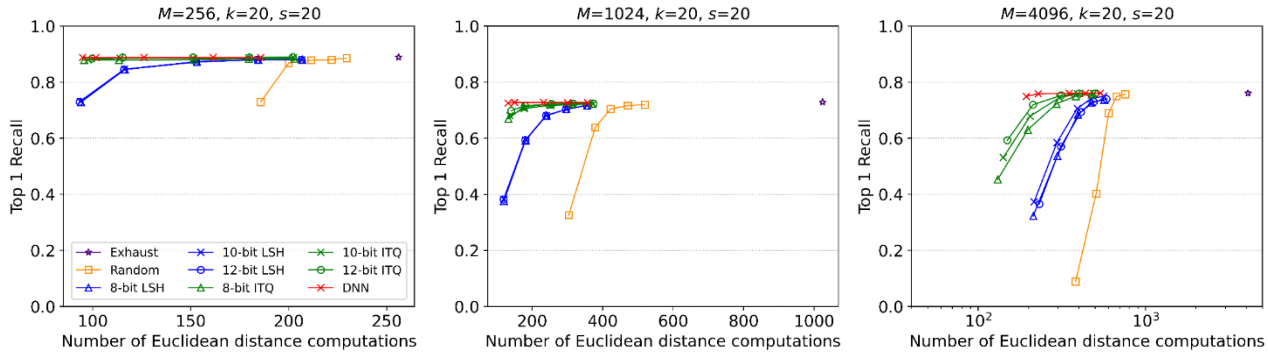

Figure 4. Recall in GIST1M with different sizes of cluster, where *k* and *s* are fixed at 20

4. Conclusions

In summary, we proposed a novel index method for ANN search that employs a *k*NN graph to accelerate the query assignment process. A modified hill-climbing algorithm is presented with the DNN-based seed generation method, which initializes high-quality seeds and thus improves the hill-climbing algorithm. Experimental results on the SIFT1M and GIST1M datasets demonstrate the superiority of the proposed method.

5. Acknowledgements

This study was supported by the Department of Computer Science and Information Engineering, National Chiayi University, Taiwan.

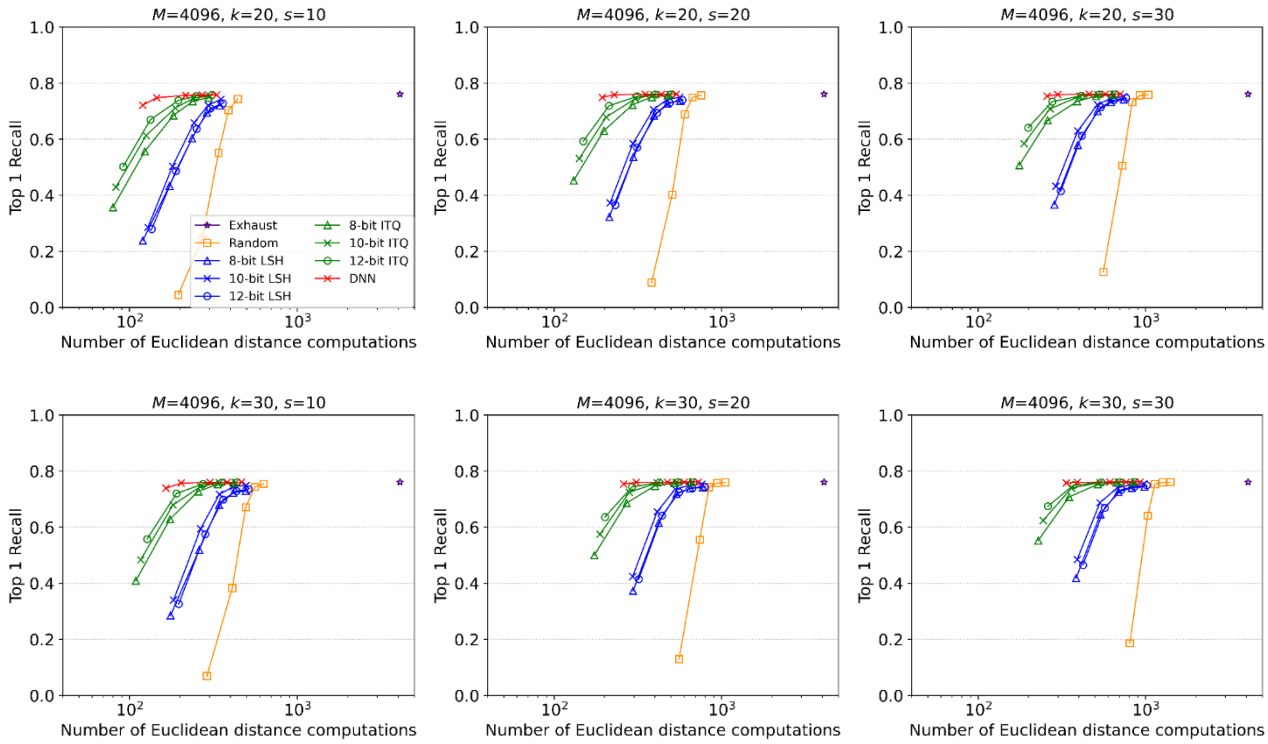

Figure 5. Recall in SIFT1M, where M is fixed at 4096.

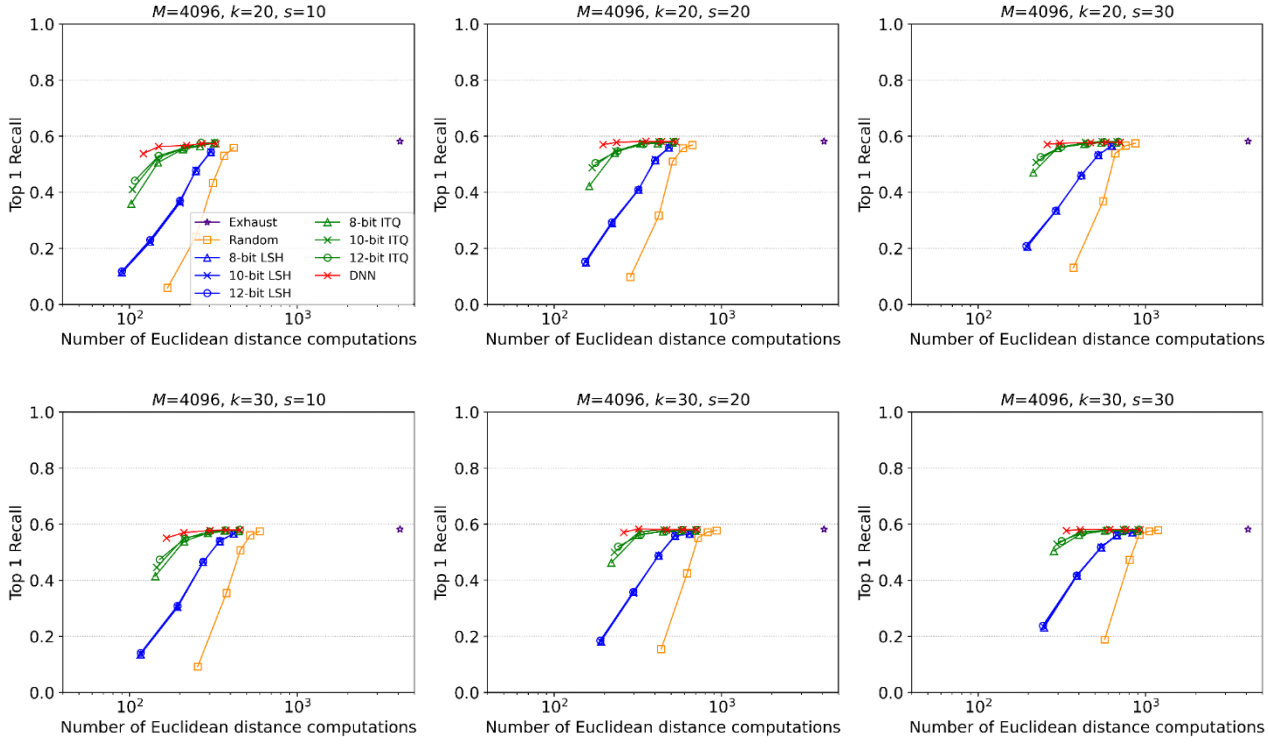

Figure 6. Recall in GIST1M, where M is fixed at 4096.

References

[1] Hu, P.; Peng, X.; Zhu, H.; Zhen, L.; Lin, J. Learning cross-modal retrieval with noisy labels. *In Proceedings of the IEEE/CVF Conference on Computer Vision and Pattern Recognition*. 2021, 5403-5413.

[2] Prétet, L.; Richard, G.; Peeters, G. Learning to rank music tracks using triplet loss. *In ICASSP 2020-2020 IEEE International Conference on Acoustics, Speech and Signal Processing (ICASSP)*, 2020, 511-515.

[3] Jegou, H.; Douze, M.; Schmid, C. Product quantization for nearest neighbor search. *IEEE transactions on pattern analysis and machine intelligence*. 2011, *33*(1), 117-128.

[4] Ge, T.; He, K.; Ke, Q.; Sun, J. Optimized product quantization for approximate nearest neighbor search. *In Proceedings of the IEEE Conference on Computer Vision and Pattern Recognition*. 2013, 2946-2953.

[5] Fu, C.; Cai, D. Efanna: An extremely fast approximate nearest neighbor search algorithm based on *k*nn graph. 2016, *arXiv preprint arXiv:1609.07228*.

[6] Muja, M.; Lowe, D. G. Scalable nearest neighbor algorithms for high dimensional data. *IEEE transactions on pattern analysis and machine intelligence*. 2014, *36*(11), 2227-2240.

[7] Heo, J. P.; Lee, Y.; He, J.; Chang, S. F.; Yoon, S. E. Spherical hashing: Binary code embedding with hyperspheres. *IEEE transactions on pattern analysis and machine intelligence*. 2015, *37*(11), 2304-2316.

[8] Malkov, Y. A.; Yashunin, D. A. Efficient and robust approximate nearest neighbor search using hierarchical navigable small world graphs. *IEEE transactions on pattern analysis and machine intelligence*. 2018, *42*(4), 824-836.

[9] Chiu, C. Y.; Prayoonwong, A.; Liao, Y. C. Learning to index for nearest neighbor search. *IEEE transactions on pattern analysis and machine intelligence*. 2019, *42*(8), 1942-1956.

[10] Zhang, Y. M.; Huang, K.; Geng, G.; Liu, C. L. Fast kNN graph construction with locality sensitive hashing. *In Proceedings of the Joint European Conference on Machine Learning and Knowledge Discovery in Databases*. 2013, 660-674.

[11] Dong, W.; Moses, C.; Li, K. Efficient k-nearest neighbor graph construction for generic similarity measures. *In Proceedings of the 20th International Conference on World Wide Web*. 2011, 577-586.

[12] Zhao, W. L.; Yang, J.; Deng, C. H. Scalable nearest neighbor search based on KNN graph. *arXiv preprint arXiv:1701.08475* 2017.

[13] Hajebi, K.; Abbasi-Yadkori, Y.; Shahbazi, H.; Zhang, H. Fast approximate nearest-neighbor search with k-nearest neighbor graph. *In Proceedings of the 22nd International Joint Conference on Artificial Intelligence*. 2011, 1312-1317.

[14] Rattaphun, M.; Prayoonwong, A.; Chiu, C. Y. Indexing in k-Nearest Neighbor Graph by Hash-Based Hill-Climbing. *In Proceedinngs of the 16th International Conference on Machine Visios Application (MVA)*. 2019, 1-4.

[15] Wang, J.; Wang, J.; Zeng, G.; Tu, Z.; Gan, R.; Li, S. Scalable k-nn graph construction for visual descriptors. In *Proceedinngs of IEEE Conference on Computer Vision and Pattern Recognition*. 2012, 1106-1113.

[16] Wang, J.; Wang, J.; Zeng, G.; Gan, R.; Li, S.; Guo, B. Fast Neighborhood Graph Search Using Cartesian Concatenation. *In Proceedings of the IEEE International Conference on Computer Vision*. 2013, 2128-2135.

[17] Fu, C.; Xiang, C.; Wang, C; Cai, D. Fast Approximate Nearest Neighbor Search with the Navigating Spreading-out Graph. *VLDB Endowment*. 2019, 461-474.

[18] Datar, M.; Immorlica, N.; Indyk, P.; Mirrokni, V. S. Locality-sensitive hashing scheme based on p-stable distributions. *In Proceedings of the 20th annual Symposium on Computational Geometry*. 2004, 253-262.

[19] Gong, Y.; Lazebnik, S.; Gordo, A.; Perronnin, F. Iterative quantization: A procrustean approach to learning binary codes for large-scale image retrieval. *IEEE Transactions on Pattern Analysis and Machine Intelligence*. 2013, *35*(12), 2916-2929.

[20] Ercoli, S.; Bertini, M.; Del Bimbo, A. Compact hash codes for efficient visual descriptors retrieval in large scale databases. *IEEE Transactions on Multimedia*, 2017, *19*(11), 2521-2532.

[21] Babenko, A.; Lempitsky, V. The inverted multi-index. *IEEE Transactions on Pattern Analysis and Machine Intelligence*. 2014, *37*(6), 1247-1260.

[22] Xia, Y.; He, K.; Wen, F.; Sun, J. Joint inverted indexing. *In Proceedings of the IEEE International Conference on Computer Vision (ICCV)*. 2013, 3416-3423.

[23] Dong, Y.; Indyk, P.; Razenshteyn, I.; Wagner, T. Learning space partitions for nearest neighbor search. *arXiv preprint arXiv. 1901. 08544*, 2019.

JSTR
ASEAN Journal of Scientific and Technological Reports

Research article

The Development of Specialty Food Application for Hat Yai: A Case Study

Aroonrak Tunpanit[1*], Patcharin Bunnoon[2], Pichet Suwanno[3] and Taksuriya Madsa[4]

[1] Business Computer Program, Rattaphum Collage, Rajamangala University of Technology Srivijaya, Songkhla, 90110, Thailand; aroonrak.t@rmutsv.ac.th
[2] Accounting Program, Rattaphum Collage, Rajamangala University of Technology Srivijaya, Songkhla, 90110, Thailand; patcharin.bo@rmutsv.ac.th
[3] Business Computer Program, Rattaphum Collage, Rajamangala University of Technology Srivijaya, Songkhla, 90110, Thailand; pichet.s@rmutsv.ac.th
[4] Department of Education Department, Rattaphum Collage, Rajamangala University of Technology Srivijaya, Songkhla, 90110, Thailand; kroodoh@gmail.com
* Correspondence: aroonrak.t@rmutsv.ac.th, Tel: 086-7617851

Abstract: Hat Yai City is the one district of Songkhla province and is an economic city that consists of a commercial district. There are entrepreneurs in a variety of professions. Unique attractions indicate the way of life. It is ethnically diverse and has to mix food with culture, a valuable cultural heritage that should be passed on. But at present, there is intense economic competition. As a result, many business and restaurant sectors get very little income. Therefore, it is necessary to bring modern applications to help the business. The objectives of this research were 1) to develop a street food application in Hat Yai, 2) to assess the efficiency of a street food application in Hat Yai, and 3) to assess satisfaction with a street food application in Hat Yai. The scope of this research was a restaurant located on Niphat Uthit 1 Road, Hat Yai District, Songkhla Province. The instruments used were the efficiency and satisfaction assessments for the street food application in Hat Yai. The restaurant operators agree to provide restaurant information and food items. The sample group used to assess satisfaction was 150 people. The application performance evaluation results It was found at the highest level ($\bar{X}$=4.75). In terms of design, it was found at the highest level ($\bar{X}$= 4.80), which could show the store location correctly and the evaluation results. The app's functional satisfaction was at a high level ($\bar{X}$ = 4.44), offering restaurant stories and food items via the mobile application conveniently and quickly.

Keywords: Development; Application; Food

Citation:
Tunpanit, A.; Bunnoon, P.; Suwanno, P.; Madsa, T. The Development of Specialty Food Application for Hat Yai: A Case Study. *ASEAN J. Sci. Tech. Report.* **2022**, *25*(3), 34-44. https://doi.org/10.55164/ajstr.v25i3.243874.

Article history:
Received: April 2, 2021
Revised: August 30, 2022
Accepted: September 21, 2022
Available online: September 29, 2022

1. Introduction

Hat Yai district it is a district of Songkhla Province, which is the largest city in the south and is a city famous for tourism. There are many natural and historical sites. It is also a transportation hub and a center for educational establishments and is a source of income-generating jobs for people in the community and foreigners. Hat Yai is like the capital of the south. In addition, Hat Yai District Songkhla also has borders adjacent to Malaysia, with convenient transportation routes that lead to transportation of goods for export and

international travel. That generates income, creates jobs, creates careers, and occurs internationally. The economy in the Hat Yai district in the past was very high income from the number of tourists that traveled heavily, causing a huge increase in hotels, shops, restaurants, and other businesses to be sufficient to accommodate tourists. And Niphat Uthit 1 Road, Hat Yai City, Songkhla Province, which is widely known among tourists as Sai 1 Road, is a major tourist attraction of Hat Yai. Crowded with shops, restaurants that prefer a variety of famous food menus, and convenient service to customers who visit all the way. There are tourists, both Thais, foreigners, or from neighboring countries. Such as Malaysia and Singapore, which often travel in Hat Yai on weekends or long consecutive holidays. One of the roads is the main tourist destination. Sai 1 Road, Hat Yai City, Songkhla Province, is the main destination for tourists to respond to their needs on vacation. Currently, the economic problems are intensely competitive, and the coronavirus disease or COVID-19 epidemic has occurred worldwide. Therefore, Thailand has measures to prevent such outbreaks.

Traveling is forbidden to enter/exit internationally, resulting in a rapid economic downturn, no tourist travel, and reduced income. These were affected universally, including the community on Niphat Uthit 1 Road (or Sai 1 Road), Hat Yai District, Songkhon Province, which was ever jolly with tourists and full of businesses, shops, restaurants, etc. Currently, there is a problem with no tourists traveling to this area, causing shops and restaurants in the community to lose income, leading to the eventual closure of the business. Therefore an important problem to be corrected by strengthening food tourism, which is an important tourist attraction of the community—corresponding to the Office of Strategic Management of the Southern Group on the Gulf of Thailand [4] The 12th National Economic and Social Development Plan (February 2018) in Strategy 1. Develop tourism in the southern region to be the world's leading quality destination in developing and supporting food tourism models with unique and different styles in each area. Culture, arts, local food, and lifestyle are unique and interesting, following the three-year development plan of Hat Yai City Municipality (2017-2019) [5] Strategy 3, Economic Development Strategy. There is a way to promote tourism, consumer goods, and consumer prices. Especially in the tourist attractions in the city, there are shops and restaurants to service tourists. To raise the standard of tourism services along with the promotion of service business continually with tourism and food.

For the above reasons, the researchers surveyed the area to assess the needs of municipal authorities and restaurant operators. It was found that there was a great need to upgrade tourism to stimulate the internal economy on Niphat Uthit 1 Road (Sai 1), Hat Yai District, Songkhla Province, which is unique in diverse food culture. The selection criteria must be a restaurant located in the area of Niphat Uthit 1 Road, to consent the information of restaurant history and food items provided. The information systems for presenting reach tourists quickly [7]. Nowadays, smartphones are another channel like a portable computer for searching for information and promoting important tourist attractions and local food. Can show the location to travel accurately Sripol, 2021. [12] Currently, the application is used to encourage food businesses, facilitate customer groups, and add channels to promote the restaurant business through online channels for continuous income. They are responding to customers who want to search for restaurants and food items with distinctive local flavors or a restaurant with a flavor that combines with culture—presenting restaurant information and food menus to tourists. Show the restaurant's old history. The story tells and informs of the restaurant coordinates, which is how to promote the restaurant. As well as being aware of the food festivals, including the location of famous restaurants nearby to receive tourists. To stimulate the economy to support the tourists who love the taste of food, help to promote tourism, and make more income for the community in the form of street food (Hatyai Gastronomy City). The objectives of this research were 1) to develop an application for street food in Hat Yai. Niphat Uthit 1 Road, Hat Yai District, Songkhla Province 2) To assess the efficiency of Hat Yai street food application development 3) To assess the satisfaction of using the Hat Yai street food application. Niphat Uthit 1 Road, Hat Yai District, Songkhla Province.

2. Materials and Methods

The researcher proceeded to the research area to study the needs of people in the community and make an application design for the street food of Hat Yai at Niphat Uthit 1 Road, Hat Yai District, Songkhla Province, is classified into 6 steps as follows:

1. During the data study stage, the researcher went to the research area to interview the restaurant business along the Niphat Uthit 1 Road, Hat Yai District, Songkhla Province. These have a length of 3 kilometers to inquire about the condition of the business performance since January 2020, which had significantly reduced revenue because no tourists are traveling in the area. Some restaurants have only been open for two months. But was affected and unable to bear the cost incurred; therefore, they had to close the business. Then the research team organized a meeting with those who participated in community development, namely, The Municipal authorities, Hat Yai Municipality Council members of district 2, community leaders, Songkhla Community Foundation, Songkhla Chamber of Commerce, and Songkhla Provincial Tourism Council. Small and Medium Enterprises (SME) foundation and restaurant operators on Niphat Uthit 1. To inquire about problems, including community needs for application development to gain access to promotional information for restaurants with outstanding good food items and directions to the restaurant (Figure 1)

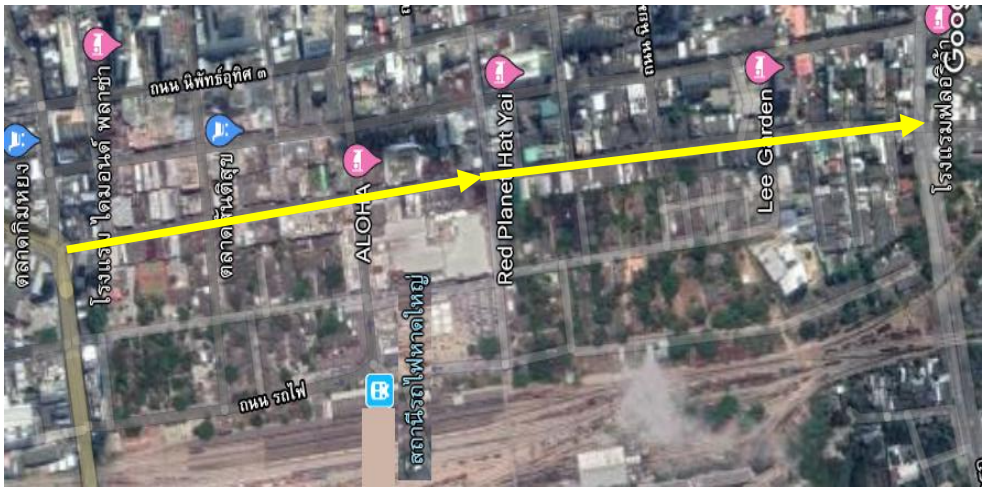

Figure 1. Niphat Uthit 1 Road Map, Hat Yai District, Songkhla Province

2. Analysis stage Data were collected from interviews to study the needs of community stakeholders and restaurant operators to promote food-based tourism. Which has the following issues

2.1 Problems with the publicity of information, which has no channel to present information about the community on Niphat Uthit 1 Road, including a lack of story presentation of the important place to encourage tourists to travel in the food of tourism.

2.2 Problems with the publicity of restaurant information. There is no restaurant database, such as the restaurant's location on Niphat Uthit 1 Road, for both Thai and foreign tourists. It also lists food items that are only shown in Thai, which does not cater to tourists with a variety of languages for communication.

3. Analysis and design stage, the researchers categorized the street food applications into command categories within the application to provide a complete overview of the use of commands from the operating system (Application Program Interface (API).

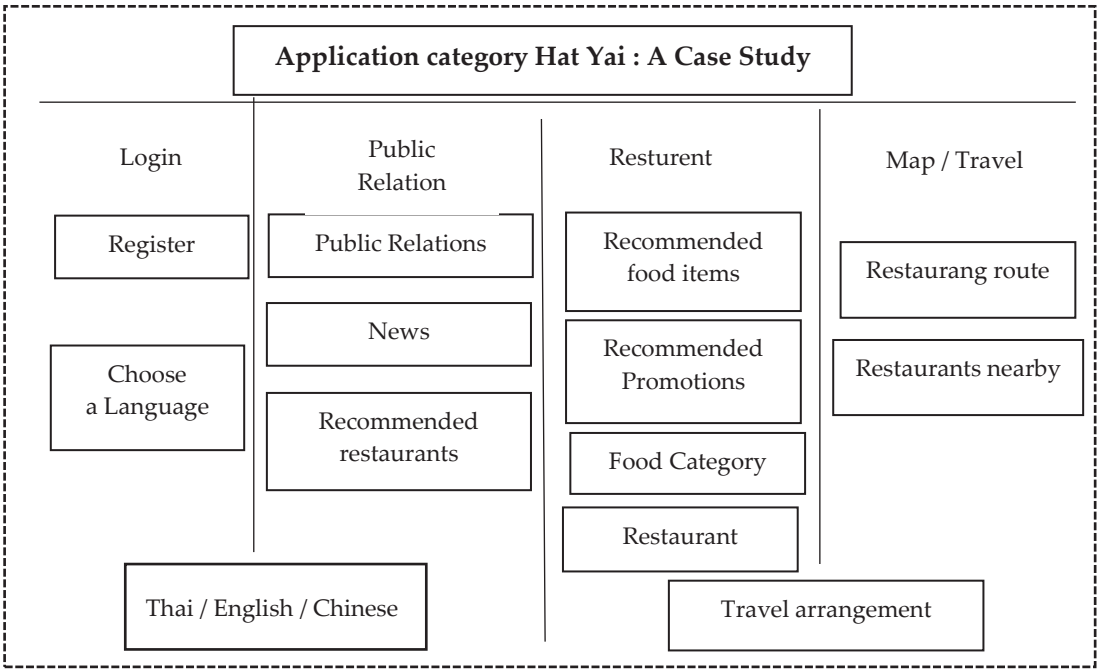

Figure 2. Hat Yai Gastronomy City Application Classification

4. The development process of the Hat Yai street food application consists of a program for developing applications, Glide Application and control commands with Apps Scripts, which can be displayed on the operating system on Android and iOS smartphones [15]. Access to full functionality and flexibility Choice of mobile devices is an important mechanism that enables users to use mobile applications. There is flexible to work on various devices and supports all smartphone operating systems [9]. It is gathering restaurant and food items and displaying them through the application. Able to define the relationship rules information acquired to manage food items to respond to customers' needs and further develop the restaurant business to generate more income.

5. Trial stage and evaluation of efficiency and satisfaction with Hat Yai street food application. This is the prototype application for the design and working system by sending a questionnaire to 7 experts with expertise in information technology and application system development. The satisfaction assessment by the sample group was the general public. A random sample of 150 application installers and trials was used.

6. Conclusion of the research results The efficacy evaluation tool was used to inquire about content integrity with the Index of Item-objective Congruence: IOC and to assess satisfaction with the Hat Yai street food application. The statistics used for data analysis were percentage, $\bar{X}$And standard deviation (S.D.).

3. Results and Discussion

The research results consisted of 3 parts as follows:

Part 1 Hat Yai Gastronomy City application development in Hat Yai District, Niphat Uthit 1 Road, Hat Yai District, Songkhla Province. Researchers have defined the category of applications for the food streets of Hat Yai. To show a data flow diagram (Data Flow Diagram) to see the overall data delivery process of the application, the data transmission and recording process is divided into two levels: Level 0 and Level 1, as shown in figure 3.

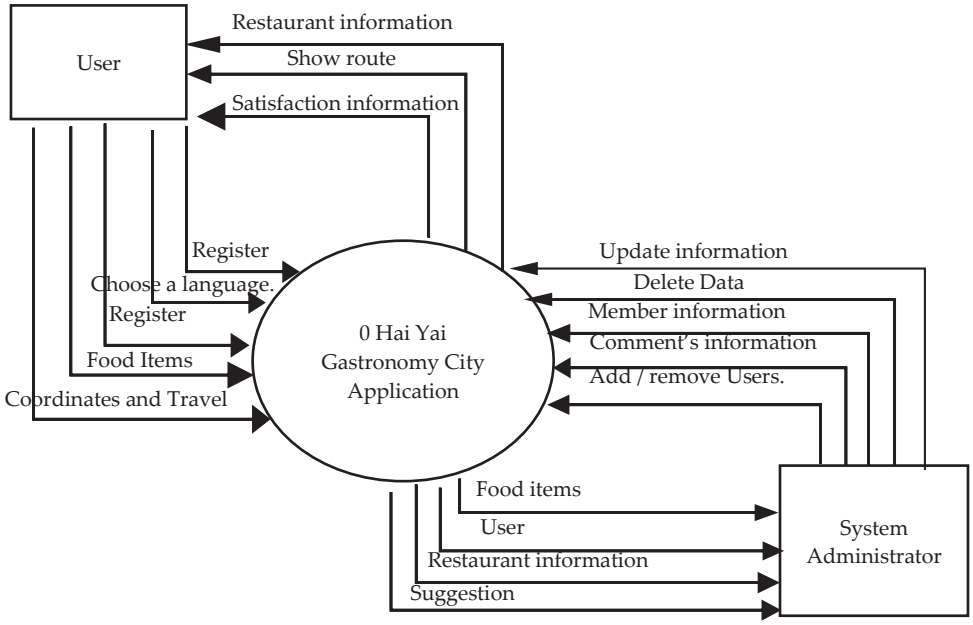

Figure 3. Data Flow Diagram Level 0

Figure 4. DFD Level 1 data stream diagram shows the storage system and workflow. Therefore, it is written as a Data Flow Diagram Level 1 by classifying tables. Storage and data delivery routes within the application. Executing various user commands, including admin rights

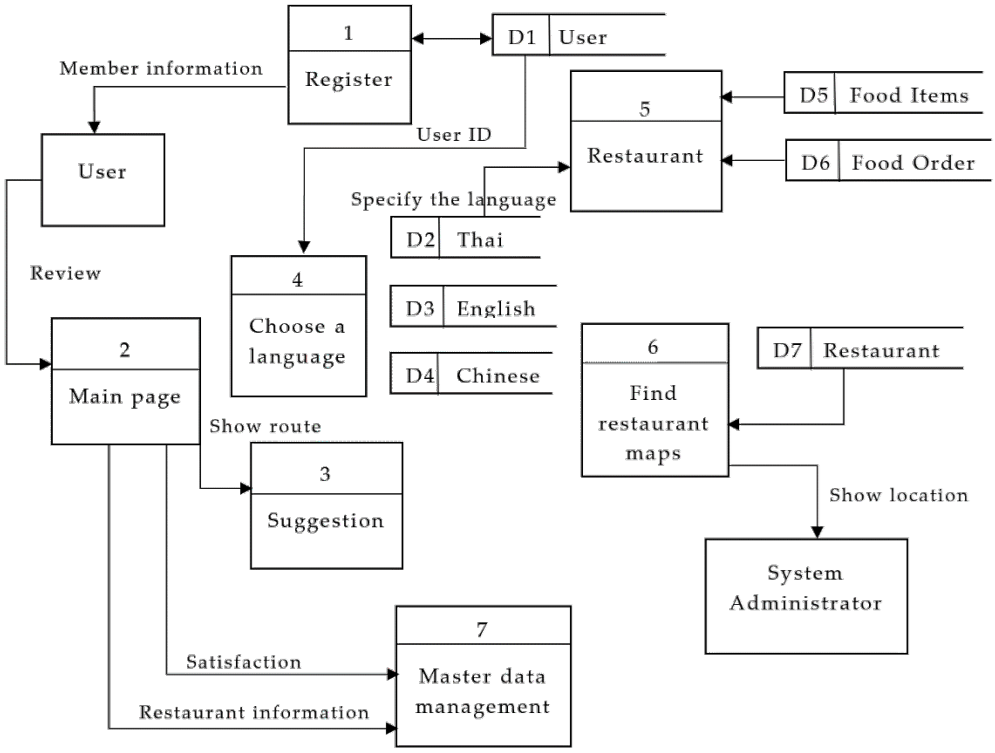

Figure 4. Data Flow Diagram Level 1

The results of the development of the application of street food in Hat Yai Niphat Uthit 1 Road, Hat Yai District, Songkhla Province, the researcher designed the main page and toolbar classified by the restaurant.

When entering the Hat Yai street food application, the main page will display four tools: home page, map, press release, and discussion. The restaurant information supporting the data is displayed in Thai, English, and Chinese. Show restaurant history information with a story (Story Telling) for Thai and foreign tourists, as shown in Figure 5.

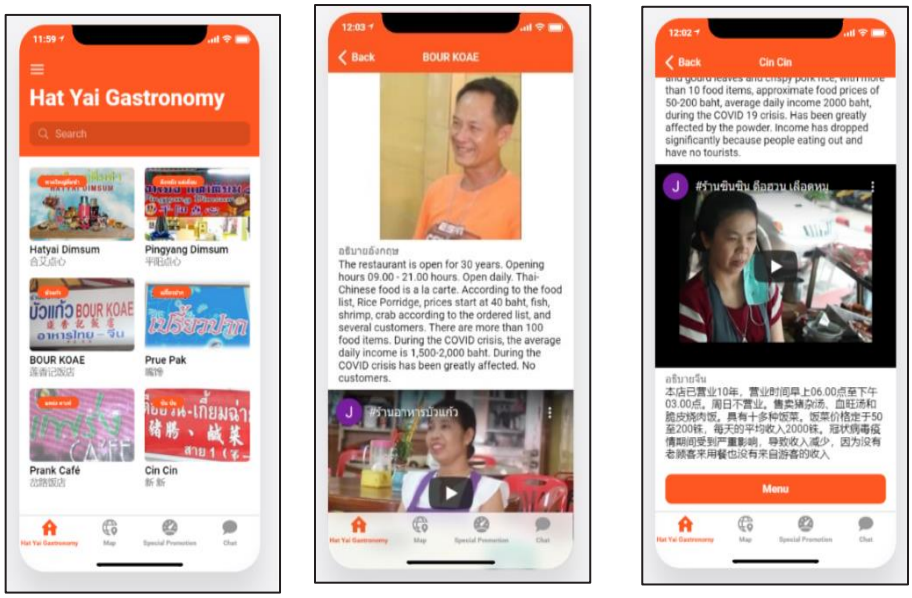

Figure 5. Main page and restaurant information

The menu bar on the top left corner shows the menus in 3 languages, classified by restaurant name, and will offer a large image via the application channel for promoting tourism in various distinctive cuisines and recommended food for tourists, as shown in Figure 6.

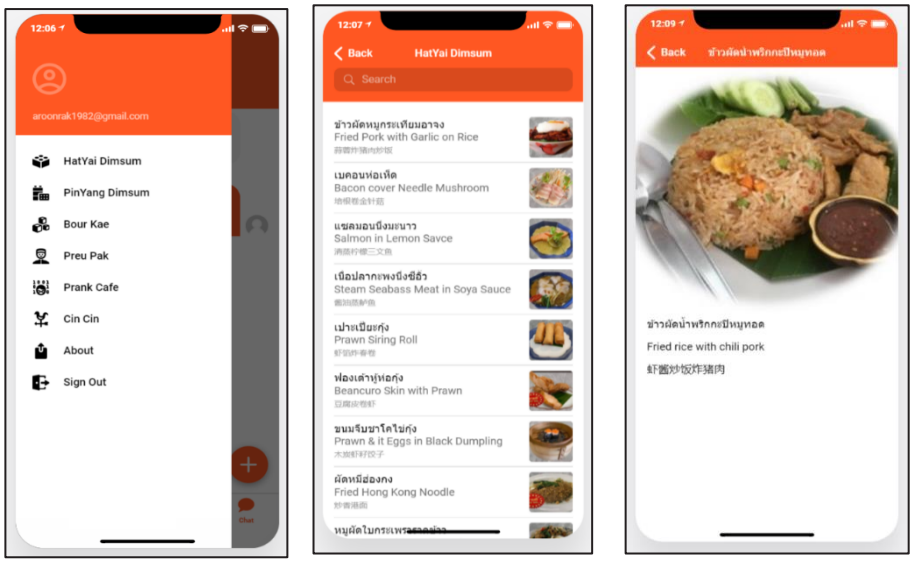

Figure 6. Restaurant and food items

The notification is the coordinates of the restaurant to support tourism in the form of food. Tourists can travel along the route to have delicious food and show news to publicize restaurant activities and be aware

of information and festivals, including chatting with the administrator to inquire about the location of famous restaurants nearby. To stimulate the economy to support tourism and tourists who love the taste of food to promote tourism and income to communities in the area, as shown in Figure 7.

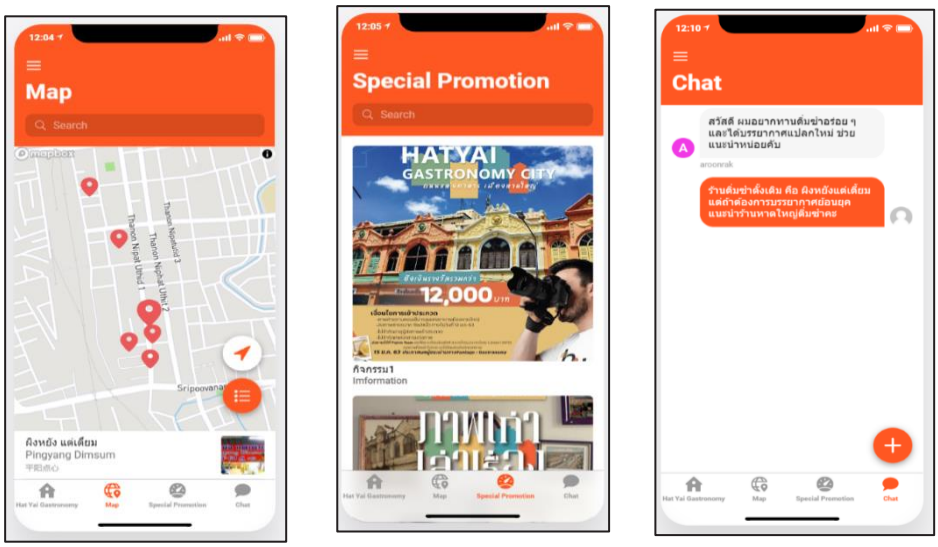

Figure 7. Restaurant map public relations and chatting through the application.

Part 2 Evaluation of application development efficiency of Hat Yai Food Road Niphat Uthit 1 Road, Hat Yai District, Songkhla Province. By evaluating the efficiency of 7 experts related to information technology development and application system development, it was found that the functionality of the application ($\bar{X}$= 4.75, SD = .160) and application design ($\bar{X}$= 4.80, SD = .180).

Table 1. Application performance evaluation results

Functional aspects of the application	$\bar{X}$	SD	Interpret results
1. Appropriately choose the type of font size displayed on the application.	4.97	.183	The most
2. Appropriateness as a four-channel for publicizing news on the application.	4.57	.679	The most
3. The suitability of using background colors. Illustrations and symbols to convey meaning	4.70	.466	The most
4. The appropriateness of choosing to watch videos and broadcasting stories about the restaurant.	4.57	.774	The most
5. Appropriate placement of components and application menus.	4.83	.461	The most
6. Appropriateness of interaction with users.	4.83	.461	The most
Total	**4.75**	**.160**	**The most**

Table 1 shows the results of the evaluation results of the performance of the street food application in Hat Yai, Niphat Uthit 1 Road, Hat Yai District, Songkhla Province, overall at the highest level ($\bar{X}$= 4.75, S.D. = .160) when considering each aspect, found. The suitability of the type The font size is displayed on the application. At the highest level ($\bar{X}$= 4.97, S.D. = .183), followed by suitability in the placement of app components and menus and user interaction at the highest level ($\bar{X}$= 4.83, S.D. = .461), respectively.

Table 2. Application design performance for evaluation results

Application design	$\bar{X}$	SD	Interpret results
1. The ability to support various phone operating systems.	4.97	.183	The most
2. A familiar text and vocabulary can be easily followed.	4.97	.183	The most
3. Arrangement of buttons for choosing using the command menu is convenient.	4.80	.484	The most
4. Ability to display information in 3 languages: Thai, English, and Chinese.	4.90	.305	The most
5. App display of food items by restaurant classification	4.83	.531	The most
6. Display search results. Navigate and display the restaurant's location through the application.	4.67	.547	The most
7. Presentation of restaurant history information and video through the app	4.47	.681	very
Total	**4.80**	**.180**	**The most**

Table 2 presents the results of the design efficiency evaluation of the Hat Yai street food application, Niphat Uthit 1 Road, Hat Yai District, Songkhla Province, overall at the highest level ($\bar{X}$= 4.80, S.D. = .180) when considering each aspect, found. The ability to support various phone operating systems and familiar texts and terms can be easily followed. At the highest level ($\bar{X}$= 4.97, S.D. = .183), followed by the ability to display data in 3 languages, namely Thai, English, and Chinese ($\bar{X}$= 4.90, S.D. = .305), respectively.

Part 3 Satisfaction with the functionality of the Hat Yai street food application Niphat Uthit 1 Road, Hat Yai District, Songkhla Province Evaluation results of the efficiency of Hat Yai street food application.

Table 3. Satisfaction results of the street food application in Hat Yai

Functional satisfaction of the application	$\bar{X}$	SD	Interpret results
1. Applications developed following actual use.	4.40	.855	very
2. The application can save the code and store the user data.	4.63	.490	The most
3. The app makes it easy to communicate with each other.	4.70	.596	The most
4. The application is fast to process.	4.40	.621	very
5. The application is reliable.	4.27	.828	very
6. The app has accurate processing capability.	4.50	.974	very
7. The application complies with the changing technology of the future.	4.20	.795	very
Total	**4.44**	**.181**	**very**

Table 3. shows the results of the satisfaction assessment of the street food application in Hat Yai, Niphat Uthit 1 Road, Hat Yai District, Songkhla Province. The overall application performance was at a high level of satisfaction ($\bar{X}$= 4.44, S.D. = .181). The application made it possible to contact, talk, and interact easily with the highest level of satisfaction ($\bar{X}$= 4.70, S.D. = .596), followed by the application to save code and store user-level data. The satisfaction level was the highest ($\bar{X}$= 4.63, S.D. = .490), and the application was capable of correct processing with a high level of satisfaction ($\bar{X}$= 4.50, S.D. = .974), respectively.

4. Conclusions

From the research results on the development of street food applications in Hat Yai. To promote tourism and income to communities in the area in the form of a food street, divided into 3 parts as follows:

1. The results of the development of the application of street food in Hat Yai Niphat Uthit 1 Road, Hat Yai District, Songkhla Province, from visits to the research area to interviews with restaurant operators along Niphat Uthit 1 Road to inquire about the reasons for no tourists and meeting of community development stakeholders, in line with Suebsom, K. and Meeplat, N., 2020 [13] joint analysis Design and implement technology that tourists in the community or the general public can access to promote tourism for tourists come to test the variety of food and outstanding food items. Able to travel according to the map, recommend restaurants to continually boost income for the community, consistent with Boonchom, V., Khamdam, K. and Kreutong, R., (2020). [1] Has developed an application. Help present cultural wisdom arising from An idea that society or community has continuously passed on from one generation to the next. The application can be installed free of charge. Registration is required for the initial use of the application to store user data. When entering the application will show restaurant information. Food items and menus with food names are displayed in Thai, English, and Chinese Show restaurant maps for traveling to nearby restaurants with Google Maps and display event press information for timely information to tourists. Comply with Dadpe Jinendra, etc., 2017. [3] Application to locate the location. Tourists can conveniently provide travel information to mobile users [13] useful for usability and responsiveness. Collect data about community attractions and restaurants to be packed in the mobile application, including the ability to display text, images, videos, and additional services anytime, anywhere.

2. The results of the evaluation of the efficiency of the application development of street food in Hat Yai can display restaurant information, food menu, and directions for tourists to guide directions to recommended restaurants. Can display images, videos, and support text in 3 languages for Thai and foreign tourist groups. The performance evaluation results showed that The application design aspect was at the highest level ($\bar{X}$= 4.80 S.D. = .180), and the application performance evaluation was at the highest level ($\bar{X}$= 4.75 S.D. = .160). The application activation is convenient by scanning the QR code, which is supported on Android and iOS operating systems, which is an operating system on smartphones with many users suitable for use in promoting tourism in the form of income promotion for restaurant operators in the community. There are restaurant details, food menus, and maps for easy access to the restaurant. Appropriate application to promote tourism in the community is appropriate and consistent with Puttitaweesri, P., Kranruang, D. and Rimphati, W., 2020. [10] Application of tourism by smartphone navigation. Community information can be displayed to find basic information conveniently. Systematic display in a form that is beautiful, proportional, color, text, images, and video that are clear, easy to use, and not complicated. Fast response to user requests corresponds to Sarayapong, 2018 [6] Mobile application technology for displaying food items Restaurant information and food ordering can be facilitated to consumers by the key factor that facilitates the display of restaurant search information and food items.

3. Satisfaction results of the Hat Yai street food application can be used on smartphones, both Android and iOS. The program can be installed free of charge. There is a simple membership storage system. The results of the satisfaction assessment revealed that the work aspect was at a high level ($\bar{X}$= 4.44 S.D. = .181), entering the application was convenient and very fast without any complicated steps. There is an interactive chat channel to help tourists and the general public with inquiries. The information presented through the application is reliable and suitable with information, activities, and restaurants that featured and recommended tourist dishes, corresponding to Chadarattiti, P. and Mrungsiri, N., 2016. [2] Android GPS-based restaurant search makes it easy to find restaurants. Because the device is compact and shows location quickly and accurately, a travel navigation system can be applied on a mobile phone application that can

display complete tourist information, work through Google Maps and suggest nearby places. To facilitate users' travel decisions in nearby areas and display information and press releases to tourists.

The research results on the development of street food applications in Hat Yai, Niphat Uthit 1 Road, Hat Yai District, Songkhla Province, has been published in the street food event on January 30 - February 3, 2021., which is attended by a large number of tourists and the general public. From an experimental trial of an application via a smartphone, it was found that It can be used and is free. The organizing committee aims to promote income and support food tourism for the community. So that the general public can access more tourists come to travel in the community, causing more income for the community, which is a potential development and sustainable self-development, consistent with Prachayaphak Laowsungsuk, 2017. [8] Applying technology to increase channels for restaurant operators to develop food items and services to satisfy consumers and the diverse information presented through easily accessible application channels and food and service types makes it easier for consumers to make informed decisions [11]. Restaurants promote tourism in the form of food by adding information about restaurants and nearby attractions to display on the map for easy search and help make traveling more convenient. So tourists can travel to nearby restaurants and eateries for famous dishes. It also supports a model of gastronomic tourism that is unique to each region and unique and interesting local food and way of life, consistent with Sornsuwan, K. and Srisawat, C., 2017. [14] Displaying detailed restaurant information and displaying its location with Google Maps allows tourists to use it on their devices quickly and efficiently. The application can present information or other activities to promote tourism in the form of food conveniently by the application, helping to manage travel time for tourists to be worthwhile. This leads to tourism with food highlights to strengthen and generate sustainable income for the community.

5. Acknowledgment

Thank you to The Community Product Value Research Unit Lower Southern Region, Rattaphum College Rajamangala University of Technology Srivijaya. That facilitated and supported this research to achieve its objective. Thank you very much to The National Research Council of Thailand (NRCT), which is giving us a subsidy for 2020 under the contract number of OR.0655/268.

References

[1] Boonchom, V.; Khamdam, K.; Kreutong, R. The Development of Android Application for Disseminating Thai Cultural Heritage of the Lower Southern Provinces of Thailand. *Thaksin University Journal*. 2020, *23*(3), 31-40.

[2] Chadarattiti, P.; Mrungsiri, N. Restaurant Search Phase Android Device with GPS System. *1 The 2nd National Conference on Technology and Innovation Management NCTIM 2016*, March 30-31, 2016, Rajabhat Maha Sarakham University. Maha Sarakham: Thailand.

[3] Dadpe, R.; Jadhav, R.; Gaidhani, Y.; Vyavahare, U.; Achaliya, N. (2017). Smart Travel Guide: Application for Android Mobile. *International Conference of Recent Trends in Engineering & Technology*, *Mar 20, 2012, Journal of electronics, Communication & Soft Computing Science & Engineering*. New Delhi: India. 2017, 115-120.

[4] Group Strategy Management Office Southern Gulf Coast. *Development Plan for the Southern Gulf of Thailand (2018-2021)* (Online). Retrieved September 23 2020, from https://www.google.com/url?sa=t&rct=j&q=&esrc=s&source=web&cd=&ad=rja&uact=8&ved=2ahUKEwis35qzssrvAhWPxzgGHSpTB70QFjAAeQIBBAD&url=http%3A%2F%2Fwww2.tsu.ac.th%2Forg%2Fplanoffice%2Fmain%2Ffiles_sec2%.

[5] Hat Yai Municipality. Three-year Development Plan (2017-2019) Hat Yai Municipality. *Administration Department and Academic and Planning Division*. 2016, 12-18. Songkhla, Thailand.

[6] Junkong, T.*Factors Impacting Usage Behavior of Mobile Apps for Order Foods of Cunsumers in Bangkok*. M.B.A. Graduate School. Bangkok University. 2016.

[7] Klubsakul, O.; Seaheng, W.; Keawle, N.; Panjasiriwattana, A.; Sriwanat, C. Application Development for Traditional Southern Food Reccomendation in Phattalung Province.*Academic Journal of Phetchaburi Rajabhat University*. 2021, *11*(3), 82-90 .

[8] Laowsungsuk, P.; Jinda, A.; Sitthisarn, S. Sentiment Analysis of Restaurant Reviews on Review Web sites. *Thaksin Journal*. 2017, *20*(1), 39-47.

[9] Pratip Na Talang, N.; Ketkul, P.; Buathong W.; Jitkamnuengsook, S. (2020). Food Recommended System Using Association Rule Technique. *PKRU SciTech Journal*. 2020**,** *4*(1), 1-12.

[10] Puttitaweesri, P.; Kranruang, D.; Rimphati, W. Development of Smartphone-based Navigation System in Ratchaburi. *Thaksin University Journal*. 2020, *22*(1), 97-108.

[11] Rukpukdi, K.; Sornpong, J.; Ornlor, N.; Sriwongsa, V. Application to find Accommodation around Yasothon Province tourist attraction with Android system. *The 4th National Conference on Business Transformation*. February 12, 2021, Chiang Rai Rajabhat University. Chiang Rai: Thailand.

[12] Sripol, P. Development of Application for food Delivery Services in Khonkaen. *Journal of Buddhist Education and Research*. 2021, *4*(1), 130-142.

[13] Sooknit. O.; Sakda, S. Local Tourism Routes from Geolocation Data using Google Maps Platform. *Thaksin University Journal*. 2020, *23*(1), 66-77.

[14] Sornsuwan, K.; Srisawat, C. Searching Restaurants System on Online Map of Pibulsongkram Rajabjat (Talekaew). *University of the Thai Chamber of Commerce Conference*. June 7, 2017, Bangkok: University of the Thai Chamber of Commerce.

[15] Suebsom, K.; Meeplat, N. The Development of Online Information System to Creat Sustainable Self-management Potential of the Community**.** *Thaksin University Journal*. 2020, *23*(3), 79-87.

JSTR
ASEAN Journal of Scientific and Technological Reports

Research article

A Period Change Study of the Contact Binary System YY Eri

Warisa Pancharoen[1] and Wiraporn Maithong[2*]

[1] Faculty of Science and Technology, Phetchaburi Rajabhat University, Phetchaburi, 76000, Thailand; warisa.pan@mail.pbru.ac.th
[2] Faculty of Science and Technology, Chiang Mai Rajabhat University, Chiang Mai, 50300, Thailand; wiraporn_mai@cmru.ac.th
* Correspondence: wiraporn_mai@cmru.ac.th

Abstract: The W UMa type of the eclipsing binary system YY Eri was observed by using a 0.7-meter telescope with a CCD photometric system in *B*, *V*, and *R* filters at the Regional Observatory for the Public, Chachoengsao, Thailand, on 5 December 2018, from 12:30 PM to 10:00 PM, UT. The obtained data were calculated using the photometry method to construct the light curve of each wavelength band and determine the minimum time. HJD 2458458.306 and HJD 2458458.144 are the minimum time of the primary and secondary eclipse, respectively. The data were used to plot the *O-C* curve. The upward parabolic curve means the period increases at the rate of 4.57×10^{-3} seconds/year. The sinusoidal curve suggests that YY Eri might have a third body which is located at a distance of about 3.45 AU from the center of mass with an orbital period of 68.6 years.

Keywords: YY Eri; Period Change; Third body

Citation:
Pancharoen, W.; Maithong, W. A Period Change Study of the Contact Binary System YY Eri. *ASEAN J. Sci. Tech. Report.* **2022**, *25*(3), 45-50. https://doi.org/10.55164/ajstr.v25i3.246953.

Article history:
Received: June 27, 2022
Revised: September 21, 2022
Accepted: September 21, 2022
Available online: September 29, 2022

1. Introduction

Most stars in our sky are binary or multiple star systems. They are the system of the stars with one center of mass. Eclipsing binaries are one binary star whose orbital plane is inclined to the observer. Therefore, we can see the eclipse when one star moves in front of the other. They showed the difference in the brightness of the stars[1]. YY Eri is a contact binary system, which is defined to be a W UMa subtype. The spectral type of both components is about G5[2], with a magnitude of 8.4 and a period of 0.32149510 days [3]. The radial velocity of YY Eri is -15 kms^{-1}[4]. The value of masses M_h =0.567 $M_\odot$ and M_c =0.967 $M_\odot$ [5]. When M_h is the mass of a hotter star and M_c is the mass of a cooler star.

The W UMa variable had nearly identical depths in primary and secondary eclipses. They show slight color variation through eclipses. The ratio of depths is related to the brightness of component stars and corresponds to the effectiveness of the temperature T_1 and T_2. The study of the light curve synthesis model and employing Roche potentials for the equilibrium surface of the star shows that the component stars in W UMa binaries exist in a state of physical contact [6]. The period of eclipsing binary corresponds to the distribution between the stars. Using the conservative mass exchange of two stars could transfer the mass from a more massive to a low massive star. The period will be decreased [1]. For this work, we study the YY Eri binary star's period change using the differential photometry technique.

2. Materials and Methods

YY Eri (RA 04h 12m 08.849 s and Dec. -10^0 28′ 09.993′′) was observed on 5 December 2018, from 12:30 PM to 10:00 PM, UT at the Regional Observatory for the Public, Chachoengsao, Thailand. The 0.7 -meter reflecting telescope and CCD with the blue (*B*), standard visual (*V*), and red (*R*) filters of the UVB system were used. The MaxIm DL6 program was used to analyze YY Eri's photometry. We obtained 150 images in *B*, 149 in V, and 149 in R filters using 30 seconds of exposure time for each image in the clear sky. We chose the TYC 5315-986-1 (RA 04h 12m 21.364s and Dec.-10^0 26′ 03.797′′) and HD 26650 (RA 04h 12m 32.596s and Dec.- -10^0 33′ 57.865′′) for comparison star and check star. The observational light curve between flux and time of YY Eri in *B*, *V*, and *R* wavelength bandwidth is shown in Figure 1.

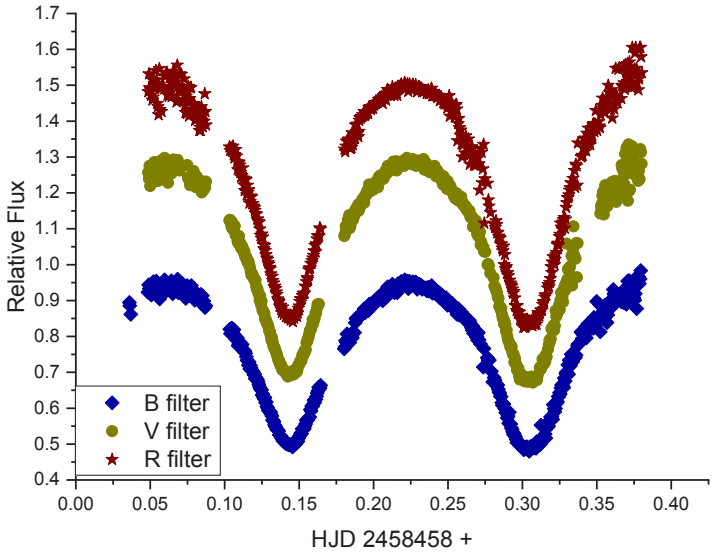

Figure 1. Light curve of the YY Eri.

3. Results and Discussion

The time of minimum light from the YY Eri light curves was determined by differential equation theory [7] and constructed in the *O-C* diagram using the Wilson-Devinney software. It is derived from the linear ephemeris equation obtained from the Database of Eclipsing Binary *O-C* Files by Bob Nelson, AAVSO [8] as follows:

$$HJD\ Min = 2441581.624 + 0.32149415E \quad (1)$$

Where *HJD Min* is the photoelectric times of the minimum light,

And *E* is the epochs of the minimum light.

In this observation, the light curves were calculated as the times of minimum light of the secondary and primary eclipses, as shown in Table 2.

Table 2. The *O-C* values of the YY Eri from this observation.

HJD Min	**Type of Minimum**	**Epoch**	***O-C***
2458458.144	secondary	52493.5	0.16685
2458458.306	primary	52494	0.16810

The *O-C* values in this research were combined with those from other astronomers in the past (979 times of minimum light) and were fitted by Quadratic Polynomial Fitting Method. The result is shown in Figure 2 [8-9].

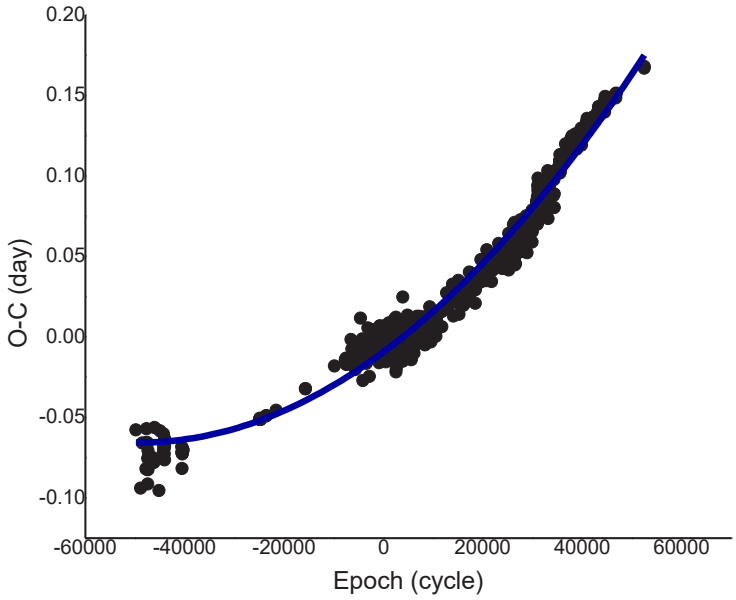

Figure 2. *O-C* Diagram of the YY Eri.

The O-C diagram, which is a plot between the observed time of minimum light (*O*) minus the calculated from ephemeris (*C*) in the y-axis with time in the x-axis, in Figure 2 shows the upward parabolic curve designated that the orbital period of YY Eri is increasing. The best solution to the quadratic ephemeris is shown as follows:

$$\text{O-C} = 2.33\times10^{-11}\text{E}^2 + 2.29\times10^{-6}\text{E} - 0.00932 \quad (2)$$

The quadratic ephemeris equation shows that the value of the period change (dP/dE) in this binary system YY Eri is $2 \times (2.33 \times 10^{-11})$ day/cycle. That means the period is increased continuously by approximately 4.57×10^{-3} seconds/year. Corresponding to the period changing rate of 5.51×10^{-3} seconds/year calculated by Ting et al. in 2018 [10]. The increase of the period showed that the distance between the stars was increased according to Thermal Relaxation Oscillation (TRO) theory. It explains the binary system evolution when the orbital period grows [11-12]. Furthermore, we present the residuals as the difference between the data (black dot) and the parabolic fitting (blue line). Besides this relation, there are periodic oscillations in the diagram, as shown in Fig 3.

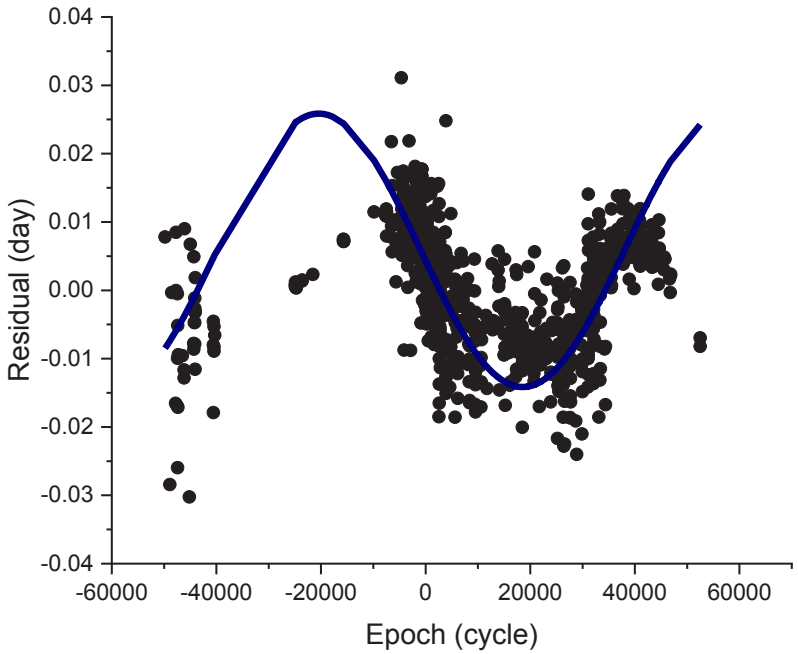

Figure 3. Residual of the YY Eri.

Figure 3 shows the sinusoidal changing of the residual. This effect may be from the apsidal motion of an elliptic orbit, the light time effect due to a third body, or cyclic changes in the magnetic activity of one of the stars[13]. However, the magnetic might be affected by the AML theory that the period change is decreasing [12]. So, the periodic residual oscillation in this study could be caused by the third body in the binary system. The best solution to the periodic oscillation is shown as follows:

$$\text{Residual} = 0.00585 + 0.02 \sin\left(\pi \frac{E - 115956.67059}{38967.43273}\right) \tag{3}$$

From the relation, we found that the YY Eri has a third body in the system. The computation method shows the distance of the third body is 3.45 AU from the center of mass and the orbital period is 68.6 years. The relation as: can calculate the mass function

$$f(m) = \frac{m_3^3}{(m_1 + m_2 + m_3)^2} \sin^3 i' = \frac{1}{P'^2} (a' \sin i')^3 \tag{4}$$

Where m_1,m_2, and m_3 are the mass of the first, the second, and the third star, respectively,

i' is the inclination,

a' is the distance of the third body from the binary system

and P' is the orbital period of the third body.

The masses of the two stars (m_1 and m_2) are 1.3 and 0.5. Solar mass in equation (4) comes from the study by Kim *et al.* in 1998 [13]. If the orbital of the third body is the circle, the calculated mass of the third

body is 0.34 Solar mass, corresponding to the studies of Ting *et al.* in 2018 [10]. They calculated the range of third mass for the inclination of 30-90 degrees are 0.17 – 0.36 Solar mass.

4. Conclusions

YY Eri, the eclipsing binary system, was observed on 5 December 2018, from 12:30 PM to 10:00 PM, UT. at the Regional Observatory for the Public, Chachoengsao, Thailand. The photometric data were analyzed at the Faculty of Science and Technology, Chiang Mai Rajabhat University, Chiang Mai, and the Faculty of Science and Technology, Phetchaburi Rajabhat University, Phetchaburi, Thailand. In Figure 5, we show *O-C* Diagram with the sinusoidal and quadratic curves of the YY Eri. We derived the solution that shows in equation (5)

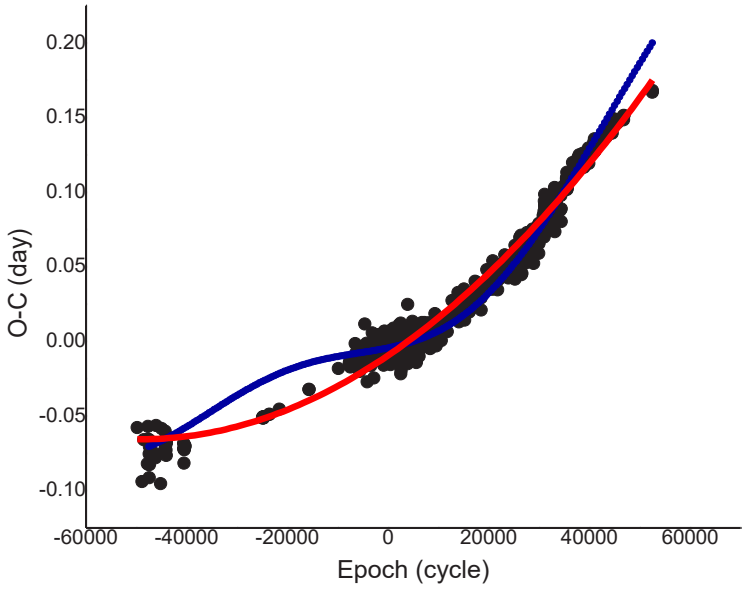

Figure 4. O-C Diagram with the sinusoidal and quadratic curves of the YY Eri.

$$\text{O-C} = 2.33\times10^{-11}\text{E}^2 + 2.29\times10^{-6}\text{E} - 0.00932 + 0.00585 + 0.02\sin\left(\pi\frac{\text{E} - 115956.67059}{38967.43273}\right) \quad (5)$$

The *O-C* diagram and the solution show that the period of YY Eri is increasing at the rate of about 4.57×10^{-3} seconds/year. In addition, the values in this diagram are variance between near-contact binary system and contact binary system corresponding to the (TRO) theory. Moreover, the O-C residuals show that their orbital periods have a sinusoidal oscillation means that the third body in this binary system with an orbital period is about 68.6 years, and the distance from the center of mass of the binary system is about 3.45 AU. Finally, if we assume the third body is a circular orbit, we can calculate its mass is 0.34 Solar mass.

5. Acknowledgements

The author would like to acknowledge the National Astronomical Research Institute of Thailand (Public Organization) for this observation.

References

[1] Skelton, P.L.; Smits, D.P. Modeling of W UMa-type variable stars. *South African Journal of Science. 105*(3/4), March/April, 2009, 120-126.

[2] Cillié, G. G. The Photoelectric Light Curve of YY Eridani. *Harvard College Observatory Bulletin No.* 1951, *920.* 41-45.

[3] Maceroni, C.; vilhu, O.; Van't Veer, F.; Van Hamme, W. Surface imaging of late-type contact binaries I:AE Phoenicis and YY Eridani., *Astronomy and Astrophysics*. 1994, 288. 529-537.

[4] Nesci, R.; Macerini, C.; Milano, I.; Russo, G. YY Eri revisited. *Astronomy and Astrophysics*. 1986, 159. 142-146.

[5] Macerini, C.; Milano, L.; Russo, G. Determination of parameters of W UMa systems.III:CC Com, YY Eri, V502 Oph and TY Pup. *Astronomy and Astrophysics Supplement Series*. 1982, 49. 123-128.

[6] Webbink, R.F.; Contact binaries. 3D stellar evolution. ASP Conference Proceedings, University of California Davis, Livermore, California, USA, 22-26 July 2002; Edited by Sylvain Turcotte, Stefan C. Keller and Robert M. Cavallo. ISBN: 1-58381-140-0, 2003. 76.

[7] Pancharoen, W.; Maithong, W. The First Study of a Period Change of the V1851 Orion Eclipsing Binary System. *ASEAN journal of Scienctific and Technological Reports*. 2021, *24*(3). 9-14.

[8] Bob Nelson's Database of Eclipsing Binary O-C Files, AAVSO. https://www.aavso.org/bob-nelsons-o-c-files (accessed on 21 Feb 2022).

[9] SIMBAD Astronomical Database - CDS (Strasbourg) http://simbad.u-strasbg.fr/simbad/ (accessed on 21 Feb 2022).

[10] Yu, T.; Hu, K.; Yu, Y.-X.; Xiang, F.-Y. Orbital period changes of the W UMa-type binary YY Eri. *Research in Astronomy and Astrophysics.* 2018, *18*(9). 106.

[11] Lucy, L.B.; Wilson, R.E. Observational Tests of Theories of Contact Binaries. *The Astrophysical Journal*. 1979, 231. 502-513.

[12] Qian, S. Orbital Period Changes of Contact Binary Systems: Direct Evidence for Thermal Relaxation Oscillation Theory. *Monthly Notices of the Royal Astronomical Society*. 2001, 328. 914–924.

[13] Kim, C.; Jeong, J.; Demircan, O.; Muyesseroulu, Z.; Budding, E. The Period Changes of YY Eridani. *Highlights of Astronomy*. 1998, *11*(1). 370-370.

JSTR
ASEAN Journal of Scientific and Technological Reports

Research article

Annual Dose Analysis of Pottery from Thoud-Ta Thoud-Yai Archaeological Site in the Songkhla Province of Southern Thailand

Tidarut Vichaidid[1*] and Piyawan Latam[2]

[1] Faculty of Science and Technology, Prince of Songkla University, Pattani Campus, 94000, Thailand; tidarut.v@psu.ac.th
[2] Faculty of Science and Technology, Prince of Songkla University, Pattani Campus, 94000, Thailand; 6420320802@email.psu.ac.th
* Correspondence: tidarut.v@psu.ac.th

Abstract: Thoud-Ta Thoud-Yai is Thailand's oldest archaeological site. Identifying the age of artifacts helps link past and present in storytelling. Absolute dating techniques are used to estimate a sample's geological age. Calculating the annual dose is the essential step. The annual dose depends on samples' concentrations of natural radionuclides and the sediment surrounding them. This research performed the annual radiation dose analysis in pottery by quantifying the concentrations of natural radionuclides using Neutron Activation Analysis (NAA). According to the volume analysis, internal dose, external dose, and cosmic rays contribute 0.180 ± 0.027, 0.959 ± 0.110, and 0.177 ± 0.009 mGy/year, respectively. The annual dose was found to be 1.139 ± 0.113 mGy/year. Annual dose measurements are necessary for determining the age of pottery samples. Since the age is determined by dividing the equivalent dose by the annual dose, this result connects the past and present at the Thoud-Ta Thoud-Yai archaeological site.

Keywords: Annual Dose, Neutron Activation Analysis, Pottery, Thoud-Ta Thoud-Yai

Citation:
Vichaidid, T.; Latam, P. Annual Dose Analysis of Pottery from in the Songkhla Province of Southern Thailand. *ASEAN J. Sci. Tech. Report.* **2022**, *25*(3), 51-58. https://doi.org/10.55164/ajstr.v25i3.247180.

Article history:
Received: Aungust 3, 2022
Revised: September 27, 2022
Accepted: September 27, 2022
Available online: September 29, 2022

1. Introduction

There are several methods of dating material samples for their age. Each is appropriate for some restricted sample structure type. The sample's aging value is also a factor. It focuses on the proportional connection between the equivalent and annual doses. In other words, the annual dose is important for determining the age. The sample's age apparent from its radionuclides is affected by radiation from the surrounding environment, so a radiation level is needed to calculate the sample's age. Most naturally radioactive elements are the radioactive series (uranium, actinium, and thorium) and some non-series nuclides (mainly potassium). This naturally occurring alpha, beta, and gamma radiation sources expose minerals to radiation continuously [1-2]. Suppose a mineral is exposed to natural radiation. In that case, some paired electrons are ionized, and trapped by impurities, and unpaired electrons, also known as lattice defects, are also formed, leading to aging [3]. The annual radiation dose must thus constantly be assessed [4]. The concentrations of U-238, Th-232, and K-40 in archaeological and geological materials will be used to calculate the

annual dose, which is the most important factor in dating. Several methods are employed to determine the contents of U-238, Th-232, K-40, and the annual dose rates of geological and archaeological material. Each method has its own merits and conveniences [5]. The aforementioned include alpha, beta, and gamma-ray spectroscopy; track detection (fission tracks and alpha-tracks); mass spectrometry: secondary ion mass spectrometry (SIMS) or with an ion micro-analyzer (IMA); inductively coupled plasma-optical emission spectrometry (ICP-OES); inductively coupled plasma mass spectrometry (ICP-MS); and chemical analyses: X-ray Fluorescence: (XRF), liquid scintillation counting (LSC), and neutron activation analysis (NAA).

Ancient materials' age is determined through annual radiation dose assessments. It is established by examining the U-238, Th-232, and K-40 concentrations. The previously mentioned NAA is an interesting technique. Archaeological artifacts contain 1-10 ppm of naturally radioactive elements, requiring careful investigation. NAA estimates long-lived radioisotopes in the environment. NAA's sensitivity and isotope specificity identify radionuclides with 104-year half-lives. Neutron activation creates radionuclides with shorter half-lives and increased specific activity. The 1950s: S.A.A. (the first artificial radionuclide was produced in 1934). Activation analysis identifies and quantifies stable elements using artificial radionuclides. Only a few stable atoms in the sample turn into radionuclides [6]. Neutron energy influences elastic collision, radiative capture, charged particle reactions, neutron reactions, fission, and fissionable isotope reactions. NAA starts nuclear processes using neutrons. Quantify neutron capture radiation. The addition of radioactive nuclei causes radioactivity. The latter kind is typically NAA [7]. Nondestructive NAA detects low background gamma radiation. In recent decades, semiconductor detectors and digital technologies have helped it advance. Gamma-ray photons generate electron-hole pairs in photon detectors such as a Highly Pure Germanium (HPGe) detector, a Ge for low energy photon spectroscopy (Ge-LEPS), and a lithium-doped Ge [Ge (Li)] detector cooled by liquid nitrogen detectors for gamma radiation. Peak current caused by electrons and holes is proportional to gamma-ray spectra used to assess U-, Th-, and K-series elements. Electrons and holes create peak currents. Gamma-ray spectroscopy can be used to find NAA's gamma-ray peaks and figure out its parts [4, 6].

The annual radiation dose must be found by adding the samples' radiation doses and the radiation dose from the environment, including cosmic rays. This study investigates the annual radiation dose of pottery at the Thoud-Ta Thoud-Yai archaeological site to determine the concentrations of natural radionuclides. By employing NAA methods and gamma spectrometry with HPGe well-type detectors, we could estimate ancient materials' U-238, Th-232, and K-40 compositions. It is important to determine the pottery samples' age and annual exposure levels. The archeological site of Thoud-Ta Thoud-Yai should link the following sequence of past and present occurrences. The 13th Songkhla Fine Arts Department has investigated the archaeological site of Thoud-Ta Thoud-Yai. The examination found that the archaeological site had several objects from antiquity. The preliminary analysis suggested that they were objects from the ancient period [8]. The annual dose levels determined in this study may be utilized to examine ages and verify the accuracy of archaeological data.

2. Materials and Methods

As indicated in Figure 1, the Thoud-Ta Thoud-Yai archeological site is situated in the Kao Daeng, Saba Yoi district of Songkhla province. As seen in Figure 2, Songkhla's 13th Department of Fine Arts unit discovered the samples in 2010. This current study used pottery samples and the surrounding environment as its study materials. The cliffs are 60 m in length and 20 m in width. There is a natural headboard slicing through the cliff shed's front face. The current is thick with vegetation. Archaeological evidence has been uncovered at several damaged sites. These include remnants of pottery containers, human skeletal fragments, steel tool components, and animal bone fragments. The archaeological site goes back to ancient periods, according to estimates. The excavation site is shown in Figure 3. Two wells, TP1 and TP2, were excavated. TP1 was the pottery excavation employed in this study's annual radiation dose analysis. At the same time, TP2 was the excavation where human skeletons were discovered, as seen in Figures 4A and 4B, while Figure 4C shows an example of pottery used in the research [8].

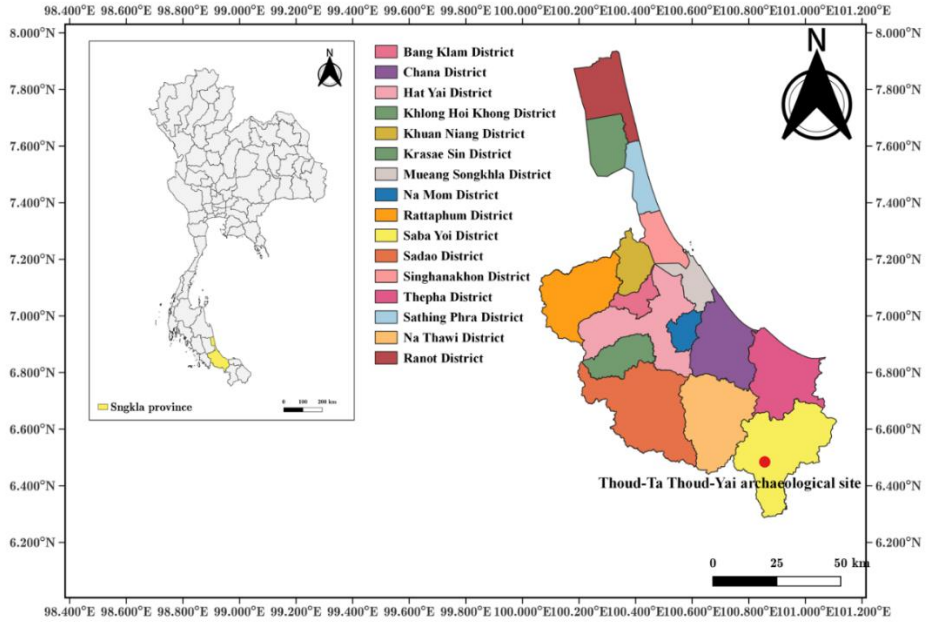

Figure 1. The Thoud-Ta Thoud-Yai archaeological site of Songkhla province.

Figure 2. The external area and the excavation site of the Thoud-Ta Thoud-Yai archaeological site [8].

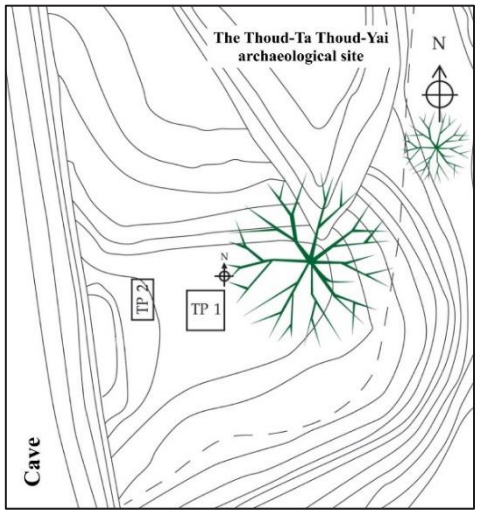

Figure 3. The excavation site. Two wells, TP1 and TP2, were excavated [8].

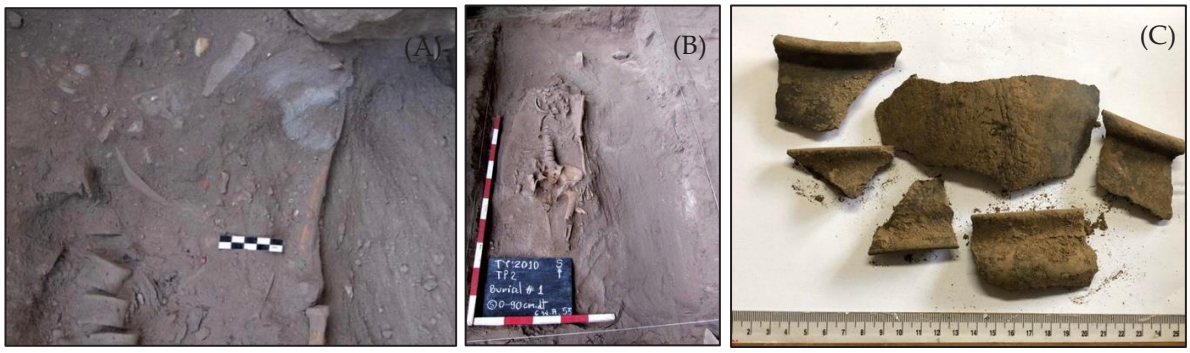

Figure 4. The excavation site (A) TP1 was the pottery excavation location used in this study's annual radiation dose analysis; (B) TP2 was the excavation where human skeletons were recovered; and (C) shows a sample of pottery used in the research [8].

The sediment and pottery samples were collected at 50–60 cm depth. All samples were dried in an oven at 60 °C for 24 h, then crushed, pulverized, and homogenized. Note that clean containers should be used for the preparation and handling stages to prevent contamination [9]. Each powdered sample was crushed to a 0-90 μm particle size and stored in polyethylene vials of the same shape and volume as those holding 150-250 mg of standard reference material. The lamp cap was heated to form a tight seal. Samples and standard references are stored in plastic cylinders in alternating order. All samples were radiation in two phases at the Thai Research Reactor-1/Modification (TTR-1/M1) at the Office of Atoms for Peace (OAP) facility. First, the concentration of U-238 and Th-232 were found by using long-term irradiation for 12 h and a cooling time of 5–6 d in the epithermal neutron flux of $2x10^9$ n/(cm^2.s). Using short-term irradiations of 10 minutes and 12 h of cooling with a thermal neutron flux of $2x10^{11}$ n/(cm^2.s), the concentration of K-40 was found [2]. The gamma-ray spectra were started. GWL series HPGe (High-purity Germanium) coaxial wells, installed in a vacuum-tight cryostat, make up the gamma spectrometer system. The aluminum absorbing layers (well wall) are 0.5 mm thick. For this purpose, we utilized the Gamma Vision-32 V 3.2 Gamma-Ray. Spectroscopy Software has a friendly graphical user interface and is great for working with and analyzing spectra on a home computer. The quantitative ratio of the gamma-ray spectrum would be altered as a consequence. A feasible method for measuring Np-239 and Pa-233 is U-238 and Th-232 because of their short half-lives, as indicated in Equation 1 (see Figure 1) [10]. Table 1 also includes important nuclear data from neutron activation studies on U-238, Th-232, and K-40. K is necessary for life. K-40 isotope abundance in nature is 0.01%, whereas K-41 is 6.7%. Hence K-40 contamination is computed from K-41. Despite its short half-life, K-42 is a common radiotracer. The only K isotope with a similar half-life is K-43, which is harder to generate than K-42. Neutron activation analysis uses K-42 to measure potassium content. [9-12]

$$\begin{aligned} &\text{U-238}(n,\gamma)\text{U-239} \xrightarrow{\beta^-} \text{Np-239}(2.55\text{d}) \\ &\text{Th-232}(n,\gamma)\text{Th-233} \xrightarrow{\beta^-} \text{Pa-233}\,(27.4\text{d}) \\ &\text{K - 41}(n,\gamma)\text{K - 42}\,(12.36\text{h}) \end{aligned} \tag{1}$$

Table 1. This study used important nuclear data from neutron activation of U-238, Th-232, and K-41 [9-10].

Element	Isotope	Half-lives	Energies of emitted Gamma ray (keV)	% of emission
U-238	Np-239	2.55 d	277.6	14.1
Th-232	Pa-233	27.4 d	311.9	33.7
K-41	K-42	12.36 h	1524.7	17.9

The annual radiation dose (D) consists of the internal dose (D_{in}), the external dose (D_{ex}), and the cosmic dose (D_{cos}). The cosmic rays were controlled by longitude, latitude, elevation, and the contributions lessened

with sample depth. Radiation from U, Th, and K in the pottery is responsible for the internal dose. Still, radiation from the same elements in the sediment around the pottery is responsible for the external dose. Radioactive element concentrations were used to analyze each contribution. U, Th, and K decay produce alpha, beta, and gamma radiation, in addition to the cosmic rays. Equation 2 may be used to determine the annual dose [6, 13].

$$D = D_{in} + D_{ex} + D_{cos} \quad (2)$$

Internal gamma radiation can be ignored since the pottery was too thin to absorb gamma rays. Due to our samples' coarse grain structure, we considered that the efficiency of the defect production (k-value) by alpha-particles in quartz remained minimal for the internal annual dose calculation. The k-value is a correction factor because an alpha particle's luminescence effects are limited to a small grain volume along the track [14]; hence, alpha particles induce less luminescence in each component of absorbed energy than beta particles and gamma radiation. Therefore, the internal dose would be exclusively determined by the beta dose rate. [6, 15]. Since the pottery surface was etched, alpha particles can be ignored when calculating the external annual dose [5]. The annual internal and external dose rates may therefore be expressed as,

$$D_{in} = kD_{\alpha} + D_{\beta} \quad (3)$$

$$D_{ex} = D_{\gamma} + D_{\beta} \quad (4)$$

In Equations 3 and 4 D_{α} , D_{β} , and D_{γ} can be determined using Equation 5. The following equation, for example, C_U is the U-238 concentration and $D_{U(\alpha)}$ a conversion factor is the alpha-particle emission rate U-238 [5, 15-16].

$$\begin{aligned} D_{\alpha} &= C_U D_{U(\alpha)} + C_{Th} D_{Th(\alpha)} \\ D_{\beta} &= C_U D_{U(\beta)} + C_{Th} D_{Th(\beta)} \\ D_{\gamma} &= C_U D_{U(\gamma)} + C_{Th} D_{Th(\gamma)} + C_K D_{K(\gamma)} \end{aligned} \quad (5)$$

The concentrations of those radioactive elements are used to estimate D_{in} and D_{ex} based on the online Dose Rate Calculator (DRAC) using the conversion factors from Guerin *et al.* [17], alpha and beta grain size attenuation factors respectively from Brennan *et al.* [18] and Guerin *et al.* [19]. Beta etch attenuation factors from Bell [20]. The cosmic dose rate, derived from the geographical location and elevation of the site, is nearly identical for each collecting site since these are in the same cosmic exposure area, with a mean square deviation of 1%. The combination of the three doses is the total annual dose of the samples [21].

3. Results and Discussion

Figure 5A shows the gamma spectra of U-238, Th-232, and their daughters, while Figure 5B shows the gamma spectrum of K-40. However, the results in Figure 5 are just an example of all the results for gamma spectra of U-238, Th-232, K-40, and daughters. Figure 5A shows a region of interest according to photopeaks at 277.60 keV and 311.90 keV for their associated radionuclides Np-239 and Pa-233, respectively. These photopeaks were used to calculate the concentrations of U-238 and Th-232, respectively. Furthermore, Figure 5B is based on photopeaks at 1524.7 keV, the associated radionuclide of K-42, and were used to calculate the concentration of K-40 [22].

The annual dose could be determined by analyzing the gamma spectra in Figure 5 for the concentrations of U-238, Th-232, and K-40 described in Table 2 (D). As indicated in Table 2, pottery samples do not contain potassium since ancient pottery was made from clay. Therefore, the majority of clays have

detectable levels of uranium and thorium. However, there is little to no potassium [23]. Using the correlation coefficients for D_{in}, D_{ex}, and D_{cos}, the Internal Dose (D_{in}), External Dose (D_{ex}), and Cosmic Dose (D_{cos}) were determined using DRAC [21]. Table 3 displays the results.

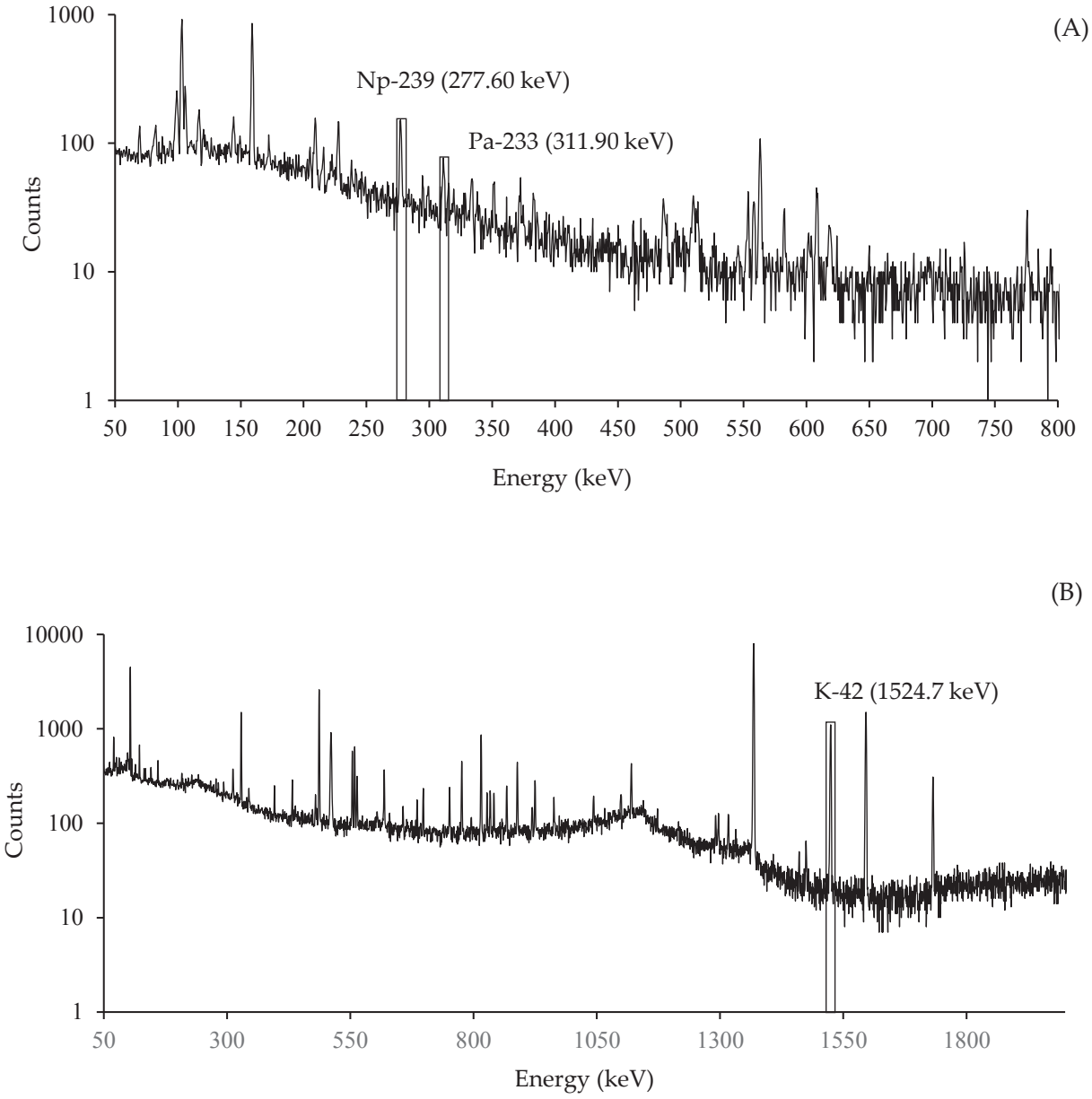

Figure 5. The significant photo peaks and associated radionuclides of sediment around the pottery are shown. (A) and (B) display gamma spectra for the radioactive elements U-238, Th-232, and K-40, respectively.

Table 2. The concentrations of U-238, Th-232 and K-40 in pottery samples and clay around pottery.

Sample	U-238 (ppm)	Th-232 (ppm)	K-40 (%)
pottery	5.61 ± 0.87	15.60 ± 1.20	-
Sediment around pottery	1.70 ± 0.66	3.27 ± 0.46	0.22 ± 0.01

Table 3. The annual levels of Internal Dose (D_{in}), External Dose (D_{ex}), Cosmic Rays Dose (D_{cos}), and the total Annual Dose (D).

Sample	D_{in} (mGy/year)	D_{ex} (mGy/year)	D_{cos} (mGy/year)	D (mGy/year)
Pottery	0.180 ± 0.027	0.959 ± 0.110	0.177 ± 0.009	1.139 ± 0.113

4. Conclusions

An annual dose assessment was performed based on the analysis of U-238, Th-232, and K-40 concentrations in pottery samples and sediment around pottery. The radiation levels of internal, external, and cosmic rays were determined. Calculated doses of radiation were 0.180 ± 0.027, 0.959 ± 0.110, and 0.177 ± 0.009 mGy/year, respectively. The annual radiation dose (D) estimate was then 1.139 ± 0.113 mGy/year. These annual dose levels can now be applied to quantify the ages of pottery samples. Such as trapping techniques (OSL, Tl, and ESR dating), [14-16, 20] age values can be used to connect historical events. The next stage is to connect to past events at the archaeological site of Thoud-Ta Thoud-Yai.

5. Acknowledgements

The authors are very grateful for the detailed survey arranged by the 13th Regional Office of the Fine Arts Department in Songkhla. We thank the Office of Atoms for Peace (OAP) for the gamma radiation measurement. We thank the Nuclear Physics Laboratory of the Faculty of Science and Technology, Prince of Songkla University, Pattani Campus, for providing the tools for measurement, analysis, and sample preparation.

Author Contributions: Tidarut Vichaidid participated in data analysis and drafted the manuscript. Piyawan Latam conceived the study, designed the study, coordinated the study, carried out data analysis, interpreted the results, and aided in drafting the manuscript. All authors gave final approval for publication.

Funding: This research received no external funding

Conflicts of Interest: The authors declare that there is no conflict of interest regarding the publication of this article.

References

[1] Hubert, L. Calibration standard for use in gamma spectrometry and luminescence dating. *Methods and Applications of Absolute Chronology*. 2001, 20, 31-38.

[2] Vichaidid, T.; Soodprasert, T.; Sastri, N. Determination of U, Th and K in Sediments and Fossil Collected from Mae Moh Mine Using Gamma-Ray Spectrometry and Neutron Activation Analysis (NAA). *Kasetsart Journal*. 2008, 42, 333-339.

[3] Shimada, A.; Toyoda, Y.; Takagi, H.; Arita, K. *ESR dating of pseudotachylite*. American Geophysical Union, Fall Meeting. 2002.

[4] Hossain, S. M.; De Cortea, F.; hauteb, P. A comparison of methods for the annual radiation dose determination in the luminescence dating of loess sediment. *Nuclear Instruments and Methods in Physics.* 2002, 490, 598-613.

[5] Adamiec, G.; Aitken, M. Dose-rate conversion factors: update. *Ancient TL*. 1998, *16*(2), 37-50.

[6] Ikeya, M. New Applications of Electron Spin Resonance Dating, Dosimetry and Microscopy. Singapore: World Scientific. 1993.

[7] Robert, R.; Peter, Bode.; Elisabete, A.; De Nadai Fernandes. 2011. Neutron activation analysis: A primary method of measurement. *Spectrochimica Acta Part B*. 2011. 66, 193-241.

[8] The 13th Songkhla Fine Arts Department. *Archaeological survey and excavation from Songkhla and Satun province Unpublished report*. 2010. 25-27, 145-154.

[9] El-Ghawi, U. M.; Bejey, M. M.; Al-Fakhri, S. M. A.; Al-Sadeq, A.; Doubali, K. K. Analysis of Libyan arable soils by means of thermal and epithermal NAA. *Arabian Journal of Science and Engineering.* 2005, 30, 147-153.

[10] Rossini, I.; Tripier, T.; Ch. Abbé, J.; Guevara, B.; Tenorio, R. Neutron activation analysis of U, Th, K and Rb in archaeological samples from Guayabo (Costa Rica) prior to thermoluminescence dating. *Journal of Radioanalytical and Nuclear Chemistry*. 1991, 154, 173-183.

[11] Ferreira Jr, F.A.; Maidana, N.L.; Vanin, V.R.; Koskinas, M.F.; Lopez-Pino, N. $^{41}K(n, \gamma)^{42}K$ thermal and resonance integral cross section measurements. *Radiochimica Acta.* 2012, 100, 871–877. https://doi.org/10.1524/ract.2012.1985.

[12] Johannes, H. A workflow for neutron activation analysis of archaeological ceramicsat the Atominstitut in Vienna, Austria. *Radioanalytical and Nuclear Chemistry*. 2018, 316, 753–759.

[13] Zimmerman, D.W. Relative thermoluminescence effects of alpha- and beta- irradiation. *Radiation Effects*. 1972, 14, 81-92.

[14] Vichaidid, T.; Youngchuay, U.; Limsuwana, P. Dating of aragonite fossil shell by ESR for paramagnetic species assignment of Mae Moh basin. *Nuclear Instruments and Methods in Physics Research Section B: Beam Interactions with Materials and Atoms*. 2007, *262*(2), 323-328.

[15] Aitken, M. J. *An Introduction to Optical Dating*. Oxford University Press, Oxford. 1998.

[16] Ikeya, M. Dating a stalactite by electron paramagnetic resonance. *Nature.* 1975, 255, 48-50.

[17] Guerin, G.; Mercier, N.; Adamiec, G.; Dose-rate conversion factors: update. *Ancient TL*. 2011, 29, 5-8.

[18] Brennan, B.J.; Lyons, R.G.; Phillips, S.W. Attenuation of alpha particle track dose for spherical grains. *International Journal of Radiation Applications and Instrumentation. Part D. Nuclear Tracks and Radiation Measurements*. 1991, 18, 249-253.

[19] Guerin, G.; Mercier, N.; Nathan, R.; Adamiec, C.; Lefrais, Y. On the use of the infinite matrix assumption and associated concepts: a critical review. *Radiation Measurements*. 2012, 47, 778-785.

[20] Ell, W.T. Attenuation factors for the absorbed radiation dose in quartz in-clusions for thermoluminescence dating. *Ancient TL*. 1979, 8, 1-12.

[21] Durcan, J.A.; King, G.E.; Duller, G.A.T. DRAC: dose rate and age calculator for trapped charge dating. *Quaternary Geochronology*. 2015, 28, 54-61.

[22] Gilmore, G.R. *Practical gamma-ray spectrometry*, 2nd edition, Appendix D, Nuclear Training Services Ltd, Warrington, UK, John Wiley & Sons Ltd. 2008.

[23] Aitken, M.J.; Zimmerman, D.W.; Fleming, S.J. Thermoluminescent Dating of Ancient Pottery. *Nature*. 1968, 219, 442-445.

JSTR
ASEAN Journal of Scientific and Technological Reports

Research article

AI System Design for Robotic Hand to Play the Piano

Wuttichon Aukkhosuwan[1*] and Wannarat Suntiamorntut[2]

[1] Faculty of Engineering, Prince of Songkla University, Songkhla, 90110, Thailand; 6210120041@psu.ac.th
[2] Faculty of Engineering, Prince of Songkla University, Songkhla, 90110, Thailand; suntiamorntut@gmail.com
* Correspondence: 6210120041@psu.ac.th;

Abstract: Robotic and Artificial Intelligent (AI) have been introduced as a key factor for industry revolution4.0. Many industries, such as manufacturing, agriculture, logistics, supply chain, and so on, are transformed and applied robotic and AI to enhance productivity and reduce cost. AI in creative work is very challenging, especially in music. This paper presents a system to enable the robotic arm to play piano notes with minimal errors. We used the knowledge of Optical music recognition (OMR), Automatic music transcription (AMT), Music source separation (MSS), and the elimination of robot arm cycle times problems for creating this system. The robotic arm used in testing with this system was LEGO. It can perform 4 functions. The first function is to play piano notes from sheet piano using Sheet Vision and Tesseract-OCR. Note reading accuracy is 21.36%, and note reading accuracy with note duration is 13.46%. The second function is to play the piano like a piano sound separate from a music file using Spleeter and Onsets and Frames. Piano note accuracy is 58.32%, piano note onset time error is ± 0.17, and piano note duration time error is ± 0.65. The third function is to play piano notes from real-time piano sounds using Onsets and Frames Real-time mode. The last function is to play the piano notes from the brain waves by comparing the frequency of the brain waves with the frequency of the piano notes. The design and experimental results are explained in this paper.

Keywords: Artificial Intelligent; Robotic; Music Source Separation; Automatic Music Transcription; Optical music recognition; Electroencephalographic

Citation:
Aukkhosuwan, W.; Suntiamorntut, W. AI system design for robotic hand to play the piano. *ASEAN J. Sci. Tech. Report.* **2022**, *25*(3), 59-68. https://doi.org/10.55164/ajstr.v25i3.246950.

Article history:
Received: July 1, 2022
Revised: September 27, 2022
Accepted: September 28, 2022
Available online: September 29, 2022

1. Introduction

Music has been a part of human culture for thousands of years. Apart from its entertainment value, music could improve people's mental and physical health. Artificial Intelligence (AI) was introduced in 1956 and had been developing from time to time. AI and creative works are very challenging, especially AI and music technology. AI in 2020 enables machine-to-human learning and problem-solving skills. Many music production tools are developed, allowing users to create beats and lyrics with a new musical experience easily.

The work of a musician career involves extracting the music notes sound from a song and trying to play them like the music notes they listened. Another task of the musician is to read music notation sheets. Musicians must play the right chords and notes at the right time.

Playing live music is very popular these days. However, people can listen to the songs of their favorite artists on many channels. But everyone still yearns for live music at restaurants or concerts. Sometimes, live music performances have issues about musicians' illnesses, accidents, or other reasons that prevent musicians from appearing on stage. Moreover, each time, the cost of hiring musicians to perform live music is high. If a restaurant has live music daily, the cost will be high. So, if we have a robotic assistant that can act as a substitute for musicians for live performances on stage, it would be great because the robot will not get sick and will also reduce the daily expenses. These problems can be solved if it's a robot with low production costs but with similar capabilities as a musician. Playing live music by robots also attracts a new audience of customers passionate about technology.

Currently, robots are being used as assistants to musicians and performing live with musicians, for example, Shimon [1]. It's a robot that composes songs according to the sounds it hears. Shimon used to perform live with the musicians. Shimon's live performance was something new and interesting to the audience. But Shimon was quite expensive to create. In addition to Shimon, there is much research about designing robotic arms to play musical instruments [2 – 5]. But designing and building these robotic arms is difficult for the average person and quite expensive. Therefore, the researchers wanted to create a system for the LEGO robotic arms to make the robot arms have the ability as close to the musician as possible. LEGO robotic arms are robotic arms that anyone can assemble, even without robotic knowledge. LEGO is not very expensive compared to other robotic arms.

The instrument the researchers chose for the system testing, and playing of the robotic arms was the piano. The piano is a simple instrument and can be performed live solo without needing another instrument.

Research on Optical Music Recognition (OMR) started a long time ago. It's the task of detecting musical characters on the five lines of the music note sheet. In 2014, a research paper used a camera to read music note sheets from paper instead of music note sheet files[6]. This research uses a method to detect bars in the music note sheet. Then zoom the camera to see notes in bars. This method is more efficient at reading music notes than reading notes from a file (depending on camera quality). But it's more costly than reading music note sheets from a file. Therefore, the researcher chose a method to read the music note sheet from files because it uses a lower cost. But the camera reading method is also an interesting alternative.

Many works in music are continually growing, such as eliminating noise and music generation. Music source separation (MSS) and automatic music transcription (AMT) are the techniques required for this study. The MSS carries out the separation of different sound sources in a song that can separate the sound of other instruments and the vocals from the music. There are many powerful MSS tools available today[7–9]. But there are a few tools that can separate piano sounds from music. Most instruments can only distinguish vocals, bass, drum, and other sounds. So Spleeter[9] is our choice.

Automatic music transcription is an audio signal analysis that produces a written transcript of a musical piece by identifying the instruments and notes played. There are many tools for automatic music transcription[10–12]. Test results show that Onsets and Frames [10] are highly efficient and easy to use. Moreover, it can work in real-time. It was therefore chosen as a tool that we used.

This work presents an AI system that can help a robotic arm to play the piano according to the music piano sound input. It can make robots the ability like musicians. Moreover, we've also added the ability to turn brainwaves into notes to provide a new alternative for live music. The tools that are used to create our system are as follows.

A. Spleeter

The Spleeter is a tool used to separate the source of the music. It contains pre-trained U-nets called the 5-stems model. The 5-stems model separates vocals, bass, drum, piano, and other sounds. The architecture of the U-nets is an encoder/decoder Convolutional Neural Network (CNN) with skip connection layers. It uses 12-layer U-nets (6 layers for the encoder and 6 for the decoder).

B. Onsets and Frames

The Onsets and Frames is a polyphonic piano music transcription tool. It uses deep convolution and recurrent neural networks to create models for predicting onsets and frames. The model was pre-trained before being used for prediction. The f1 score of the note with offset detection of Onsets and Frames is 50.22. Onsets and Frames can now process in real-time.

C. Optical Character Recognition

Optical Character Recognition (OCR) is an electronic process for translating text images into the computer's editable text. The OCR's performance depends on the image's quality for processing. This research uses OCR to convert music sheets (image files) into MIDI files.

D. Tesseract-OCR

Tesseract is an optical character recognition engine that detects text in images and converts it into computer-editable text. It is a tool developed by Google. In version 4, the Long Short-Term Memory (LSTM) mechanism and model have been added, enabling Unicode (UTF-8) support and recognizing up to 116 languages.

E. Music Instrument Digital Interface

Music Instrument Digital Interface (MIDI) is a protocol used for communication between electronic musical devices. The MIDI files store instruction sets for operating an electronic musical device. Parts of the instruction set contain controls to play the notes, the ordinal number of the musical notation, the volume, and the duration.

F. MindWave Mobile 2

MindWave Mobile 2 is a Bluetooth brainwave reader tool based on the TGAM1 module. The output of the sensor is 12-bit raw brainwaves (3-100Hz) with a sampling rate of 512Hz, EEG power spectrums (alpha, beta, etc.), NeuroSky eSense meters (attention and meditation), and eye blinks.

2. Materials and Methods

The robot arm already tested with this system is the Lego Mindstorms EV3. The main components used to build the robot arm to test the system are seven large motors, two EV3 bricks, as shown in Figure 1, one medium motor, and two Edimax EW-7811Un, as shown in Figure 1. The large motor is used to control the finger press of the robot arm, as shown in Figure 2. One large motor can now control two fingers at different times. EV3 bricks are clients that receive server commands to run the motor. One EV3 brick can control only four motors. The medium motor is used as a left and proper motion control on the belt of the robot arm, as shown in Figure 2. The Edimax EW-7811Un is a wireless adapter used to connect to the internet of the EV3 bricks.

Figure 1. Shows EV3 brick (left) and Edimax EW-7811Un (right).

Figure 2. It shows the robotic arm that contains seven large motors (left) and a medium motor (right).

Only four variables in the MIDI file were interested while LEGO was playing music. They are music notes, offsets (or duration), onsets, and velocities. Before playing the song, LEGO has been ordered to move to the octave, where the music notes are played. The note variable holds the information of the note played, with the onset as the start time and the offset as the stop time. The velocity in the MIDI file stated the speed of pressing a musical note. The fast pressing of the notes makes the sound of the notes louder. The value of this variable is sent as the motor speed for pressing the musical notes to increase the music's dynamic. Adding dynamic to the song makes the song more beautiful. The robot arm is still unable to press the sharp and flat note. The system needed to change the music key to C major before sending it to the robot to play.

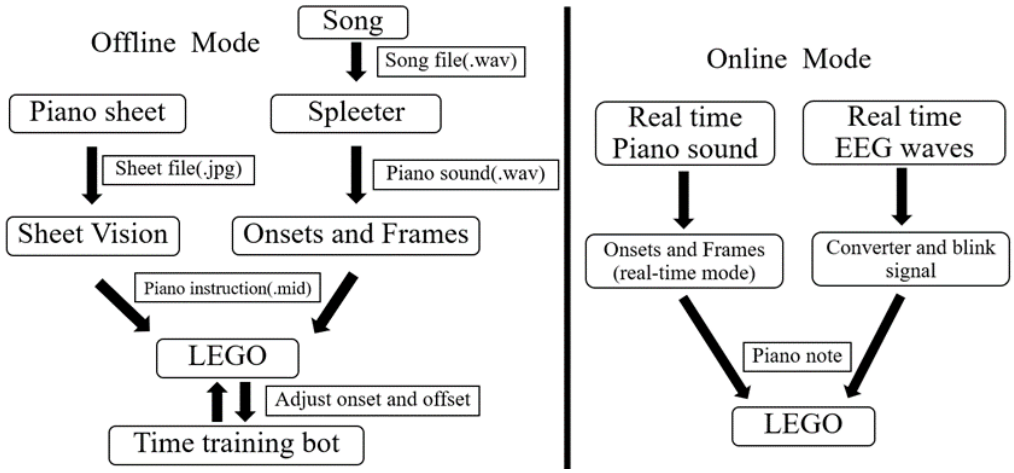

Figure 3. Shows the system processing diagram.

The built system can do 4 things. The first is that the system can read the brain waves of the wearer Mind Wave Mobile 2. After that, the system turns the read data into a series of notes and sends it to LEGO to play in real-time. It is a prototype and a method of sending brainwave data for those interested in further developing music playing through brainwaves.

Second, the system can turn the piano sound heard into piano note data. The system transmits piano notes to LEGO to play the piano in real time. It's useful for live music and piano copy shows. It can be improved by adding the song predictions function of the piano sound detected. In the end, it can be developed into a robot performing live with musicians and can play together at the same time.

Third, the system can separate the piano sound of the song. Then turn the piano sound into a piano note dataset and send it to LEGO. This will allow us to know the note and chord of the new song that does not have public information of note and chord. It is a skill that musicians must have. In the end, we don't need to add piano notes of the new song to the system. Just insert a new music file into the system. LEGO will be able to play piano.

Lastly, the system can convert the piano sheet files (JPEG files) to piano note data. Then send it to LEGO. It is a skill that every musician must have. That is to read the music sheet and play the notes in the correct rhythm. LEGO has a limitation regarding moving speed. The operating time of each motor is 0.7 s. It is average time it takes to move (test move 30 times).

Moreover, the moving speed of the motor will gradually decrease with increasing service life. So, these motors of LEGO cannot play songs with more tempo than 85 bpm. The tempo is the speed at which a musical note is played, usually using beats per minute (bpm).

From Figure 3, the system it has built can perform two functions. The first function is the online mode (real-time). The first step is to import real-time piano sound. Second, use Onsets and Frames to transcribe the received piano sound and convert it to piano notes. After receiving the musical note data, the system transformed it into a LEGO instruction set, as shown in figure 4. The last step is to send an instruction set to LEGO to play music notes.

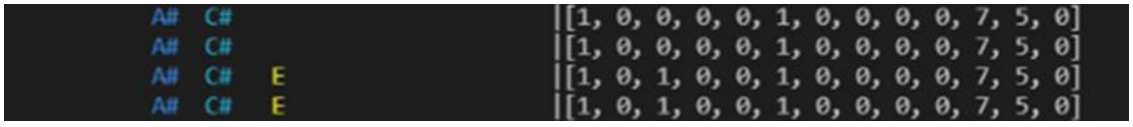

Figure 4. Shows the music notes detected from real-time piano sound by Onsets and Frames (left), and the message has been sent to LEGO (right).

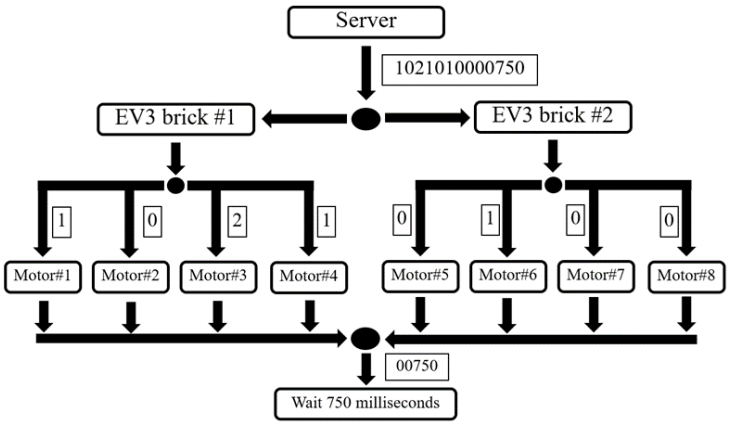

Figure 5. It shows a diagram of operating the LEGO motors from the server.

In Figure 5, the server has sent instructions to both EV3 bricks. The EV3 bricks have sent commands to each motor based on its position. The first seven motors are used to control the press. Code 0 is the order to do nothing—codes 1, 2, 3, and 4 spin forward to command the first finger to press. The higher the number, the higher the speed. Pressing an electric piano at high speed will make the sound even louder. Pressing it slowly makes the sound softer. It is to control the weight of each music note for a more melodious song. Codes 5, 6, 7, and 8 are to spin back to order the second finger to press. The 8th motor is used to move on the belt.

Code 0 is the order to do nothing. Code 1, 2, 3, and 4 are to order the robot arm to move to the left. The higher the number, the greater the distance. Codes 5, 6, 7, and 8 are to order the robot arm to move to the right. In the last step, the server ordered both EV3 bricks to wait. The last five digits are the waiting time. This function cannot use the time training bot. The operation of this function is in real-time. Therefore, it cannot reconfigure the onset and offset values before sending them to the robot arm.

The second function instructs LEGO to play music based on brainwaves read from the EEG sensor. The system reads brainwave data from the Neuro Sky Mind Wave Mobile 2 Headset. The system converts the read data into music notes in the specified frequency range. The system turns the music notes into LEGO instructions. The brainwave data used in the test are attention (any value read from the EEG sensor can be used). The note's frequency range is limited to two octaves. The command to instruct the robotic arm to press a music note is blink action. When the user blinks, the blink value read from the EEG sensor will be greater than 0 (if not blink, the value will be 0). When the blink value is greater than 0, the system sends information to LEGO for music note pressing, shown in figure 6.

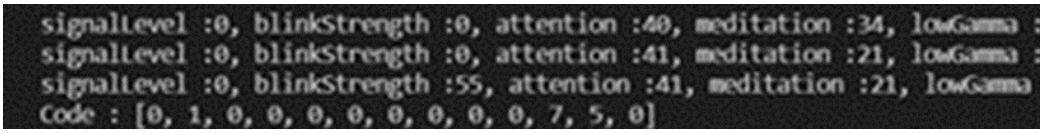

Figure 6. It shows the data from the EEG sensor and the code sent to the robot arm.

The second mode is offline mode. This mode can import two types of data, a JPEG piano note sheet, and a music WAV file. The piano sheet input solution uses a field Optical Character Recognition (OCR) tool called Sheet Vision. It is a python programming language developed by Calvin Gregory and Calvert Pratt. It detects musical characters such as notes, flats, and sharps in an imported piano sheet. Sheet Vision changes the result of detection to a dataset of musical notes. Sort music notes by time and export them as MIDI files.

This system has added tempo detection from piano note sheets using Tesseract version 4.1.1. Set the OCR engine to default and page segmentation mode to sparse text, and crop the image to make it easier to check. A way to detect tempo in a song is to extract the text with an equal sign in front of the number. The number after the removed equal sign is the song's tempo or speed.

For WAV file imports, the system sent imported data files to Spleeter. Spleeter separates various instrument sound sources using the 5-stems model and exports the separated instrument sound WAV files. The system sends WAV files of piano sounds to Onsets and Frames. It detects onsets and frames of the music note and exports it as a MIDI file.

MIDI files are converted to LEGO instruction sets and sent to LEGO. The robotic arm has the time it takes to move (cycle time). The cycle time distorts the time each note plays. Therefore, the last stage of the mode offline mode is a time correction of each music note. The time training bot runs this process. The bot records the robotic arm playing through the midi interface of an electric piano using a python library called Pygame. The robotic arms music playback is saved in MIDI file format. The new files resulting from playback are compared with the old MIDI files received. A different time is the cycle time of the robotic arm. The bot corrects the time in old MIDI files by reducing music note playback time with the cycle time of the robotic arm. With the bot's functionality, the robot can play the notes at the correct time of the song.

3. Results and Discussion

The data set for testing the performance of the WAV import system is The Lakh MIDI Dataset v0.1 (LMD) [13]. The LMD dataset is chosen because it has a large amount of quality data. It has piano tracks and is a popular MIDI data set. The total number of files tested was 5373, which is only part of the LMD data set. Every file is a MIDI file that contains a piano track. The data on the piano track analyzed were music notes, onset, duration, and velocity. The test aims to verify the performance of MIDI files generated by WAV files that Spleeter and Onsets and Frames have processed.

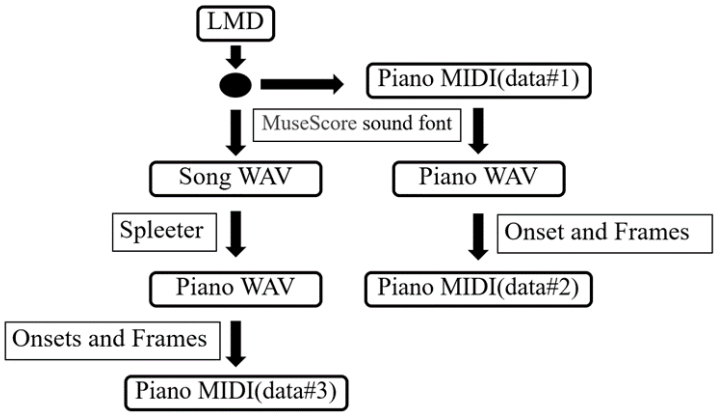

Figure 7. Shows data test set creation diagram.

From Figure 7, the first data set comes from creating a new file that copies only piano tracks from the original data set. The second data set is obtained by converting the MIDI files from the first to WAV files. The sound font converted is Muse Score versions 2.2 and 3 with GM (General MIDI). Use Onsets and Frames to convert WAV files back to MIDI files. This second data set was created to test the performance of Onsets and Frames. The third data set was obtained by a method like the second but used Spleeter to separate piano MIDI files. This third data set was created to test the effectiveness of Spleeter implementation. Finally, compare the first and second data set versus the similarity between the first and third data set.

The first step of the midi file comparison is to split the onset interval of the notes in the first MIDI data set. The upper boundary of the first note interval is in the middle of the first note and the second note onset time. It is the same value as the lower boundary of the second note interval. The lower boundary of the first

note is double the onset time minus the upper boundary time. The upper boundary of the last note is double the onset time minus the lower boundary time.

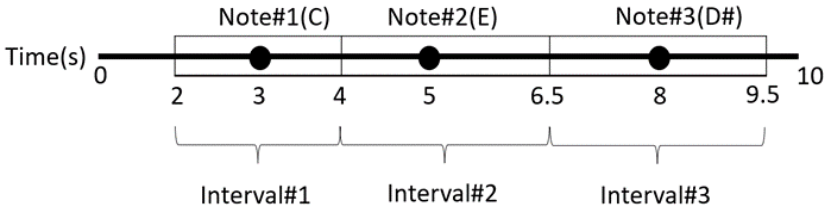

Figure 8. Show the segmentation of the onset interval of the musical notes in dataset 1.

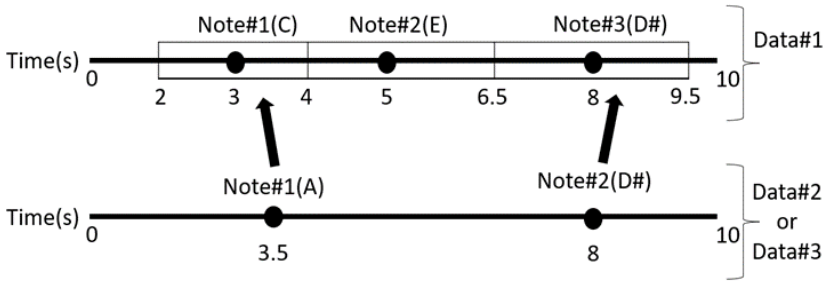

Figure 9. Show music note matching (paired by nearest time).

In Figures 8 and 9, The black point is the time when the music notes begin to sound (onset). The construction of the lower and upper bound of intervals depends on the start time of nearby music notes. If the lower bound of the first note is less than 0, it will be rounded to 0. The real reason for creating the onset interval is to eliminate the issue where some music notes are not detected. The onset interval help match music note for comparisons.

The music notes in the first and the matched second (or third) files are compared. MIDI files contain every music note's note type, onset, duration, and velocity information. Those data of the music notes were compared. They are weighted as one and tested for onset, duration, and velocity errors if they are the same note. But if they don't match, it's weighted as zero, and no tests are performed.

We used baseline statistics, weighted average, and error range to measure the experimental results' effectiveness. We examined the number of notes detected by the Onsets and Frames against the song's notes and displayed them as percentages. The accurate note of the measured music notes is compared to all the notes and is expressed as a percentage. As for the time discrepancy, the note starts playing (onset). We will calculate it as the interval of error. It then shows the range of potential errors. The duration of the note played and the volume of the notes are also checked similarly. We use this test method not to find the F1 score because we want details about the time the note starts, the duration of the press stop and the volume of the note press. This information can better control the robot in playing the piano notes.

Table 1. Show the results of Onsets and Frames and Spleeter tested

Onsets and Frames	Detecting (%)	Accuracy (%)	Onset errs (sec)	Duration errs (sec)	Velocity errs
Without Spleeter	91	75.72	± 0.025	± 0.51	± 24.93
With Spleeter	150.63	58.32	± 0.17	± 0.65	± 43.88

From Table 1, testing of Data Set 1 and Data Set 2, Onsets and Frames had a note detection average of 91 notes (input 100 notes). The accuracy rate was 75.72 percent. Accurate notes have an average onset time error of ± 0.025 seconds, a duration time error of ± 0.51 seconds, and a velocity error of ± 24.93. The test results

of data set 1 and data set 3 (Spleeter was added), Onsets and Frames had a note detection average of 150.63 (input 100 notes). The number of extra notes caused by noise was averaged at 50.63. Of all the notes detected, the accuracy rate was only 58.32 percent. Accurate notes have an average onset time error of ± 0.17 seconds, a duration time error of ± 0.65 seconds, and a velocity error of ± 43.88. The MIDI velocity range is from 0–127.

This test also has issues with noise caused by Spleeter operation. It caused the note detection rate to be much higher than expected, and the accuracy was not as good as expected. The researchers speculated that what caused these problems was the size of the processing window of Spleeter. This is because selecting the Processing window affects the performance of music source separation [14].

The second tests the performance of reading piano sheet music and converting it to MIDI files by Sheet Vision. The dataset that was used to test was TheoryTab Database from Hooktheory. They are MIDI files and sheet music JPEG files. The total amount of data used in the test was 1160 files. This testing compares MIDI files output from Sheet Vision with MIDI files from the TheoryTab Database.

However, this process is to read the piano notes on the five lines from piano sheet music. The performance testing method compares the detected notes in pairs in sequence from two MIDI files and scores them shown in Figure 10. Scoring will be stopped when notes do not match, and subsequent notes will not be counted, as shown in Figure 11.

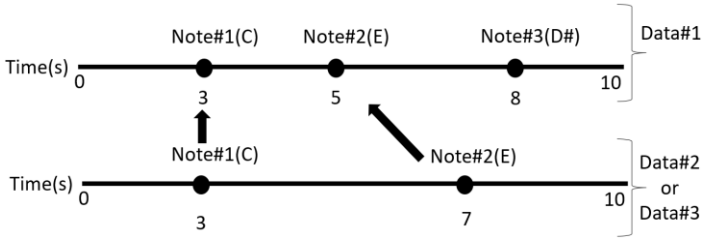

Figure 10. Show music note matching (paired by sequent).

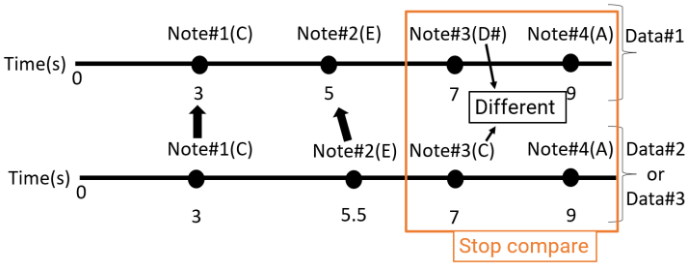

Figure 11. Show music note matching (paired by sequent) and stop scoring when the paired notes differ.

This test does not indicate how effectively detect notes and convert them to note values in a MIDI file. This test is based on a real robot arm's piano playing. If the robot misses a note, any subsequent notes are considered distorted.

Table 2. Show the result of testing

Tempo accuracy (%)	Note detecting (%)	Note accuracy (%)	Note with duration accuracy (%)
87.41	77.01	21.36	13.46

From Table 2, the result is the percentage of the correct interval size measured from the beginning of the sheet music. The note detection average of this system is 77.01 notes (input 100 notes). The accuracy of the note reading is 21.36 percent. The accuracy of the note reading with playtime duration is 13.46 percent. The tempo reading accuracy of this system by Tesseract is 87.41 percent.

The 2 functions only send data from Onsets and Frames (online mode) with hardware Mindwave mobile 2 to the system to convert to MIDI and then forward to LEGO. The performance data of both tools is pre-existing.

4. Conclusions

The system can read piano sheet music and WAV music files and export them as MIDI files. But the efficiency of reading piano notes is still low. The system can turn the resulting piano sound and brainwave data that reads from the EEG sensor into musical notes in real-time. The system can convert MIDI files and music notes into LEGO instructions. The system can also eliminate the excess time caused by the robotic arm's cycle times to play the electric piano.

Most of the limitations are in the part of the robotic arm that cannot play music at too high a speed. The robotic arm can't press the black electric piano keys (sharp and flat keys). The system needs to convert the music key signature into the C major keys before sending them to the robotic arm to play.

The system limitation for real-time conversion of piano sounds to piano notes is that it must operate in a quiet environment. Because the system may change the noise into piano notes, the system also can't extract only piano sounds of songs in real-time. So, the interesting future works are to build a system that can reduce noise and develop an AI that can extract piano sounds in real-time. Moreover, it is also interesting to apply this system to other instruments.

The future task of reading brainwaves if we can convert the brainwave signals of highly concentrated people into music. Then playing this song frequently to someone with ADHD may help them to improve their concentration. Moreover, music created by brain waves during activities may enhance the performance of the activity.

5. Acknowledgements

I would like to express my sincere thanks to my thesis advisor, Asst. Prof. Dr. Wannarat Suntiamorntut for her invaluable help and support throughout this research. Moreover, I would like to thank the Digital Research and Innovation Institute (DRii) for funding and research equipment.

In addition, I am grateful for Asst. Prof. Dr. Sakuna charoenpanyasak, Asst. Prof. Dr. Watcharin Kaewapichai and the researchers from Digital Research and Innovation Institute (DRii) for their suggestions and help.

Finally, I most gratefully acknowledge my parents and friends for all their support throughout this research.

References

[1] Weinberg, G.; Raman, A.; Mallikarjuna, T. Interactive jamming with Shimon: A social robotic musician. In: *2009 4th ACM/IEEE International Conference on Human-Robot Interaction (HRI)*. 2009, 233-234. https://doi.org/10.1145/1514095.1514152.

[2] Lin, JC.; Huang, HH.; Li, YF.; Tai, JC.; Liu, LW. Electronic piano playing robot. In: *2010 International Symposium on Computer, Communication, Control and Automation (3CA)*. 2010, 2, 353-356. https://doi.org/10.1109/3CA.2010.5533457.

[3] Zhang, D.; Jianhe, L.; Beizhi, L.; Lau, D.; Cameron, C. Design and analysis of a piano playing robot. In: *2009 International Conference on Information and Automation*. 2009, 757-761. https://doi.org/10.1109/ICINFA.2009.5205022.

[4] Zhang, A.; Malhotra, M.; Matsuoka, Y. Musical piano performance by the ACT Hand. In: *2011 IEEE International Conference on Robotics and Automation*. 2011, 3536-3541. https://doi.org/10.1109/ICRA.2011.5980342.

[5] Li, YF.; Chuang, LL. Controller design for music playing robot — Applied to the anthropomorphic piano robot. In: *2013 IEEE 10th International Conference on Power Electronics and Drive Systems (PEDS)*. 2013, 968-973. https://doi.org/10.1109/PEDS.2013.6527158.

[6] Fahn, CS.; Lu, KJ. Humanoid recognizing piano scores techniques. In: *2014 International Conference on Information Science, Electronics and Electrical Engineering*. 2014, 3, 1397-1402. https://doi.org/10.1109/InfoSEEE.2014.6946149.

[7] Luo, Y.; Mesgarani, N. Conv-TasNet: Surpassing Ideal Time–Frequency Magnitude Masking for Speech Separation. *IEEE/ACM Trans Audio, Speech, Lang Process*. 2019, 27(8), 1256-1266. https://doi.org/10.1109/TASLP.2019.2915167.

[8] Defossez, A.; Usunier, N.; Bottou, L.; Bach, F. *Music Source Separation in the Waveform Domain*. Published online 2019.

[9] Hennequin, R.; Khlif, A.; Voituret, F.; Moussallam, M. Spleeter: a fast and efficient music source separation tool with pre-trained models. *Journal of Open Source Software*. 2020, 5, 2154. https://doi.org/10.21105/joss.02154

[10] Hawthorne, C.; Elsen, E.; Song, J.; Roberts, A.; Raffel, C.; Engel, J.; Oore, S.; Eck, D. Onsets and Frames: Dual-Objective Piano Transcription. in *Proceedings of the 19th ISMIR Conference, Paris, France, September 23-27*, 2018. 50-57.

[11] Trabelsi, C.; Bilaniuk, O.; Zhang, Y.; et al. *Deep Complex Networks*. Published online 2017. https://doi.org/10.48550/ARXIV.1705.09792.

[12] Hawthorne, C.; Simon, I.; Swavely, R.; Manilow, E.; Engel, J. *Sequence-to-Sequence Piano Transcription with Transformers*. Published online 2021. https://doi.org/10.48550/ARXIV.2107.09142.

[13] Raffel, C. *Learning-Based Methods for Comparing Sequences, with Applications to Audio-to-MIDI Alignment and Matching*. Columbia University, 2016.

[14] Sharma, S.; Mittal, VK. Window selection for accurate music source separation using REPET. In: *2016 3rd International Conference on Signal Processing and Integrated Networks (SPIN)*. 2016, 270-274. https://doi.org/10.1109/SPIN.2016.7566702.

JSTR

ASEAN Journal of Scientific and Technological Reports

JSTR
ASEAN Journal of Scientific and Technological Reports

Article type

Type of the Paper (Article, Review, Communication, etc.) *about 8,000 words maximum*

Title (Palatino Linotype 18 pt, bold)

Firstname Lastname[1], Firstname Lastname[2] and Firstname Lastname[2*]

[1] Affiliation 1; e-mail@e-mail.com
[2] Affiliation 2; e-mail@e-mail.com
* Correspondence: e-mail@e-mail.com; (one corresponding authors, add author initials)

Abstract: A single paragraph of about 400 words maximum. Self-contained and concisely describe the reason for the work, methodology, results, and conclusions. Uncommon abbreviations should be spelled out at first use. We strongly encourage authors to use the following style of structured abstracts, but without headings: (1) Background: Place the question addressed in a broad context and highlight the purpose of the study; (2) Methods: briefly describe the main methods or treatments applied; (3) Results: summarize the article's main findings; (4) Conclusions: indicate the main conclusions or interpretations.

Keywords: keyword 1; keyword 2; keyword 3 (List three to ten pertinent keywords specific to the article yet reasonably common within the subject discipline.)

1. Introduction

The introduction should briefly place the study in a broad context and highlight why it is crucial. It should define the purpose of the work and its significance. The current state of the research field should be carefully reviewed and critical publications cited. Please highlight controversial and diverging hypotheses when necessary. Finally, briefly mention the main aim of the work. References should be numbered in order of appearance and indicated by a numeral or numerals in square brackets—e.g., [1] or [2,3], or [4–6]. See the end of the document for further details on references.

2. Materials and Methods

The materials and methods should be described with sufficient details to allow others to replicate and build on the published results. Please note that your manuscript's publication implicates that you must make all materials, data, computer code, and protocols associated with the publication available to readers. Please disclose at the submission stage any restrictions on the availability of materials or information. New methods and protocols should be described in detail, while well-established methods can be briefly described and appropriately cited.

Interventional studies involving animals or humans, and other studies that require ethical approval, must list the authority that provided approval and the corresponding ethical approval code.

Citation:
Lastname, F.; Lastname, F.; Lastname, F. Title. *ASEAN J. Sci. Tech. Report.* **2022**, *25*(X), xx-xx. https://doi.org/10.55164/ajstr.vxxix.xxxxxx

Article history:
Received: date
Revised: date
Accepted: date
Available online: date

2.1 Subsection

2.1.1. Subsubsection

3. Results and Discussion

This section may be divided by subheadings. It should provide a concise and precise description of the experimental results, their interpretation, as well as the experimental conclusions that can be drawn.Authors should discuss the results and how they can be interpreted from previous studies and the working hypotheses. The findings and their implications should be discussed in the broadest context possible. Future research directions may also be highlighted.

3.1. Subsection

3.1.1. Subsubsection

3.2. Figures, Tables, and Schemes

All figures and tables should be cited in the main text as Figure 1, Table 1, etc.

Figure 1. This is a figure. Schemes follow the same formatting.

Table 1. This is a table. Tables should be placed in the main text near the first time they are cited.

Title 1	Title 2	Title 3
entry 1	data	data
entry 2	data	data [1]

[1] Table may have a footer.

3.3. Formatting of Mathematical Components

This is example 1 of an equation:

$$a = 1, \tag{1}$$

The text following an equation need not be a new paragraph. Please punctuate equations as regular text. This is example 2 of an equation:

$$a = b + c + d + e + f + g + h + i + j + k + l + m + n + o + p + q + r + s + t + u \tag{2}$$

The text following an equation need not be a new paragraph. Please punctuate equations as regular text. The text continues here.

4. Conclusions

Concisely restate the hypothesis and most important findings. Summarize the significant findings, contributions to existing knowledge, and limitations. What are the future directions? Conclusions MUST be well stated, linked to original research question & limited to supporting results.

5. Acknowledgements

Should not be used to acknowledge funders – funding will be entered as a separate. As a matter of courtesy, we suggest you inform anyone whom you acknowledge.

Author Contributions: For research articles with several authors, a short paragraph specifying their individual contributions must be provided. The following statements should be used "Conceptualization, X.X. and Y.Y.; methodology, X.X.; software, X.X.; validation, X.X., Y.Y. and Z.Z.; formal analysis, X.X.; investigation, X.X.; resources, X.X.; data curation, X.X.; writing—original draft preparation, X.X.; writing—review and editing, X.X.; visualization, X.X.; supervision, X.X.; project administration, X.X.; funding acquisition, Y.Y. All authors have read and agreed to the published version of the manuscript." Please turn to the CRediT taxonomy for the term explanation. Authorship must be limited to those who have contributed substantially to the work reported.

Funding: Please add: "This research received no external funding" or "This research was funded by NAME OF FUNDER, grant number XXX" and "The APC was funded by XXX". Check carefully that the details given are accurate and use the standard spelling of funding agency names at https://search.crossref.org/funding. Any errors may affect your future funding.

Conflicts of Interest: Declare conflicts of interest or state "The authors declare no conflict of interest." Authors must identify and declare any personal circumstances or interest that may be perceived as inappropriately influencing the representation or interpretation of reported research results. Any role of the funders in the design of the study; in the collection, analyses or interpretation of data; in the writing of the manuscript, or in the decision to publish the results must be declared in this section. If there is no role, please state "The funders had no role in the design of the study; in the collection, analyses, or interpretation of data; in the writing of the manuscript, or in the decision to publish the results".

References

References must be numbered in order of appearance in the text (including citations in tables and legends) and listed individually at the end of the manuscript. We recommend preparing the references with a bibliography software package, such as EndNote, ReferenceManager to avoid typing mistakes and duplicated references. Include the digital object identifier (DOI) for all references where available.

Citations and references in the Supplementary Materials are permitted provided that they also appear in the reference list here.

In the text, reference numbers should be placed in square brackets [ ] and placed before the punctuation; for example [1], [1–3] or [1,3]. For embedded citations in the text with pagination, use both parentheses and brackets to indicate the reference number and page numbers; for example [5] (p. 100), or [6] (pp. 101–105).

[1] Author 1, A.B.; Author 2, C.D. Title of the article. *Abbreviated Journal Name* Year, *Volume*, page range.

[2] Author 1, A.; Author 2, B. Title of the chapter. In *Book Title*, 2nd ed.; Editor 1, A., Editor 2, B., Eds.; Publisher: Publisher Location, Country, 2007; Volume 3, pp. 154–196.

[3] Author 1, A.; Author 2, B. *Book Title*, 3rd ed.; Publisher: Publisher Location, Country, 2008; pp. 154–196.

[4] Author 1, A.B.; Author 2, C. Title of Unpublished Work. *Abbreviated Journal Name* stage of publication (under review; accepted; in press).
[5] Author 1, A.B. (University, City, State, Country); Author 2, C. (Institute, City, State, Country). Personal communication, 2012.
[6] Author 1, A.B.; Author 2, C.D.; Author 3, E.F. Title of Presentation. In Title of the Collected Work (if available), Proceedings of the Name of the Conference, Location of Conference, Country, Date of Conference; Editor 1, Editor 2, Eds. (if available); Publisher: City, Country, Year (if available); Abstract Number (optional), Pagination (optional).
[7] Author 1, A.B. Title of Thesis. Level of Thesis, Degree-Granting University, Location of University, Date of Completion.
[8] Title of Site. Available online: URL (accessed on Day Month Year).

Reviewers sugestion

1. Name, Address, e-mail
2. Name, Address, e-mail
3. Name, Address, e-mail
4. Name, Address, e-mail

URL link:

Notes for Authors >> https://drive.google.com/file/d/1r0zegnIVeQqe4iLQyT1xDEIinNggINPD/view?usp=sharing
https://drive.google.com/file/d/1r0zegnIVeQqe4iLQyT1xDEIinNggINPD/view?usp=sharing

Online Submissions >> https://ph02.tci-thaijo.org/index.php/tsujournal/user/register

Current Issue >> https://ph02.tci-thaijo.org/index.php/tsujournal/issue/view/16516

AJSTR Publication Ethics and Malpractice >> https://ph02.tci-thaijo.org/index.php/tsujournal/ethics

Journal Title Abbreviations >> http://library.caltech.edu/reference/abbreviations


มหาวิทยาลัยทักษิณ THAKSIN UNIVERSITY
ปัญญา จริยธรรม นำการพัฒนา Intelligence and Ethics guide Development

สถาบันวิจัยและพัฒนา มหาวิทยาลัยทักษิณ
222 หมู่ 2 ต.บ้านพร้าว อ.ป่าพะยอม จ.พัทลุง 93210
โทรศัพท์ 074-609-600 ต่อ 7242 โทรศัพท์ 074-609-655
E-mail Address: aseanjstr@tsu.ac.th